Neuropilin-1-dependent modulation of T cell responses during blood-stage and experimental cerebral malaria

Inaugural-Dissertation

zur

Erlangung des Doktorgrades

Dr. rer. nat.

der Fakultät für

Biologie

an der

Universität Duisburg-Essen

vorgelegt von

Hanna Sophie Elisabeth Abberger

aus Singen (Hohentwiel)

Oktober 2020

Die der vorliegenden Arbeit zugrunde liegenden Experimente wurden am Institut für Medizinische Mikrobiologie des Universitätsklinikums Essen unter der Leitung von Prof. Dr. Wiebke Hansen durchgeführt.

1. Gutachter: Prof. Dr. Wiebke Hansen

2. Gutachter: Prof. Dr. Stefanie Flohé

Vorsitzender des Prüfungsausschusses: Prof. Dr. Ulf Dittmer

Tag der mündlichen Prüfung: 08.02.2021

DOI: 10.17185/duepublico/74532
URN: urn:nbn:de:hbz:465-20220905-144336-2

Table of contents

1 Zusammenfassung

Neuropilin-1 (Nrp-1) ist ein Ko-Rezeptor für VEGF, Semaphorine und TGF-β, der bei der neuronalen Entwicklung und Angiogenese eine wichtige Rolle spielt. Nrp-1 wird von verschiedenen Zellen exprimiert, unter anderem von Tumor- und Endothelzellen, aber auch von Immunzellen, wo es an der Aktivierung von T-Zellen beteiligt zu sein scheint. Darüber hinaus zeigte eine frühere Studie unserer Forschungsgruppe, dass regulatorische T-Zellen (Tregs) über die Nrp-1/VEGF-Achse in Tumorgewebe einwandern und die anti-tumorale Immunantwort beeinflussen.

In der vorliegenden Studie wurde die Nrp-1-Expression im Zusammenhang mit Malaria im Blutstadium in *Plasmodium yoelii* (PY)-infizierten Mäusen analysiert. Die Charakterisierung von PY-infizierten Balb/c-Mäusen zeigte eine signifikante Erhöhung von Nrp-1 auf $CD4^+FoxP3^-$ Effektor-T-Zellen, die neben B-Zellen die Hauptakteure bei der Eliminierung der Parasiten in diesem Modell sind. Die $Nrp\text{-}1^+CD4^+$ T-Zellen zeigten einen hoch aktivierten Phänotyp, der während der PY-Infektion von T-Zell-spezifischen Nrp-1-depletierten $Nrp\text{-}1^{fl/fl}$ x $CD4cre^{tg}$ Mäusen reduziert war, ohne jedoch die Parasitenlast zu beeinflussen.

In einem zweiten experimentellen zerebralen Modell der Malaria (ECM) wurde der Einfluss der Nrp-1-Expression auf die Aktivierung sowie die Migration von T-Zellen in *Plasmodium berghei ANKA* (PbA)-infizierten C57BL/6-Mäusen untersucht. Während einer PbA-Infektion sind $CD8^+$ T-Zellen die Zellen, die zur zerebralen Pathologie führen, indem sie von der Milz ins Gehirn wandern und eine Störung der Blut-Hirn-Schranke induzieren, was eine Neuroinflammation zur Folge hat. Normalerweise exprimieren $CD8^+$ T-Zellen nur sehr geringe Mengen an Nrp-1, die durch die ECM jedoch signifikant induziert wurden. Microarray-Analysen und durchflusszytometrische Untersuchungen zeigten einen hoch aktivierten Phänotyp der $Nrp\text{-}1^+CD8^+$ T-Zellen. Tatsächlich korrelierte die Nrp-1-Expression auf $CD8^+$ T-Zellen mit dem Schweregrad der ECM-Pathologie. PbA-infizierte Mäuse mit einer T-Zell-spezifischen Depletion von Nrp-1 zeigten im Vergleich zu Wildtyp-Geschwistertieren eine signifikant reduzierte Anzahl zytotoxischer T-Zellen im Gehirn. Folglich führte dies zu einer verringerten ECM-Pathologie in $Nrp\text{-}1^{fl/fl}$ x $CD4cre^{tg}$ Mäusen. Die Blockade der Nrp-1-VEGF-Interaktion war während der PbA-Infektion vernachlässigbar, was durch die Tatsache unterstrichen wurde, dass die VEGF-vermittelte Migration von Nrp-1-exprimierenden

oder -depletierten $CD8^+$ T-Zellen nicht verändert war. Im Gegensatz dazu deutete die *In-vitro*-Aktivierung von $CD8^+$ T-Zellen aus WT- und KO-Mäusen eher darauf hin, dass Nrp-1 nicht nur ein Aktivierungsmarker ist, sondern den Aktivierungszustand der $CD8^+$ T-Zellen direkt beeinflusst.

Dies macht Nrp-1 zu einem potenziellen therapeutischen Ziel für die Behandlung von schwerer Malaria und könnte auch für andere $CD8^+$ T-Zell-vermittelte Krankheiten von Bedeutung sein.

2 Summary

Neuropilin-1 (Nrp-1) is a co-receptor for VEGF, semaphorins as well as TGF-β and plays a role in neuronal development and angiogenesis. It is expressed by various cells, including tumour and endothelial cells, but also immune cells, where it seems to be involved in the activation of T cells. In addition, a previous study of our research group showed that regulatory T cells (Tregs) migrate into tumour tissue via the Nrp-1/VEGF axis and influence the anti-tumour immune response.

In the present study, Nrp-1 expression was analysed in the context of blood-stage malaria. The characterisation of *Plasmodium yoelii* (PY)-infected Balb/c mice showed a significant increase of Nrp-1 on $CD4^+FoxP3^-$ effector T cells, which are the main actors in parasite clearance in this model, besides B cells. These $Nrp\text{-}1^+CD4^+$ T cells showed a highly activated phenotype, which was reduced during PY infection of T cell-specific Nrp-1-ablated $Nrp\text{-}1^{fl/fl}$ x $CD4cre^{tg}$ mice without affecting the parasitic load.

In an experimental model of cerebral malaria (ECM), the impact of Nrp-1 expression on activation as well as migration of T cells was analysed in *Plasmodium berghei ANKA* (PbA)-infected C57BL/6 mice. During PbA infection, $CD8^+$ T cells are the main pathology-driving cells, as they migrate from the spleen to the brain and induce a disruption of the blood-brain barrier leading to neuroinflammation. It is striking that $CD8^+$ T cells, which normally express very low frequencies of Nrp-1, significantly upregulated Nrp-1 during ECM. Microarray and flow cytometric analyses revealed a highly activated phenotype of $Nrp\text{-}1^+CD8^+$ T cells. In fact, Nrp-1 expression on $CD8^+$ T cells correlated with the severity of ECM pathology. PbA-infected mice with a T cell-specific ablation of Nrp-1 showed significantly reduced numbers of cytotoxic T cells in the brain compared to wildtype littermates. Consequently, ablation of Nrp-1 in $Nrp\text{-}1^{fl/fl}$ x $CD4cre^{tg}$ mice resulted in improved ECM pathology. The blockade of the Nrp-1-VEGF interaction was negligible during PbA infection, which was underlined by the fact that VEGF-mediated migration was not altered in Nrp-1-expressing or –depleted $CD8^+$ T cells. Instead, *in vitro* activation of $CD8^+$ T cells from WT and KO mice indicated that Nrp-1 was not only an activation marker, but was directly involved in the activation state of $CD8^+$ T cells.

This makes Nrp-1 a potential therapeutic target for the treatment of severe malaria and could also be relevant for other $CD8^+$ T cell-mediated diseases.

3 Introduction

3.1 Immune system

The immune system is a complex system consisting of soluble and cellular components that protect the body from exogenous pathogens like bacteria, viruses and parasites as well as endogenous pathological processes. It is thereby essential to keep the immune response balanced to achieve immune defence without an overshooting immune reaction that could lead to tissue damage or autoimmunity. Immune cells derive from hematopoietic stem cells and have their origin in the bone marrow. They differentiate into myeloid or lymphoid progenitor cell lines and further develop into different leukocyte populations. Myeloid cells play an important role in the innate immune system, while lymphocytes are part of the adaptive immunity [1].

3.1.1 Innate immunity

The innate immune system is the first line of defence that is fully functional from birth on. It acts rapidly within minutes after infection and can sense a broad variety of molecular patterns, which makes it very versatile. It contains various mechanisms starting with anatomical and chemical barriers like the skin and antimicrobial substances of the mucosa [1]. The innate immune response includes soluble proteins that are for example involved in the complement system. The detection of pathogens induces a proteolytic cascade that marks the infected cell with a protein complex that can be recognised by the cellular defence and results in the lysis of cells and foreign components [2]. The cellular innate immune response encompasses phagocytic macrophages, granulocytes and dendritic cells (DCs) as well as mast cells and natural killer cells [1]. With their pattern recognition receptor (PRR), they recognise antigens like pathogen-associated molecular patterns (PAMPs) of microorganisms or damage-associated molecular patterns (DAMPs), cell-derived structures released upon stress or infection. Extracellular structures are recognised by transmembrane receptors such as Toll-like receptors (TLRs), while intracellular PAMPs and DAMPs are primarily sensed by nucleotide-binding oligomerisation domain (NOD)-like receptors (NLRs), but also i.e. certain TLRs located in the cytoplasm. The resulting release of cytokines and chemokines potentiates immune effector functions that lead to the degradation of the foreign molecules and attract further immune cells that initiate adaptive immunity [3].

3.1.2 Adaptive immunity

The adaptive immune system is activated by innate immune reactions leading to a delayed but due to antigen-specificity, very efficient immune response. In contrast to the innate immune reaction, adaptive immunity has to be developed with increasing age. The immunological memory is important for rapid elimination of pathogens upon re-infection and forms the basis for vaccinations. Lymphocytes are the cells involved in specific immune defence. Depending on the location of differentiation within the primary lymphoid organs, they are categorised into thymic T lymphocytes and B lymphocytes differentiated in the bone marrow [1]. T and B lymphocytes differ in their antigen-specific receptors: In contrast to the T cell receptor (TCR), the B cell receptor (BCR) also exists as a soluble form, also known as immunoglobulins (Igs) or antibodies. Upon antigenic activation of B cells, they mature into antibody-producing plasma cells. These secreted antibodies correspond to the antigen specificity of the BCR of the plasma cell; they subsequently bind the target structure, resulting in phagocytosis or neutralisation by innate immune cells [4].

T lymphocytes or short T cells are the cellular components of the adaptive immune response. They are categorised into three main populations: T helper cells, regulatory T cells and cytotoxic T cells. Initially, naïve T cells, which have not previously been in contact with antigens, circulate in the blood system. In secondary lymphoid tissues like the spleen, naïve T cells are activated, a process known as T cell priming that requires different signals. First, in the context of the innate immune response, innate immune cells degrade and process antigen structures and characteristic peptides are loaded onto major histocompatibility complex (MHC) class I or II molecules. Extracellular antigens like self-antigens and bacteria are phagocytosed and presented on MHC class II molecules. MHC II is specifically expressed by antigen presenting cells like DCs, monocytes, macrophages as well as B cells and is recognised by $CD4^+$ T cells. Cytoplasmic peptides from pathogens such as viruses that invade cells are cleaved into short peptides that can be loaded onto MHC class I receptors. The MHC I molecules are expressed on all nucleic body cells except of erythrocytes and interact with $CD8^+$ T cells [5]. Primarily DCs can cross-present [6]: They take up extracellular antigens and present them on MHC class I molecules to support the initiation of the immune response [7]. The binding of the TCR of lymphocytes to antigen-loaded MHC molecules is simplified by the formation of an immunological synapse between antigen presenting cells (APCs) and lymphocytes. This cell junction gathers adhesion and

signal molecules in the synapse and enables stable cell contacts [8]. In addition to TCR-MHC interaction, it polarises co-stimulatory receptors like CD28 that are involved in a secondary signal, which is essential for T cell priming. The stimulation of APCs by PAMPs leads to the activation and expression of CD28 ligands such as CD80 and CD86 on the surface of these cells [5]. Usually, other immune cells expressing MHC molecules do not express CD28 ligands and therefore limit the autoreactivity of T lymphocytes. $CD4^+$ T cells use their CD28 receptor to bind costimulatory molecules, are activated, produce the soluble survival signal IL-2 and start to proliferate [5]. To keep the immune system in check, T cells can be inhibited in their function by co-inhibitory receptors like programmed cell death 1 (PD-1) and cytotoxic T lymphocyte antigen 4 (CTLA-4), interacting with PD-L1/2 and CD80/CD86, respectively. In 2018, James P. Allison and Tasuku Honjo received the Nobel Prize for their discovery of the immune checkpoint inhibitors that are used in tumour therapy. The third signal of T cell activation is the release of cytokines, soluble signal molecules derived from both activated T cells and APCs that induce the proliferation of T cells and their differentiation into effector T cells with specialised functions described in the following sections [5].

3.1.2.1 $CD4^+$ T cells

During priming, different pathogen species lead to the presence of specific cytokines that determine the differentiation of naïve $CD4^+$ T lymphocytes into the most effective T helper (T_H) subpopulation. T_H1, T_H2, T_H17 and T_{FH} as well as regulatory T cells, which balance the immune response, are part of the $CD4^+$ T cell compartment [1]. Their differentiation is regulated by defined transcription factors and the specialised helper cells differ in their secreted cytokine profile and the immune cells they interact with to fight the pathogen (Figure 1).

Interferon γ (IFN-γ) and interleukin 12 (IL-12) that originate from innate immune cells and natural killer (NK) cells induce the transcription factor T-bet that drives the differentiation of naïve $CD4^+$ T cells into T_H1 cells. T_H1 cells control infections with viruses, protozoans like *Plasmodium spp.* and bacteria by releasing both IFN-γ themselves as well as tumour necrosis factor α (TNF-α). Intracellular pathogens are usually phagocytosed by macrophages, which present antigens on their surface [1]. T_H1 cells can trigger macrophage activation and the activity of NK cells by releasing IFN-γ. They also support the differentiation of cytotoxic $CD8^+$ T cells [5].

Naïve T cells differentiate into T_H2 cells when extracellular parasites like helminths and the cytokine IL-4 are present. T_H2 cells are defined by GATA-3 expression and secrete IL-4, IL-5 and IL-13 to induce an inflammatory response characteristic for allergies and asthma, which includes activation of eosinophilic granulocytes, mast cells and the plasma cell-produced antibody class IgE [1].

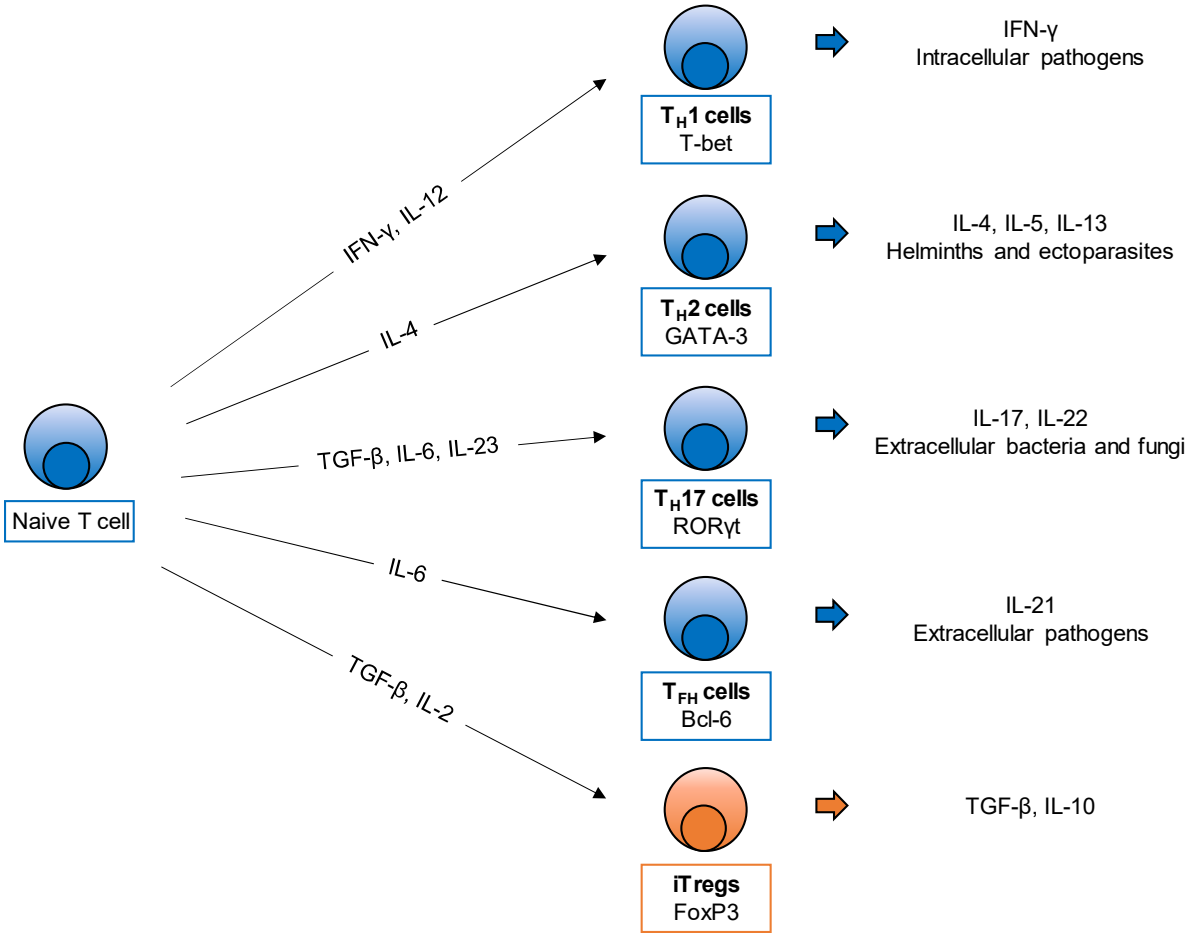

Figure 1: Cytokines involved in the differentiation of $CD4^+$ T helper cells, summarised from Bröker et al. 2019 [5]

Various pathogens activate an innate immune response, which subsequently induces the priming of naïve T cells. Specific cytokines favour the development of different T helper (T_H) subsets with highly specific effector functions. Intracellular pathogens are accompanied by the presence of IFN-γ and IL-12 inducing the transcription factor T-bet and form T_H1 cells, which amplify the IFN-γ secretion. T_H2 cells differentiate in the presence of IL-4 during helminth infection and express the transcription factor GATA-3. Characteristic T_H2 cytokines are IL-4, IL-5 and IL-13. TGF-β in the presence of IL-6 and IL-23 results in the differentiation of $RORγt^+$ T_H17 cells that express IL-17 and IL-22 and contribute to immune response upon infection with extracellular bacteria and fungi. Follicular helper T cells (T_{FH}) are $Bcl\text{-}6^+$ and need IL-6 for differentiation as a response to infection with extracellular pathogens. They secrete IL-21. Induced regulatory T cells (iTregs) develop in the presence of TGF-β and IL-2 and can be identified by expression of FoxP3. Immunosuppression is mediated by TGF-β and IL-10 cytokine release.

Extracellular bacteria and fungi are phagocytosed by innate immune cells, which release IL-6, IL-23 and TGF-β and induce the T_H17 response. IL-17 producing T helper cells express the transcription factor RORγt and indirectly activate neutrophils: IL-17 induces the production of granulocyte-colony stimulating factor (G-CSF) and chemokines by stroma cells, resulting in the emigration of neutrophils from the bone marrow and induces their maturation. Additionally, T_H17 cells secrete IL-22, which

enhances the production of anti-microbial peptides by epithelial cells, strengthening the first-line barrier [5].

Follicular T helper cells (T_{FH}) support the germinal centre reaction and provide B cell help, whereby inducible T cell costimulator (ICOS) expression is essential. Current research suggests that IL-6 and the transcription factor B cell lymphoma 6 (Bcl-6) play a crucial role in the development of T_{FH} cells [1]. Bcl-6 is associated with the surficial expression of chemokine receptor type 5 (CXCR5), a receptor required for cell migration into B cell follicles. T_{FH} cells mainly secrete IL-21, which induces B cell proliferation and differentiation into plasma cells, resulting in the production of highly affine antibodies against the specific class of pathogen [5].

In general, immune responses against pathogens have to be tightly controlled to guarantee pathogen clearance and to avoid overshooting immune reaction, which might lead to immunopathologies. In this process, regulatory T cells (Tregs) play a crucial role by suppressing autoimmune reactions and controlling overwhelming immune responses. Tregs occur as natural Tregs (nTregs) or can be induced by naïve $CD4^+$ T cells (iTregs) and are distinguished from effector T cells by their unique expression of the transcription factor *forkhead box P3* (FoxP3) [9]. nTregs develop in the thymus together with conventional $CD4^+$ T cells in an IL-2-dependent manner and can strongly bind to MHC complexes loaded with self-antigens, which makes them different from conventional T cells [1]. iTregs are induced in secondary lymphoid organs upon antigen stimulation together with the cytokine stimulus of IL10 or TGF-β, lacking the T_H17-driving cytokine IL-6 [1]. Regardless of the origin of the Tregs, they have different mechanisms for the suppression of immune cells [10]: Tregs release cytokines like IL-10, TGF-β and IL-35 that lead to inhibitory signals for other immune cells [11]. Tregs express a variety of surface molecules similar to those that are expressed by activated conventional T cells, which enables the binding to APCs. They bind directly to MHC class II molecules via lymphocyte activation gene 3 (Lag-3) and inhibit antigen presentation. Binding of CTLA-4 to CD80/CD86 of APCs interferes with co-stimulatory signals required for T cell priming [12, 13]. Furthermore, Tregs intervene in the metabolism of target cells. Since they are unable to produce the survival cytokine IL-2, Tregs express CD25 on their surface, which binds IL-2 with a very high affinity. Usually, only activated $CD4^+$ T cells express this receptor, and thus Tregs consume and deprive the target cells of their survival signal, resulting in controlled cell death

called apoptosis [10, 14]. Tregs might also actively kill target cells by releasing granzyme from intracellular vesicles [15].

3.1.2.2 CD8⁺ T cells

$CD8^+$ T lymphocytes have the special feature that they can kill the body's own cells. Whenever viruses and intracellular bacteria infect a cell with a nucleus or cells in tumour environments are transformed, they can process the antigen and present it on MHC class I molecules. In addition, extracellular pathogens can be cross-presented by APCs, as described earlier. Naïve $CD8^+$ T cells recognise peptides loaded onto MHC receptor I and differentiate into cytotoxic T lymphocytes (CTLs). CTLs can selectively direct their cytotoxic potential against infected cells and rapidly kill them. They have several killing mechanisms (summarised in Figure 2): Activated $CD8^+$ T cells induce programmed cell death, also known as apoptosis, by releasing cytotoxic granules in response to antigen-recognition (Figure 2A). These granules contain perforin and granzymes, especially granzyme A and B (Gzm A/B). Human granules additionally contain granulysin with antimicrobial functions [1]. As the name suggests, perforin perforates the membrane of the target cells and allows granzymes, which were transported together with the perforins by the scaffolding protein serglycin, to enter the cytoplasm and induce apoptosis. The vesicles of CTLs contain fully functional proteins that are inactive within the granules. However, once released, they are rapidly effective in killing and can be constantly restocked by synthesis of the cytotoxic proteins [1]. An alternative way of cytotoxicity is killing via the Fas/Fas-L system (Figure 2B). CTLs express Fas ligands (Fas-L, also called CD95L) on their cell membrane, which interact with the Fas receptor of target cells. The binding results in the activation of the signalling cascade of apoptosis [16]. Metalloproteases are able to cleave Fas-L molecules and release them as soluble form. In this way, Fas-L activation affects many surrounding cells and induces cell death without antigen recognition [5]. Besides direct cell-death-inducing mechanisms, $CD8^+$ T cells secrete cytokines to boost the general immune response (Figure 2C). IFN-γ inhibits viral amplification and promotes MHC class I production, enhancing antigen presentation by infected cells [1]. It also attracts macrophages, triggers phagocytosis and induces Fas-signalling in target cells that are in turn killed by the binding of Fas-L on CTLs [1, 16]. Additionally, TNF-α is released by CTLs and binds to the TNF receptor (TNFR) on the target cell. The signalling induces caspases and ends in apoptosis [16].

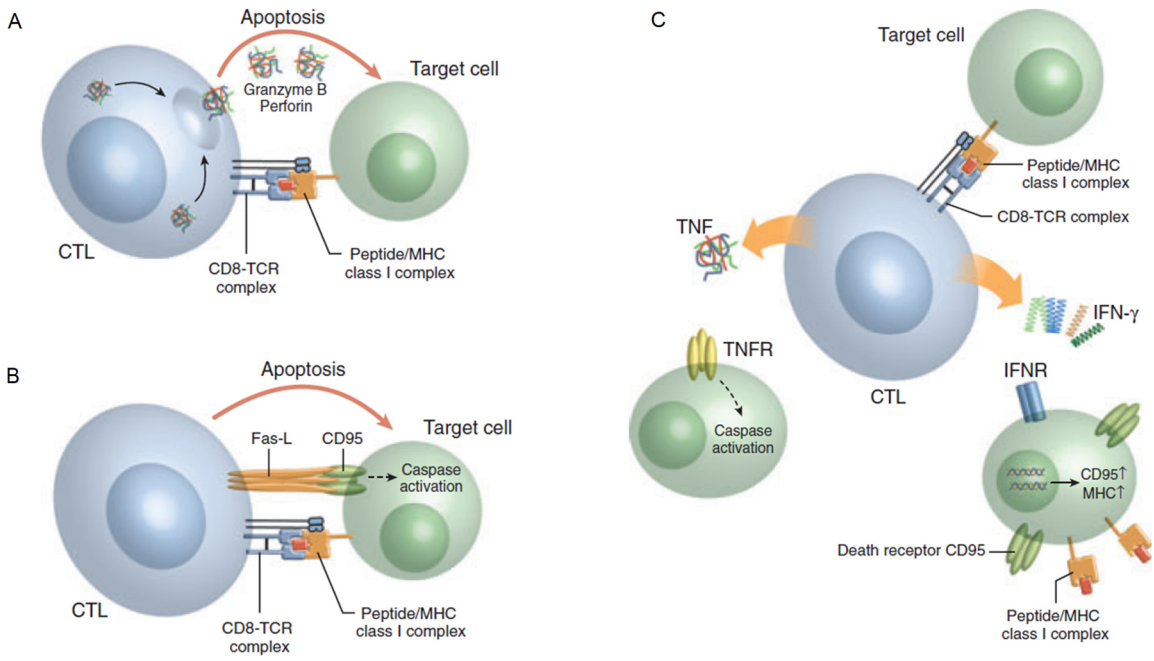

Figure 2: Killing mechanisms of CD8⁺ CTLs, modified by Andersen et al. 2006 [16]

Cytotoxic CD8⁺ T cells (CTLs) have direct and indirect mechanisms to kill their target cells. (**A**) Upon recognition of antigens presented on MHC class I molecules, CTLs can release their granules. Toxic perforin perforates the target membrane and granzyme B can enter the cell and kill it. (**B**) Target cells that express MHC class I and CD95/Fas on their surface can be killed by the interaction of Fas Ligand (Fas-L) on the surface of CD8⁺ T cells. Subsequent activation of the caspases induces apoptosis. (**C**) Indirect killing mechanisms of CTLs are cytokine-mediated. For example, CTLs release TNF and IFN-γ, which binds to the appropriate receptor on the target cells (TNFR and IFNR, respectively). This activates apoptosis signalling or induces the expression of CD95 and MHCI.

In summary, the immune system is a highly specialised system where innate immune cells sense PAMPs and DAMPs via their PRRs, phagocyte pathogens and produce cytokines. DCs bridge innate and adaptive immune response by presenting antigens. The adaptive immune system includes antibody-producing plasma cells and T lymphocytes that differentiate into effector CD4⁺ T helper cells and cytotoxic CD8⁺ T cells to fight pathogens. Suppressive Tregs prevent an overshooting immune reaction and restore the balance of the immune system.

3.1.3 Immune status of the brain

The brain is a vital organ and is therefore particularly well protected against pathogens by various mechanisms. It is embedded into the skull, which protects against physical shock from the outside and has a tissue barrier regulating the in- and efflux from the blood to the brain. It is independent of the lymphatic system to prevent extracellular fluids from entering and it has a unique immune status [1].

The blood-brain barrier (BBB) is a structure of different cells that controls the supply of nutrients and oxygen to the brain and ensures the disposal of waste with the aid of highly specific transporters and channels [17]. In addition, it physically protects the brain from pathogens and peripheral immune cells. Endothelial cells are interconnected via tight junction proteins and form the basic structure of the BBB. Endothelial cells are covered by a basal lamina and surrounded by pericytes (Figure 3). Astrocyte end feet have stabilising function, provide the connection to neurons and are supported by brain-resident macrophages, also known as microglia [18]. The disruption of the blood-brain barrier is characteristic for neurological disorders such as multiple sclerosis, Alzheimer and hypoxia-ischemia, but also for the late phase of experimental cerebral malaria (ECM) and allows peripheral immune cells to enter the brain and damage brain-resident cells [19].

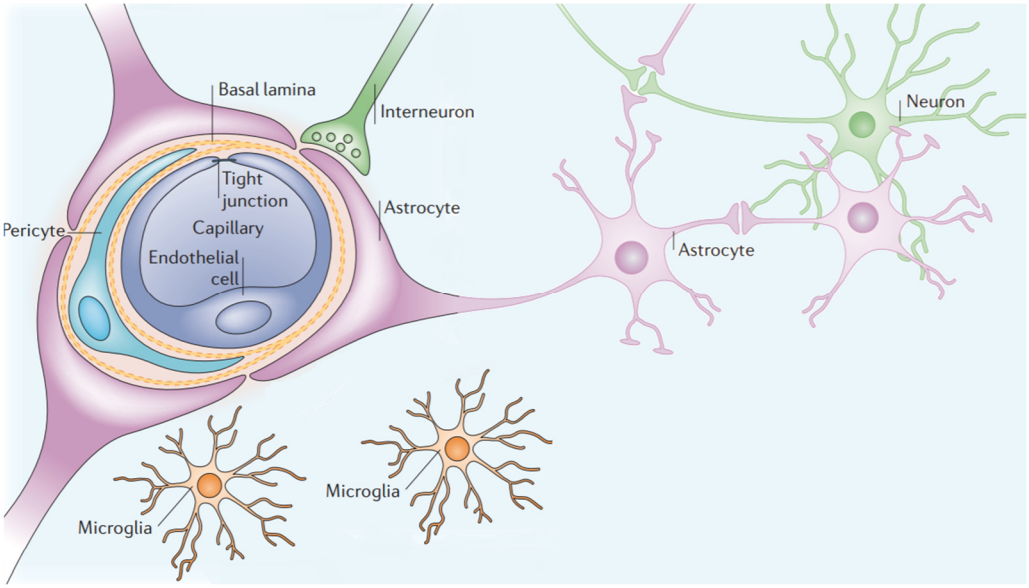

Figure 3: Structure of the blood-brain barrier, modified by Abbott et al. 2006 [20]

The blood-brain barrier (BBB) is a selective barrier between the blood and the brain. It consists of endothelial cells surrounded by a basal lamina. Pericytes support stability and co-localise microglia. It is known that astrocyte end feet play an important role in the function of the BBB and are the link to neurons in the brain parenchyma.

Under physiological conditions, the brain is considered as immune-privileged, which means that the brain is restricted in the induction of immune responses in order to assure the survival and function of neuronal activities. Immune cells like APCs that express MHC molecules are not able to invade the brain due to the BBB [1]. Immunosuppressive molecules such as the apoptosis-inducing factor Fas-L, which binds to immune cell-expressed Fas, PD-1 and adenosine receptors are present at privileged sites to prevent activation of immune cells and neuroinflammation in case of intruding pathogens and immune cells [1, 21]. Anti-inflammatory mediators like TGF-β

are synthesised *in situ* to promote the induction of anti-inflammatory Tregs upon antigen contact in the brain. In recent years, the paradigm of the immune-privilege has been questioned as more and more studies suggest an interaction of the peripheral immune system with the central nervous system (CNS). In addition, an immune function is attributed to brain-resident cells, which shifts the immune privilege towards an immune specialisation of the brain [22]. To fully understand the complex processes in the brain, further research is essential.

3.2 Neuropilin-1

Neuropilins are glycoproteins that are found in all vertebrates and were first described in neuronal development, precisely in axonal guidance [23, 24]. Furthermore, they are involved in heart development, angiogenesis and the interaction of immune cells, influencing immune responses [25-29]. These transmembrane receptors are expressed by multiple murine immune cells including DCs, T cells and Tregs, but also by endothelial cells and tumour cells [25, 26, 29]. The importance of Neuropilin-1 (Nrp-1) during development is demonstrated in Nrp-1 knockout and overexpressing mice, which suffer from severe neuronal impairment and are lethal in the embryonic stage [24, 28, 30]. Neuropilins are additionally involved in pathologies like cancer and in experimental autoimmune encephalomyelitis (EAE), the rodent model of the autoimmune disease multiple sclerosis [31-33].

Two isoforms of Neuropilin are known: Nrp-1 and Nrp-2, both existing as transmembrane receptors and soluble truncated forms [34]. Both Neuropilin molecules have an extracellular domain at the N-terminus, a transmembrane domain and a cytoplasmic tail in the cytosol [35]. The extracellular domain has different subunits, which are used by different interaction partners (Figure 4): a1 and a2 are part of the CUB domain (complement binding factors C1r/C1s, sea urchin epidermal growth factor, bone morphogenetic protein 1), which together with b1 bind to semaphorins. The subunits b1 and b2 are factor V/VIII coagulation factor homology domains (FV/VIII) in which the amino-terminal b1 interacts with vascular endothelial growth factors (VEGFs) [36]. It is further suggested that Neuropilins form homo- and heterodimers with the meprin, A5 protein, protein tyrosine phosphatase μ (MAM) domain located at subunit c [37].

The cytoplasmic domain contains a PSD-95/Dig/ZO-1 (PDZ)-binding motif with three C-terminal amino acids: SEA [38]. Since Nrp-1 is a co-receptor that is not connected to a kinase, it is thought to require interaction partners with a PDZ domain to induce signalling, but further research is needed to unravel the Nrp-1 signalling pathway [39].

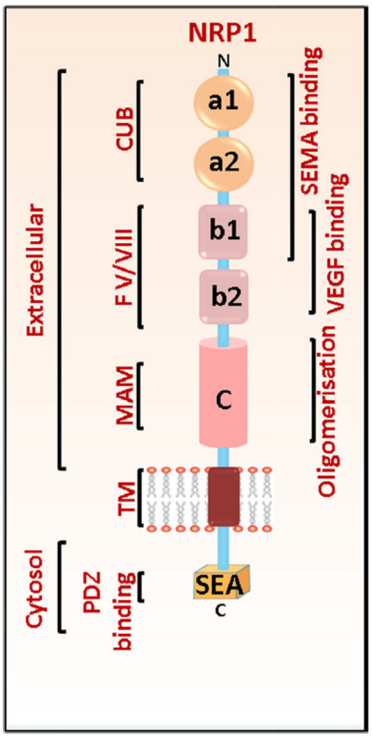

Figure 4: Structure of Neuropilin-1, modified by Roy et al. 2017 [40]

Neuropilin-1 (Nrp-1) encompasses three domains: An N-terminal extracellular domain, a transmembrane (TM) region and a C-terminal cytosolic tail. The extracellular domain is subdivided into a CUB domain (complement binding factors C1r/C1s, sea urchin epidermal growth factor, bone morphogenetic protein 1) with subunits a1 and a2. Followed by factor V/VIII coagulation factor homology domains (FV/VIII) b1 and b2. Semaphorins bind to CUB and b1, while VEGFs bind within the FV/VII region. The MAM (meprin, A5, μ) region might play a role in dimerization. The cytosolic tail has a PDZ (PSD-95/Dig/ZO-1) binding site with three amino acids (SEA) and needs to be occupied to induce a signalling cascade.

3.2.1 Ligands of Neuropilin-1

Neuropilin-1 binds class III semaphorins and isoforms of the growth factor VEGF as well as other growth factors such as TGF-β. Class III semaphorins, predominantly semaphorin 3A (sema3A) and with lower affinity semaphorin 3F (sema3F), bind to Nrp-1, which forms a complex with plexins A1 or A2, inducing the signalling cascade [40, 41]. Sema3A plays a role in cytoskeletal reorganisation and reduces lymphocyte activation, proliferation and the viability of endothelial cells [42, 43]. Sema3A and VEGF have overlapping binding sites on the Nrp-1 molecule and may therefore compete with each other during angiogenesis. It has been shown that sema3A inhibits endothelial cell motility, while $VEGF_{165}$ has stimulatory function [44]. The importance of class III semaphorins has been demonstrated in knockout mice in which 70 % die within the first three days after birth and the survivors suffer from severe impairments of spinal cord and nervous system development [45]. Delgoffe and colleagues suggested class IV semaphorins as interaction partners for Nrp-1 and published a study in which sema4A was bound to Nrp-1 by a slightly lower affinity compared to sema3A [33]. Naïve DCs and low frequencies of B cells express sema4A on their surface, which are increased after stimulation. Upon activation, sema4A expression is also present on T cells [46].

VEGFs play a crucial role in vasculogenesis and angiogenesis, the formation of new blood vessels in physiological development and in pathological surroundings like tumours [47-49]. VEGF has four different isoforms, numbered from A to D, the viral VEGFE and VEGFF in snake venom as well as the placental growth factor (PGF) [50-55]. VEGF expression is induced by hypoxia e.g. in tumour environment and has three VEGF receptors (VEGFR1-3) [56, 57]. The splicing variant $VEGF_{165}$ binds to its receptor VEGFR2 and Nrp-1 is involved in the complex as a co-receptor enhancing signal transduction, which results in enhanced mitogenic activity of endothelial cells [29, 58]. Nrp-1 also forms complexes with other receptors like VEGFR1, but the molecular mechanisms and effects need further validation [59]. The A7R peptide consisting of the seven amino acids ATWLPPR was identified to specifically block the binding of $VEGF_{165}$ to Nrp-1 and is used to analyse the role of VEGF/Nrp-1 binding in the context of different mechanisms and diseases [60, 61].

Nrp-1 can also act as an co-receptor for other growth factors including TGF-β, a cytokine known to influence tumour manifestation and metastasis, but also to have protective properties in the brain parenchyma [1, 62]. Nrp-1 is a co-receptor that forms a complex with the TGF-β receptor TGF-βRI/II/III and augments the signal transmission [63]. Additionally, Nrp-1 can stimulate the latent form of TGF-β, the membrane-associated LAP-TGF-β [64].

In the context of tumorigenesis, it is known that Nrp-1 interacts with epidermal growth factor, hepatocyte growth factor and placenta-derived growth factor (PDF) [65]. Most recently, an interaction of Nrp-1 and CD4d, a factor of the complement system, and an interaction of Nrp-1 with MHC class I tetramers was suggested [66]. Additional research is necessary to validate these data and to identify the underlying mechanisms. Finally, Nrp-1 can form homophilic bindings with itself, which will be discussed in detail in the following chapter.

3.2.2 Function of Neuropilin-1 in immune cells

In naive mice, Nrp-1 is mainly expressed on mast cells, tissue-resident macrophages, DCs, conventional $CD4^+$ T cells and has been described as a Treg marker [40, 67]. In human blood, Nrp-1 expression was only reported for pDCs [25].

In DCs, Nrp-1 has an essential function in the formation of the immunological synapse, which is involved in T cell activation and thus in the adaptive immune response. Mizui and Kikutani named Nrp-1 the “glue” between immune cells [68]. By polymerase chain

reaction (PCR) and immunofluorescence staining, Tordjman and colleagues described Nrp-1 on resting T cells from human blood, which formed homophilic bindings with Nrp-1 molecules of DCs. Pre-incubation of the cells with Nrp-1-blocking antibodies weakened the cell contacts [25]. Sema3A binds to Nrp-1 and disturbs the reorganisation of the cytoskeleton and therefore the formation of the immunological synapse in DC/T cell co-cultures. The resulting reduced activation of T cells can be rescued by blocking sema3A [42]. In mice, it could be confirmed that Nrp-1 plays a role not only in the event of cell-cell contact, but also in the duration of the interaction of immune cells. DCs and Nrp-1-expressing Tregs bind longer to each other than DCs to conventional T cells, which express lower frequencies of Nrp-1 on their surface [26]. The longer the cells are in contact, the more MHC class II molecules polarise in the immunological synapse and the stronger the activation stimulus is for the T cells. Blocking Nrp-1 with an antibody abrogates the advantage of Tregs over effector T cells, which consequently proliferate stronger than without the blocking [26].

Murine Tregs express high concentrations of the Nrp-1 glycoprotein, which correlates with FoxP3 expression [67]. Precisely, Nrp-1$^+$ T cells had a significantly higher suppressive capacity than Nrp-1$^-$ T cells *in vitro* [31]. Nrp-1 plays a role not only in the function, but also in the stability and survival of Tregs. Sema4A derived from immune cells interacts with Nrp-1 on Tregs, inhibits a signalling cascade that limits the Foxo transcription factor in the cell nucleus and therefore provides a stable FoxP3 signal [33]. Furthermore, Nrp-1 has an indirect effect on the generation of Tregs as it can induce the latent form of TGF-β, latency associated peptide (LAP)-TGF-β, leading to the differentiation of naive T cells into Tregs with suppressive capacities [64]. Beside its role in immune suppression, several studies have described the induction of Nrp-1 expression on FoxP3$^-$ T cells e.g. from human blood by stimulation with αCD3 and αCD28 *in vitro* [69]. This result triggered an ongoing debate about the use of Nrp-1 as an activation marker. The transcription marker Helios correlates significantly with Nrp-1 and Helios was previously described as an activation marker [70, 71]. In contrast, both molecules Nrp-1 and Helios were also proposed as specific marker molecules for nTregs. However, iTregs uregulate Nrp-1 on their surface upon inflammation such as EAE or asthma [70]. Hence, the underlying mechanism of Nrp-1 induction is not entirely solved. Initially, trogocytosis was discussed, in which Nrp-1 from Nrp-1$^+$ DCs is packed into vesicles and transferred onto CD4$^+$ T cells, which were pretreated with cycloheximide and therefore unable to synthesise Nrp-1 themselves [72]. However, it

was later shown that increased frequencies of T cells express Nrp-1 in the absence of APCs during *in vitro* stimulation than in the presence, refuting the trogocytosis hypothesis [69]. Nevertheless, Nrp-1 is a promising candidate for a therapeutic target in immune-driven pathologies due to its immune modulating functions.

3.2.3 Neuropilin-1 in pathologies

The function of Nrp-1 has been analysed in various diseases, most of which are in the context of cancer. In tumours, effector T cells are important for cancer control, while Tregs are known to suppress anti-tumoural immune responses and are therefore associated with tumour progression [73]. A previously published study by our research group showed that Tregs use Nrp-1 to migrate into tumour tissue via a VEGF gradient released by the tumour itself [32]. Ablation of Nrp-1 on T cells reduced the frequency of intratumoural Tregs, increased the number of $CD8^+$ T cells and their activation status, resulting in decreased tumour size and improved survival. The neutralisation of VEGF and VEGFR2 in human patients with metastatic colorectal cancer and in CT26-bearing mice reduced the proliferation of Tregs and might support anti-tumoural immune responses in future experiments [74].

In EAE, the Nrp-1 ligand VEGF is also upregulated in the brain, indicating a role for Nrp-1 in neuroinflammation [75]. In the murine model of multiple sclerosis, primarily $CD4^+$ T cells enter the brain and demyelinate neuronal axons, leading to inflammation [31]. T cell-specific ablation of Nrp-1 resulted in increased disease severity due to decreased suppressive capacity of Tregs accompanied by an enhanced inflammatory T_H17 response [31]. In atherosclerosis, T cell-restricted Nrp-1 deficiency ameliorated the disease [76]. The authors hypothesise that Nrp-1 is involved in the migration of disease-causing $CD4^+$ T cells into the aorta [76].

Recently, various studies analysed Nrp-1 expression in $CD8^+$ T cells, which is usually very low in the naïve state. Within pathological surrounding like tumours, viral infection and immune tolerance, there is growing evidence that Nrp-1 expression is induced on $CD8^+$ T cells [77-79]. One study detected tumour-infiltrating $Nrp\text{-}1^+CD8^+$ T cells in human non-small cell lung cancer tissue [77]. Nrp-1 expression correlated with $PD1^{high}$ expression as well as with several exhaustion-associated markers like T cell immunoglobulin and mucin-domain containing 3 (Tim-3), Lag-3 and CTLA-4. *In vivo*, a αNrp-1 antibody in combination with the neutralisation of PD-1 led to improved migration capacity and cytotoxic function of $CD8^+$ T cells and thus a better anti-

tumoural immune response [77]. In addition, Nrp-1 is also described to play a role in the secondary immune response upon re-transplantation of tumour cells. Due to the suggested Nrp-1-associated exhaustion of $CD8^+$ T cells it is hypothesised that Nrp-1 presence might interfere with appropriate memory differentiation. Liu and colleagues therefore proposed Nrp-1 as an “immune memory checkpoint” [80].

Another study detected Nrp-1 on $CD8^+$ T cells during gamma herpesvirus infection and also provided evidence for a role of Nrp-1 in the formation of T cell memory [79]. The deletion of Nrp-1 led to the formation of a precursor stage of memory T cells without affecting the resting memory stage and could influence the recall response during secondary virus infection [79]. In autoimmunity, it is known that self-reactive $CD8^+$ T cells express Nrp-1 in the liver, but do not influence the tolerant phenotype [78]. The expression profile of $Nrp\text{-}1^+CD8^+$ T cells was comparable to tumour-infiltrating $CD8^+$ T cells but the presence of Nrp-1 did not influence the effector functions like cytotoxicity or IFN-γ production.

In summary, Nrp-1 is expressed on a variety of body and immune cells and has multiple functions both under homeostasis as well as under pathological conditions, but many open questions remain to be answered in future research studies.

3.2.4 Neuropilin-1 in therapies

Not only because Nrp-1 is expressed by immunosuppressive Tregs, which effectively suppress anti-tumoural immune response, but also by tumour cells themselves, the targeting of Nrp-1 could have several benefits in cancer therapy. Nrp-1 is described to be expressed by various cancer cell types including non small cell lung cancer tumours or gastric cancer. Nrp-1 is associated with proliferation and angiogenesis within tumours and is associated with a poor outcome [81, 82]. Multiple monoclonal antibodies (mAbs) have been developed and inhibit the binding of Nrp-1 to its ligands [83]. One promising candidate is the mAb MNRP1685A, that blocks Nrp-1/VEGF interaction, leading to reduced angiogenesis and thus restricts tumour growth in xenograft tumour models [84]. Hence, phase I clinical trials using the MNRP1685A antibody in combination with bevacizumab, a VEGF blocking antibody, have been conducted in patients with solid tumours [85]. However, recent results indicated that this combination therapy results in proteinuria and therefore led to the termination of the study [85]. Another therapeutic approach is the use of synthesised peptides, which are small enough to penetrate deep into tumour tissue and target the cells, a limiting

factor in cancer treatment. So-called cell- or tumour-penetrating peptides (CPPs or TPPs) are designed to deliver drugs into the tumour tissue. One Nrp-1-specific peptide is known that alters endothelial structures and influences the invasion of lymphocytes into the tumour [86]. Considering the fact, that tumour cells also express Nrp-1, these TPPs could be used to specifically target tumour cells or transport drugs, mAbs and nanoparticles into the tumour.

Altogether, Nrp-1 is expressed by a large variety of immune cells, endothelial cells and tumour cells. It binds to semaphorins, VEGF and TGF-β and has far-reaching functions. It is a marker for murine Tregs, is involved in the interaction and migration of immune cells and thus in the modulation of immune responses. In cancer and other pathologies, the induction of Nrp-1 on for example $CD8^+$ T cells was observed and influences the outcome of the diseases. It is therefore conceivable that Nrp-1 has the potential as a therapeutic starting point in infectious diseases such as cerebral malaria.

3.3 Malaria

Malaria has been known for thousands of years as an infectious disease caused by the parasite species *Plasmodium*. As early as 2700 B.C., chinese documents reported cases with repetitive fever and enlargement of the spleen, indicating an ancient malaria disease [87]. In 1880, Charles Louis Alphonse Laveran, an army officer in Algeria, discovered a protozoan parasite that infects red blood cells, which could be eliminated by quinine. He was the first who refuted the assumption of a bacterial infection as a cause of malaria, suggested by Louis Pasteur and Robert Koch. He was awarded with the Nobel Prize for his discovery of the *Plasmodium* parasite in 1907 [87]. For a long time it was assumed that malaria was caused by bad air, from the Italian “*mala aria*”, of standing water, until Battista Grassi and Ronald Ross identified the *Anopheles* mosquito as malaria vector in the 1890s. The latter was also awarded with the Nobel Prize in 1902 [88].

Today, the World Health Organization (WHO) estimates 228 million cases of malaria worldwide, with 405,000 people dying from the disease in 2018, mainly infants under five years of age [89]. Every two minutes one child succumbs to *Plasmodium* infection [90]. The disease is most prominent in sub-Saharan Africa, where 93 % of the cases are registered, 3.4 % occur in South-East Asia and 2.1 % in the Eastern Mediterranean region (Figure 5) [89]. Characteristic symptoms of infection are recurring fever and chills, headache and nausea. Severe cases develop anaemia, respiratory distress,

hypoglycaemia, acidosis and can culminate in cerebral malaria with convulsions, coma and multiple organ failure, resulting in death [91]. High drug resistance and the lack of an approved vaccine made malaria still the sixth most common cause of death in low-income countries in 2016 [92].

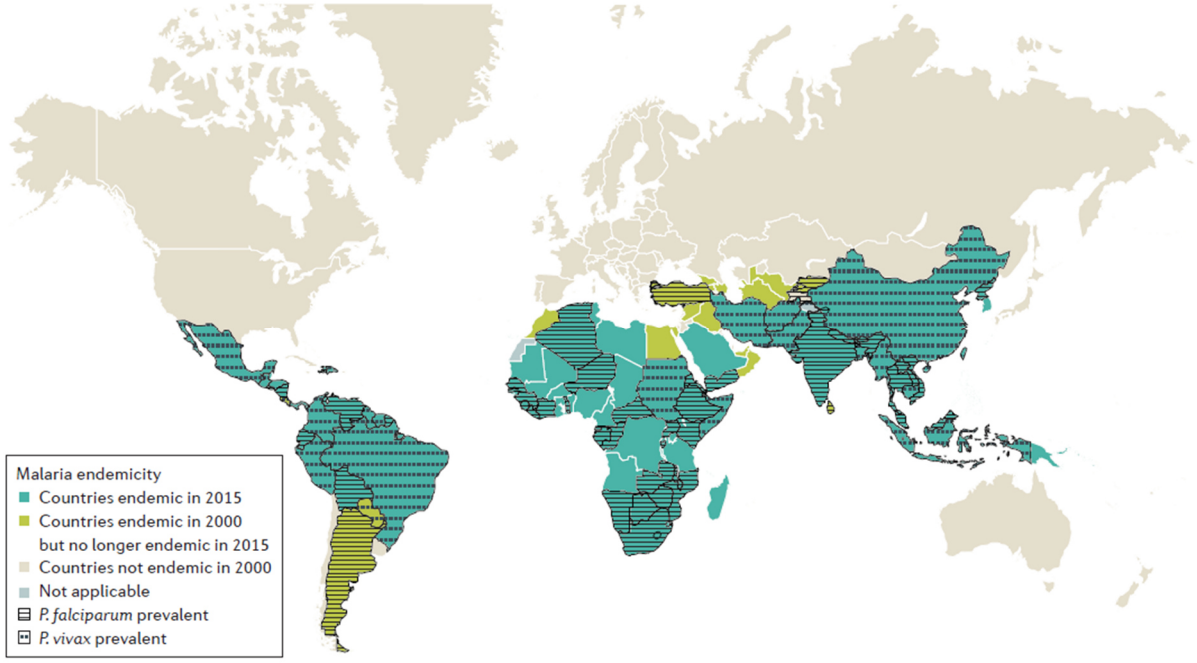

Figure 5: Map of malaria-endemic regions, modified by Phillips et al. 2017 [93]

The majority of *Plasmodium* infections are located in Africa, fewer cases occur in South-East Asia and the Eastern Mediterranean region. While *P. falciparum* is the predominant species in Africa, *P. vivax* is more common in the Asian region. Turquoise areas are malaria endemic areas in 2015. Green areas indicate regions that were endemic in 2000, but are no longer endemic in 2015. Countries marked in grey are considered malaria-free since 2000. Dark grey countries were not included into the survey. Striped or dotted lines indicate prevalence of *P. falciparum* or *P. vivax*, respectively.

Prevention of the disease by controlling the vector with mosquito nets, indoor residual spraying of insecticides and the larval source management is essential to control malaria [94]. The larval source management includes manipulation of the breeding areas of the mosquitos, including the drainage of stagnant waters, the addition of insecticides or natural enemies like fish into the water to kill the larvae [95]. One ethically controversial strategy is the application of genetically modified mosquitoes. In theory, the clustered regularly interspaced short palindromic repeats/CRIPR-associated protein 9 (CRISPR/cas9) gene editing system could be used to make the mosquitoes resistant to *Plasmodium* strains or inhibit the reproducibility of the vector [96].

As many parasites are resistant to classic malaria drugs like quinine and chloroquine, the most effective treatment of malaria is currently an artemisinin-based combination therapy with artemisinin derivates together with other drugs [97]. Tu Youyou isolated

artemisinin from a herb and was awarded the Nobel Prize in 2015 for the drug's high efficacy in clearing multi-resistant *Plasmodium* strains [97]. The mechanism of action is still under debate, but it is assumed that the parasite produces the hemoglobin food residue heme that activates artemisinin, which produces free radicals [98]. Intracellular targets, which are essential for the survival of the parasite, are modified restricting the parasitic survival [99]. Nevertheless, more than several dozen cases of artemisinin resistance were reported in Southeast Asia in the past few years, highlighting the need for fundamental malaria research to increase the efficacy of future treatments [100].

Currently, one promising vaccine candidate is RTS,S, also called Mosquirix, that shows promising results in reducing the number of *Plasmodium falciparum* malaria cases. The first pilot studies started in Ghana, Kenya and Malawi with vaccination of children [90].

3.3.1 Life cycle of *Plasmodium*

The lifecycle of *Plasmodium* parasites takes place in two different hosts: Sporogony is the sexual amplification of parasites in the mosquito and schizogony defines the asexual phase in vertebrates (Figure 6) [101]. During the bite of a female *Anopheles* mosquito, up to 100 sporozoites are released from the salivary glands into the host. In the pre-erythrocytic phase, the sporozoites migrate to the liver, actively invade hepatocytes and build up a parasitophorous vacuole [102, 103]. In this clinically asymptomatic phase, the parasites develop into schizonts that contain several thousand merozoites, which, depending on the reproductive cycle of the *Plasmodium* species, egress into the bloodstream after several days [101]. In the blood stage, merozoites actively invade erythrocytes and develop into different ring stages, grow and amplify into trophozoites. Within the erythrocyte, the parasite forms a food vacuole and uses intraerythrocytic hemoglobin as nutrient [103]. The degradation of hemoglobin forms toxic heme, which is detoxified into hemozoin that can be visualised under the microscope as crystalline structures [104]. After 24 to 72 hours, depending on the *Plasmodium* species, the red blood cells rupture and release blood-schizonts, each harbouring 16-32 merozoites that can infect new naïve erythrocytes. The rupture of the red blood cells is clinically depicted by the malaria characteristic fever [101, 105].

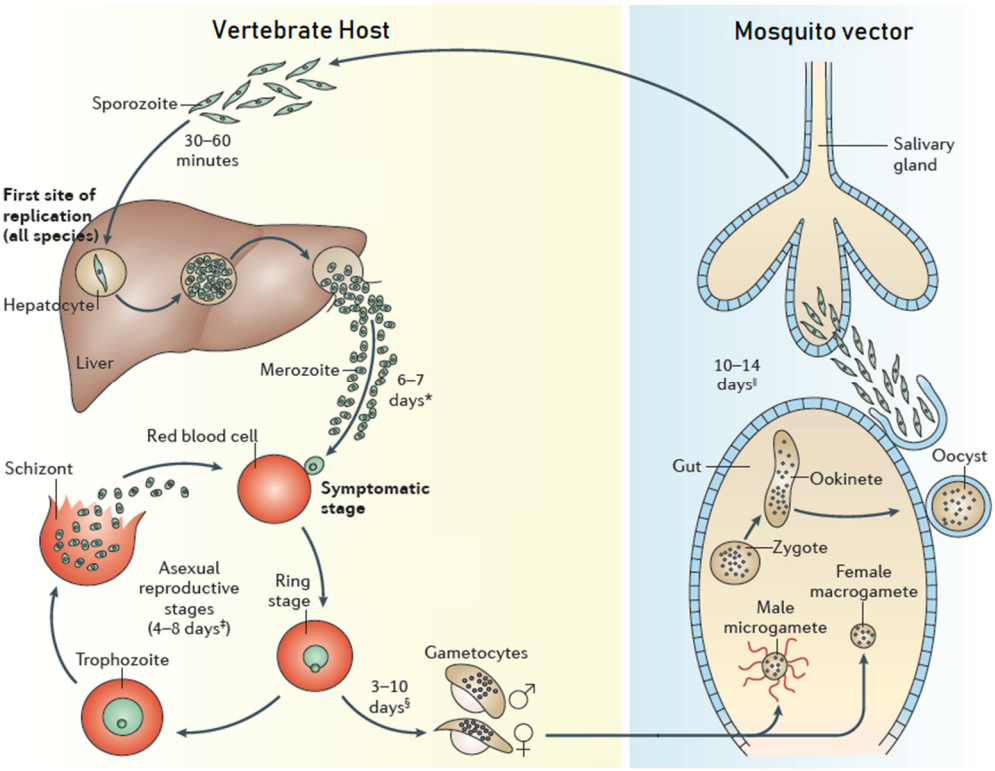

Figure 6: *Plasmodium* life cycle, modified by Phillips et al. 2017 [93]

A female *Anopheles* mosquito injects sporozoites into a vertebrate host and induces the asexual *Plasmodium* life cycle called schizogony. The parasites migrate into the liver, infect hepatocytes and develop into schizonts that host thousands of merozoites. The asymptomatic pre-erythrocytic phase ends with the release of merozoites into the blood stream. In the blood stage, a merozoite penetrates an erythrocyte, develops into a ring stage and forms trophozoites. The developed schizonts release new merozoites into the blood, and the erythrocytic cycle begins anew. At the same time, some merozoites form gametocytes: female macrogametocytes and male microgametocytes, which can be taken up by the mosquito in another blood meal. Gametogenesis is part of the sexual replication in the gut of the mosquito. The gametes fuse and form a zygote, develop into an ookinete and migrate through the midgut epithelium. In the oocyte, several new sporozoites are produced that are released and migrate to the salivary glands, where they wait to be injected into a new vertebrate host. *Merozoites of some *Plasmodium* species can remain dormant in the liver as hypnozoites. ‡Corresponds to the interval of fever attacks and is species-dependent. §Species-dependent. ||Temperature-dependent.

In parallel, some of the merozoites develop into gametocytes: female macrogametocytes and male microgametocytes, which are taken up by the mosquito during another blood meal [101].

The sexual replication phase of *Plasmodium* is induced by gametogenesis in the vectors' gut, which leads to the fusion of the gametes to form a zygote [104, 106]. It develops into an ookinete that penetrates the midgut epithelium, transforming into an oocyst with new sporozoites. These sporozoites migrate to the salivary glands of the mosquito to be transmitted to a new mammalian host [104].

3.3.2 Plasmodium species

Currently, five unicellular *Plasmodium* (P.) species are known to infect humans and result in different clinical outcomes of malaria. Based on the reproductive cycle of the different parasite species, the infections differ in their febrile periods and their prepatency, defining the time frame from the mosquito bite to the detectability of trophozoites in the patients' blood [101].

The development of the five *Plasmodium* strains requires different temperatures in the mosquitoes, which reflect the geographical prevalence of the species (Figure 5). It is expected that if global warming increases the global temperature by 2-3°C, 3-5 % more malaria cases will appear in the world [107]. *P. falciparum* has a pre-patent period of nine days and is the predominant parasite in Africa with development cycles at more than 21°C in the mosquito [93]. *P. falciparum* causes malaria tropica with 48 hours of erythrocytic stage, leading to fever attacks of 16-36 hours or longer. It displays very high levels of parasites in the blood and can result in life-threatening cerebral malaria (CM). The underlying mechanisms of CM development are not fully understood yet. The current knowledge will be discussed in the following sections.

In the South-East Asian region, *P. vivax,* which replicates at average temperatures of 16°C [93], causes tertian fever with a hot stage lasting for 8-12 hours. After 11-13 days of infection, only very low frequencies of parasites are detected in the blood [89, 101]. Nevertheless, *P. vivax* can also cause severe malaria, including cerebral malaria and multi-organ failure. In contrast to *P. falciparum*, *P. vivax* can form hypnozoites, a dormant stage of the parasite that can re-induce malaria after several years and represents an unsolved challenge in therapy [108]. *P. vivax* uses the Duffy glycoprotein receptor to penetrate erythrocytes. Former research studies showed that this receptor is absent in the majority of African people, explaining the low numbers of cases in this area (Figure 5) [109]. *P. ovale* and *P. malariae* are very rare occurring parasites that cause tertian or quartan malaria, respectively, and usually do not show a severe course of disease [101]. The fifth species of human *Plasmodium* is *P. knowlesi,* which was originally a species that infected macaques, but has lately been reported to have spread to humans in Malaysian Borneo and other countries in South-East Asia [101]. It has a unique amplification cycle in erythrocytes that is completed within 24 hours. *P. knowlesi* patients usually have high levels of parasitemia, often associated with a severe course of malaria [110]. In general, research studies report co-infections with various *Plasmodium* species, which complicates diagnosis and the choice of

treatment. Especially *P. knowlesi* co-infections with *P. falciparum* or *P. vivax* were reported in Maynmar or Vietnam [111, 112].

To study underlying mechanisms of *Plasmodium* infection in detail, rodent malaria models were established. Naturally occurring *Plasmodium* parasites were isolated from infected rodents from Africa. Four *Plasmodium* species with several subspecies are currently used for animal studies*: P. yoelii*, *P. berghei*, *P. chabaudi* and *P. vinckei* [113]. The course of infection and the symptoms of malaria vary between the different species and mouse strains. Infection with *P. vinckei vinckei* is lethal whereas *P. vinckei petteri* is a non-lethal parasite. *P. chabaudi* infection is popular for the analysis of immune regulations, the influence of cytokines and chronic progressions [113]. While *P. chabaudi adami* is characterised by a mild infection, *P. chabaudi chabaudi AS* infection can be fatal [114]. *P. yoelii* is used to study liver and blood-stage malaria and is either cleared within 21 days (*P. yoelii 17XNL*) or lethal (*P. yoelii 17XL*). *P. berghei ANKA* (PbA) parasites result in severe pathology inducing experimental cerebral malaria (ECM) in C57BL/6 mice, but not in Balb/c mice and serve as a model for human *P. falciparum* infection. In this work, *P. yoelii 17XNL*- (hereafter referred to as PY) infected Balb/c mice and PbA-infected C57BL/6 mice were used as murine malaria models.

3.3.3 Immune response during malaria

The immune response to malaria is very complex and varies between *Plasmodium* species and the developmental stage of the parasite in the liver, blood and brain. Upon recurrent infections, a partial immunity is achieved as the patients are infected but often lack malaria-characteristic symptoms [114]. The immune defence mechanisms must be strictly controlled, to clear the parasites without inducing an overshooting immune reaction that can harm healthy tissue and induce severe cerebral malaria [114].

3.3.3.1 Immune response during liver-stage malaria

The liver phase of *Plasmodium* infection proceeds without clinical symptoms. As described earlier, *Plasmodium* infection starts with the transmission of sporozoites into the skin of the host by a mosquito bite. Some parasites are immediately phagocytosed by skin-resident APCs and some migrate via the lymphatics to the lymph nodes and stimulate the antigen-presentation [102, 115]. In the liver, cytosolic fragments produced by transmigration of parasites through hepatocytes induce the signalling cascade of the myeloid differentiation gene 88 (MyD88), which leads to the activation

of the nuclear factor κ-light-chain-enhancer of activated B cells (NF-κB) [116]. The subsequently generated nitric oxide (NO) is toxic to cells and parasites resulting in death [117]. Recent reports suggest that the sporozoites themselves are able to interfere with NF-κB and suppress this toxicity by releasing circumsporozoite protein (CSP) [118]. This protein plays an essential role in the RTS,S vaccine, where CSP is fused to the surface protein of the hepatitis B virus and should induce an immune response [119]. In general, several PRRs like TLRs, NLRs and C-type lectin receptors (CLRs) are still under debate to be involved in innate immune reactions in the liver, but need to be further analysed [102].

In other diseases, it has been reported that liver-resident APCs present antigens to T cells via MHC class I, independently of peripheral APCs and thus activate $CD8^+$ T cells [120]. In livers of PY-infected mice, increased concentrations of type I interferons and IFN-γ were measured [121]. Since it is well known that $CD8^+$ as well as $CD4^+$ T cells release IFN-γ upon antigen contact, it is speculated that $CD8^+$ T cells can kill infected hepatocytes directly or indirectly via the production of toxic NO, induced by IFN-γ [117, 122]. The involvement of antibodies in liver-stage defence is still controversially discussed, and future research is decisive to identify the underlying mechanisms of plasma cell differentiation in the liver of malaria patients and the corresponding mouse models.

3.3.3.2 Immune response during blood-stage malaria

The erythrocytic phase begins with the release of merozoites from the liver into the blood stream, where they invade erythrocytes. The blood stage is characterised by recurrent fever attacks caused by the rupture of erythrocytes and subsequent release of cytokines like TNF-α, IL-1β and IL-6 by immune cells [123]. The spleen plays a central role in the parasite clearance during malaria, as it filters the blood and eliminates old or infected erythrocytes. At the same time, it harbours high frequencies of immune cells, which come in close proximity to the parasites [124, 125]. Immune responses against blood-stage malaria are thus primarily initiated in the spleen (Figure 7) [126].

DAMPs and parasitic structures, the PAMPs, induce the innate immune response. The three most important ones are hemozoin, glycosylphosphatidylinositol (GPI) anchors and DNA fragments of the parasites [127-129]. As described previously, parasites use the hemoglobin of erythrocytes as nutrient. The degradation product is toxic heme,

which stimulates the immune system as DAMP [128]. GPI anchors are crucial for the viability of the parasite as they anchor surface molecules to its membrane [130]. TLRs are important to recognise these GPI anchors and activate the NF-κB signalling cascade resulting in the synthesis of toxic NO, equivalent to the liver phase, and pro-inflammatory cytokines like TNF and IL-1β [127]. This activates macrophages, leading to phagocytosis of infected red blood cells (iRBCs), without the presence of opsonising antibodies. Macrophages can further sense the *P. falciparum*-encoded erythrocyte membrane protein 1 (PfEMP1) through their scavenger receptor CD36 and phagocyte iRBCs [114]. DCs are important in the early phase of infection as they are responsible for the activation of T cells and the production of systemic levels of pro-inflammatory cytokines [131]. Infected erythrocytes activate DCs that upregulate costimulatory molecules like CD40 and CD80, secrete IL-12 and present antigen fragments on MHC class II [132]. NK cells are likely to be activated by the presence of IL-12 and IL-18 and produce IFN-γ or directly lyse iRBCs [133-135]. The antigen-presentation of DCs and the presence of IL-12 and IFN-γ leads to the differentiation of $CD4^+$ T cells into T_H1 cells that secrete IL-2, IFN-γ and TNFα [132]. According to the current state of knowledge, T_H1 cells are essential for the clearing of blood-stage parasites, since $CD4^+$ T cells are the main producers of IFN-γ during *Plasmodium* infection [136]. In addition, they are thought to support antibody specification and production [137]. Innate immune cells and T cells can reduce levels of parasitemia to a minimum, but antibodies from plasma cells are essential for the complete clearance [114]. $CD8^+$ T cells are negligible during the immune response in the acute blood-stage because RBCs do not express MHC molecules and therefore the cytotoxic function of $CD8^+$ T cells cannot be provoked.

A *Plasmodium* infection induces a very strong immune response with high concentrations of pro-inflammatory cytokines, which must be kept in balance in order to avoid tissue damage. The depletion of suppressive $FoxP3^+$ regulatory T cells during blood-stage malaria led to a significantly reduced parasitic load [138]. Moreover, the expression of the immunosuppressive cytokine IL-10 was increased during PY infection [138]. IL-10 producing T_H1 cells, so-called Tr1 cells, are described to play a role in the control of the excessive immune response during malaria [139]. DCs produce IL-10 that promotes Tr1 differentiation, leading to a feedback loop with the re-secretion of IL-10 [140]. The Tr1 cells inhibit the humoral immune response in *P. yoelii*

infection, decrease parasite clearance but prevent tissue damage in *P. chabaudi AS* infected mice [141, 142].

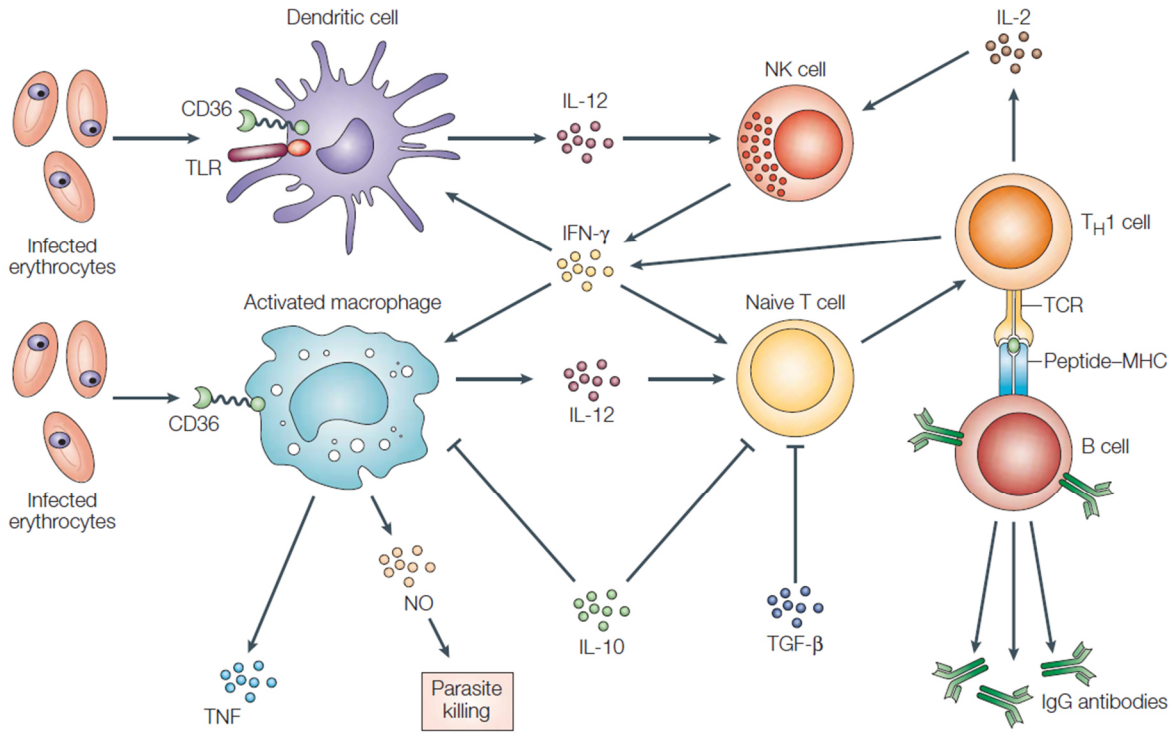

Figure 7: Immune response to blood-stage malaria, adopted by Stevenson and Riley, 2004 [114]

In the blood-stage of malaria, *Plasmodium* parasites infect erythrocytes. Innate immune cells like macrophages and DCs recognise PAMPs and DAMPs via their PRRs, while toll-like receptors (TLRs) and CD36 (in humans) play an important role. The NF-κB signalling cascade induces the secretion of pro-inflammatory cytokines and nitric oxide (NO) that can directly kill the parasites. The parasites and IL-12 activate NK cells that produce IFN-γ. IFN-γ and IL-12 as well as antigens presented by DCs promote T_H1 cell differentiation in the spleen, which can fight the parasites by releasing cytokines. T_H1 cells are also reported to initiate B cell maturation and antibody production. IL-10 and TGF-β prevent an excessive immune response.

3.3.3.3 Cerebral malaria

A *Plasmodium* infection can cause an imbalance between pro- and anti-inflammatory immune responses, which, together with cross-presentation by endothelial cells and the breakdown of the blood-brain barrier, causes cerebral malaria. Cerebral malaria is primarily known to be caused by *P. falciparum* in humans and can be modelled by PbA infection in mice. The exact mechanism by which cerebral malaria develops has not been fully elucidated yet, but several processes have been described that could potentially cause the pathology.

The immune response in the blood-stage is the initiator of the development of cerebral malaria. In this phase, priming and proliferation of antigen-specific $CD8^+$ T cells occurs in the spleen 3-5 days post infection, even though they are negligible in the clearance of the parasites [126]. Conventional $CD8\alpha^+$ DCs cross-present parasite peptides on MHC class I molecules to $CD8^+$ T cells and activate them (Figure 8, step 1) [143, 144].

In the blood, *P. falciparum*-infected RBCs express PfEMP1 on their surface and interact with adhesion molecules on platelets and endothelial cells promoting the accumulation of iRBCs in brain vessels (Figure 8, step 2) [145]. Large plaques of erythrocytes in the blood vessels can cause ischemia and reduce the availability of oxygen in the brain, damaging surrounding tissue [146]. At the same time, immune cells release pro-inflammatory cytokines like IFN-y in response to PbA antigens in the blood, as described in the previous section. As a result, endothelial cells of PbA-infected mice as well as humans with CM upregulate adhesion molecules like intercellular adhesion molecule 1 (ICAM-1), vascular cell adhesion molecule 1 (VCAM-1) and P-selectin or CD36 (Figure 8, step 3) [147-150]. Mice lacking expression of ICAM-1 exhibit improved stability of the blood-brain barrier and are protected from ECM. The blockade of lymphocyte function-associated antigen 1 (LFA-1) and very late antigen 4 (VLA-4), the molecules interacting with ICAM-1 and VCAM-1, respectively, clear $CD8^+$ T cells from the lumen of brain vessel, highlighting the role of adhesion molecules during ECM pathology [151, 152].

The accumulation of parasites and activation of the endothelium further amplifies the release of pro-inflammatory cytokines and chemokines (Figure 8, step 4). IL-5, IL-1β, IL-10 and IL-2 have been detected in human serum or plasma during *P. falciparum* infection, while IL-12, IL-5, IL-6 and IFN-γ are present in severe forms of malaria. Specifically high concentrations of IL-1β are characteristic for cerebral malaria [153]. Patients who succumbed to CM showed particularly elevated plasma concentrations of the chemokines CXLC10 and CXCL4 [154]. During murine PbA infection, not only CXCL9 and CXCL10, but also CCL2, CCL4 and CCL5 are elevated in the brain, but their exact function needs further investigation [155, 156]. It has been shown that chemokines and cytokines play an important role in the migration of peripheral immune cells, especially $CD8^+$ T cells, from the periphery into the immune-specialised brain. During PbA-infection, the majority of $CD8^+$ T cells express CXCR3, a chemokine receptor for CXCL9 and CXCL10 that plays a central role in the migration of T cells into the brain and the manifestation of ECM pathology (Figure 8, step 5) [155, 156]. The source of CXCL9 and CXCL10 is still controversially discussed. One study suggests the expression of CXCL9 on endothelial cells, while CXCL10 was found on neurons and less frequently on endothelial cells [155]. IFN-γ is the key cytokine responsible for the development of ECM, since it upregulates CXCL9 and CXCL10 and supports the migration of immune cells into the brain [133, 150, 156, 157]. Leukocytes

from Balb/c mice express lower levels of CXCR3 during PbA infection, which might contribute to the fact that Balb/c mice are usually protected from ECM [156]. CXCL4, an additional chemokine recognised by the CXCR3 receptor, is upregulated in the plasma and brain of PbA-infected mice and further enhances T cell migration. CXCL4 depletion led to reduced concentration of IFN-γ and TNFα and an increased survival of PbA-infected mice [158].

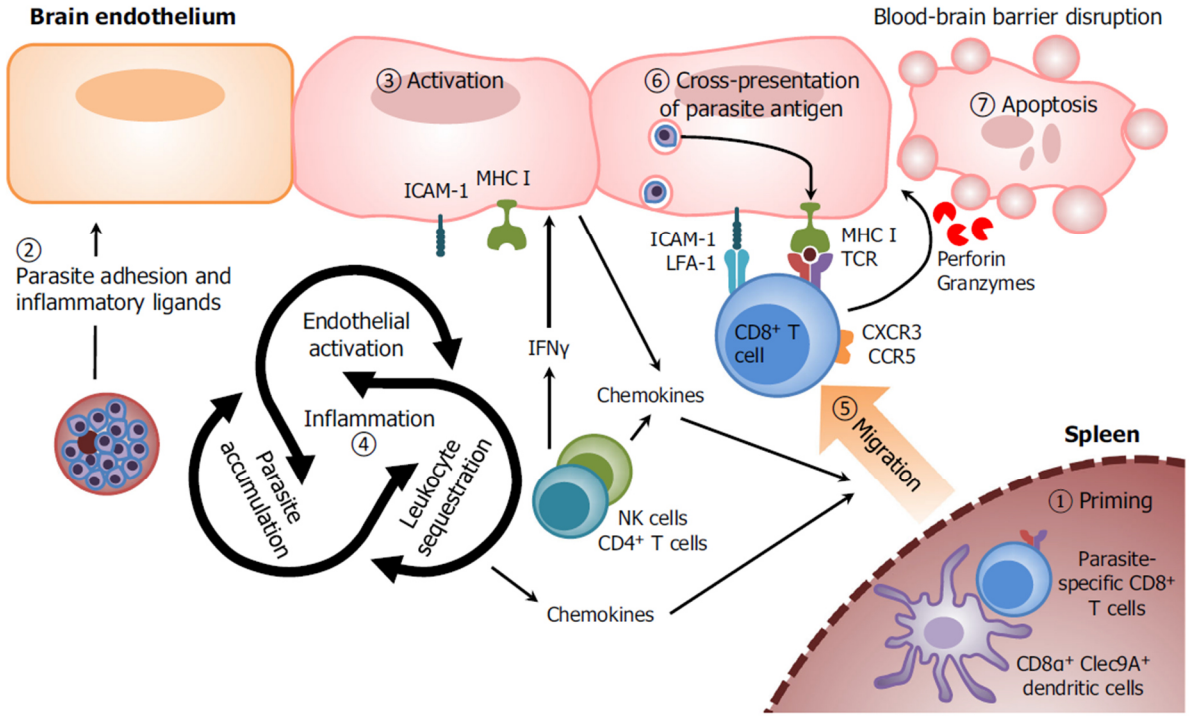

Figure 8: Immune response in ECM pathology, adapted by Howland et al. 2015 [159]

During the blood-stage of *Plasmodium* infection, essential mechanisms occur that induce the development of cerebral malaria. (1) CD8α⁺ DCs cross-present *Plasmodium* antigens to CD8⁺ T cells in the spleen. (2) Parasites accumulate in the brain, which activates endothelial cells via PRRs. (3) Furthermore, IFN-γ secreted by T_H1 cells in the periphery induces adhesion molecules like the intercellular adhesion molecule 1 (ICAM-1) on the endothelium. (4) These events amplify the release of cytokines and chemokines and lead to the migration of peripheral immune cells, especially CD8⁺ T cells, into the brain (5). (6) Brain endothelial cells have the unique ability to cross-present parasite antigens, which can be recognised by CD8⁺ T cells. (7) This leads to the killing of endothelial cells and hence to the breakdown of the blood-brain barrier. ECM results in cerebral inflammation, which is associated with neurological symptoms and often fatal.

Moreover, current understanding of ECM development includes the assumption that cerebral endothelial cells of mice infected with ECM-inducing *Plasmodium* strains have the rare ability to present antigens, although the exact mechanism remains elusive (Figure 8, step 6) [160]. When iRBCs accumulate in cerebral vessels, they might adhere to endothelial cells in the brain and activate them [161]. The latter recognise PAMPs via TLRs and NLRs [145], internalise the iRBCs and process *Plasmodium* parasites to cross-present them on MHC molecules on their surface [160]. Higher percentages of PbA parasites compared to non-ECM causing parasites have been found in perfused brains, which could affect the amount of antigen and thus cross-

presentation [160]. Only endothelial cells of mice infected with ECM-causing parasites showed cross-presentation *in vitro*, which may further explain why only some of the parasite strains induce neuropathological symptoms [160]. In brain vessels, the recruited antigen-specific $CD8^+$ T cells from the spleen recognise the peptides loaded onto MHC class I molecules and kill the endothelial cells via perforin/granzyme B release, resulting in a destabilisation of the blood-brain barrier (Figure 8, step 7) [160]. The resulting migration of leukocytes, soluble factors like cytokines and chemokines as well as parasite fragments into the brain can activate astrocytes and microglia and induce neuroinflammation [162]. The impaired neuronal function is characteristic for cerebral malaria and is clinically depicted by behavioural deficits, convulsions and coma, which can be fatal [91].

In summary, current research suggests that ECM is caused by cytotoxic $CD8^+$ T cells, pro-inflammatory cytokines like IFN-γ and TNFα as well as cross presentation by endothelial cells. The breakdown of the blood-brain barrier is the crucial event of ECM, allowing peripheral immune cells to invade the brain to induce neuronal damage.

3.3.3.4 The role of co-inhibitory receptors on T cells during malaria

As reviewed by Montes de Oca and colleagues, both murine and human T cells with chronic contact to *Plasmodium* parasites express co-inhibitory receptors like CTLA-4, Lag-3, Tim-3 and PD-1 [139]. During *P. berghei* infection, the expression of CTLA-4 was increased by $CD4^+$ T cells, and the blockade by a mAb resulted in an elevated T cell response and thus increased pathology [163]. Furthermore, higher levels of IFN-γ led to an enhanced accumulation of iRBCs and $CD8^+$ T cells in brain vessels, resulting in the manifestation of ECM in usually resistant Balb/c mice [164]. Several human studies also report that high frequencies of CTLA-4 and PD-1 expressing $CD4^+$ T cells exaggerate the pathology [165, 166]. The blockade of PD-1/PD-L1 and CTLA-4 *in vitro* resulted in increased cytokine production [166]. The expression of lymphocytic molecule Tim-3 was enhanced during infection with human *P. falciparum* and murine PbA. In contrast to the previously described blockade of co-inhibitory receptors, the blockade of Tim-3 reconstituted activation of T cells resulting in a better elimination of *Plasmodium* parasites [167]. In PY-infected mice, the blockade of PD-L1 and LAG-3 resulted in an elevation of the T_{FH} and B cell response, which was associated with increased antibody concentrations and thus improved clearance of the parasites [165].

Although the blocking of co-inhibitory receptors represents a promising therapy for the treatment of tumours [168], it remains to be elucidated whether it is also suitable for the treatment of malaria. Different *Plasmodium* species and hence variable immune mechanisms in different organs, including the susceptible brain, require efficient peripheral T cell responses to eliminate the parasites, but low activation in the brain and therefore a delicate balance of co-inhibitory molecules.

3.4 Objectives

Nrp-1 is a transmembrane protein that binds to VEGF, semaphorins and TGF-β and is involved in neuronal development and angiogenesis. Endothelial cells, tumour cells and immune cells, especially high frequencies of murine Tregs, express Nrp-1. During immune cell priming, Nrp-1 plays a role in the formation of the immunological synapse, where immune cell receptors polarise to interact with each other, and can therefore modulate T cell activation. Furthermore, our research group published previously that Nrp-1 is involved in cell migration along a VEGF gradient.

In PY infection, the priming of immune cells in the spleen plays a central role for the clearance of malaria parasites. The influence of Nrp-1 expression on activation of immune cells will be analysed in spleens of Balb/c mice during blood-stage malaria. A characterisation of Nrp-1^{+} conventional CD4^{+}FoxP3^{-} T cells will be conducted in the naïve and PY-infected state. T cell-specific or Treg-specific ablation of Nrp-1 in Nrp-1$^{fl/fl}$ x CD4cre^{tg} or Nrp-1$^{fl/fl}$ x FoxP3cre^{tg} mice shall provide insights in the role of T cell-expressed Nrp-1 during blood-stage malaria.

In the second part, the role of Nrp-1 expression will be studied in the context of ECM. PbA infection is driven by CD8^{+} T cells that are activated in the spleen and then migrate to the brain, where they lead to blood-brain barrier instability. Subsequent cerebral T cell infiltration leads to neurological deficits, which usually ends fatal. To find out, whether Nrp-1 is expressed on CD8^{+} T cells, immune cells of naïve and PbA-infected C57BL/6 mice will be characterised. Microarray analysis shall provide information about differentially regulated genes of Nrp-1^{+} and Nrp-1^{-}CD8^{+} T cells and their activation phenotype will be analysed by flow cytometry. To study whether Nrp-1 expression has an influence on migration and activation of CD8^{+} T cells during ECM, Nrp-1 will be specifically ablated on T cells and/or Tregs in Nrp-1$^{fl/fl}$ x CD4cre^{tg} and Nrp-1$^{fl/fl}$ x FoxP3cre^{tg} mice. The T cell phenotype as well as peripheral immune cell numbers in the brains of these mice will be analysed and their impact on ECM severity

determined. VEGF, as a Nrp-1 ligand known to be involved in Nrp-1-mediated Treg migration, will be analysed in the brains and sera of PbA-infected C57BL/6 mice. Furthermore, the influence of the Nrp-1/VEGF interaction will be investigated by the treatment of C57BL/6 mice with the A7R peptide. Since $CD8^+$ T cell migration and activation is important during ECM pathology, *in vitro* migration assays of Nrp-1-expressing and -deficient $CD8^+$ T cells will be conducted. Stability of Nrp-1 expression and potential roles in T cell activation will be analysed on *in vitro* stimulated $CD8^+$ T cells to identify the underlying mechanism.

4 Material

4.1 Mice

Experimental mice were kept in individually ventilated cages at the animal facility of the Robert-Koch-Haus of the University Hospital Essen. To ensure specific pathogen-free conditions, every three month, sentinel mice were examined for serological, histological and parasitological health. Animals used in experiments were at least six weeks old and all experiments were conducted in accordance to the ethical principles and guidelines of the state authorities of Nature, Environmental and Consumer Protection (LANUV), North Rhine-Westphalia.

4.1.1 Balb/c

Albino inbred Balb/cOlaHsD mice were bred in the animal facility of the Robert-Koch-Haus of the University Hospital Essen.

4.1.2 C57BL/6

Female C57BL/6JOlaHsd mice were purchased from Envigo (Horst, The Netherlands) with an age of 6-8 weeks.

4.1.3 Nrp-1flxCD4cre

Nrp-$1^{fl/fl}$ x CD4$cre^{wt/tg}$ mice were used on a Balb/c (PY infection) and C57BL/6 (PbA infection) background. Nrp-$1^{fl/fl}$ mice with two loxP sites flanking exon 2 of the *nrp-1* gene [169] were crossed with CD4cre mice with a cre recombinase under the control of the CD4 promoter. In Nrp-$1^{fl/fl}$ x CD4cre^{tg} mice the floxed exon 2 of the *nrp-1* gene was eliminated resulting in an ablation of Nrp-1 expression specifically in T cells. Nrp-$1^{fl/fl}$ x CD4cre^{wt} littermates were used as wildtype controls for *in vivo* studies and Nrp-$1^{+/+}$ x CD4cre^{tg} mice for *in vitro* studies.

4.1.4 Nrp-1flxFoxP3cre

Nrp-$1^{fl/fl}$ mice were crossed with FoxP3cre mice that expressed the cre recombinase under the control of the FoxP3 promotor [170]. $Nrp1^{fl/fl}$ x FoxP3cre^{tg} mice had an Nrp-1 ablation in Tregs and not in conventional $CD4^{+}FoxP3^{-}$ T cells. Nrp-$1^{+/+}$ x FoxP3cre^{tg} littermates with a WT *nrp-1* gene lacking the loxP sites (Nrp-$1^{+/+}$) and an active cre recombinase were used as wildtype controls.

4.2 Plasmodium species

Two murine parasite strains were used in this work to model malaria in mice. *Plasmodium yoelii XNL* (PY) is a parasite strain inducing blood-stage malaria characterised by high parasitic loads that can be cleared by the mice within approximately 21 days. *Plasmodium berghei ANKA* (PbA) is a lethal parasite strain that is used to study experimental cerebral malaria (ECM). The frequencies of PbA-infected erythrocytes is relatively low and untreated infection is accompanied by neurological deficits and death. Prof. Kai Matuschewski (Humboldt University of Berlin) kindly provided PY and GFP-tagged PbA parasite strains.

4.3 Buffer and Media

Table 1 Buffers and media

Buffer/Medium	Ingredients/Company
ACK lysis buffer (pH 7.2-7.4)	8,30 g/l [NH4Cl] 1,00 g/l [KHCO3] 200 µl/l EDTA
FACS buffer	1x PBS-Puffer 2 % (v/v) FCS 2 mM EDTA
Giemsa buffer (pH 7.2)	0,49 g [KHCO3] 1,14 g [Na2HPO4 * 2 H2O] ad 1000 ml H2O
Giemsa staining solution	10% Giemsa dye in Giemsa buffer
Go Taq 5x Flexi reaction buffer	Promega, Mannheim, Germany
$IMDM_{complete(c)}$	„Iscove's Modified Dulbecco's Medium" with GlutaMAX™ - I and 25 mM Hepes 10 % heat-inactivated FCS (v/v) 2,5 µM β-Mercaptoethanol 100 µg/ml Penicillin/Streptomycin
M-MLV Reverse Transcriptase buffer (5x)	Promega, Mannheim, Germany
PBS buffer (pH 7.0)	8 g/l NaCl 0,2 g/l KCl 1,44 g/l [Na2HPO4 * 2 H2O] 0,2 g/l [KH2PO4]
RPMI 1640	„Roswell Park Memorial Institute"-Medium with GlutaMAXTM -I and 25mM Hepes
Tail buffer	100 mM Tris HCL (pH 8,5) 200 mM NaCl

	0,2 % SDS 5 mM EDTA
TBE buffer	89 mM Tris 89 mM Boric acid 2,53 mM EDTA
TE buffer (10x)	10 mM Tris/Hcl (pH 8.0) 1 mM EDTA
Trypan blue solution	0,5 g Trypan Blue 0,9 g NaCl ad 100ml H2O

4.4 Material and Instruments

Table 2 Material and Instruments

Instrument	Company
6.5 mm Transwell plates 24 wells 5.0 µm Pore Polycarbonate Membrane Insert, sterile	Corning, Corning, USA
7500 Fast Real-Time PCR System	Applied Biosystems, Waltham, USA
AutoMACS (AutoMACS pro)	Miltenyi Biotec, Bergisch Gladbach, Germany
Centrifuge (Centrifuge 5417R)	Eppendorf, Hamburg, Germany
Centrifuge (MULTIFUGE 3SR+)	Thermo Fisher scientific, Waltham, USA
FACS (BD ARIA II)	BD Biosciences, Heidelberg, Germany
FACS (BD LSR II)	BD Biosciences, Heidelberg, Germany
FACS (Canto)	BD Biosciences, Heidelberg, Germany
Fast Prep®-24	MP Biomedicals, California, USA
GelDoc Station	BD Biosciences, Heidelberg, Germany
Incubator (HERA cell 150)	Thermo Electron Corporation, Waltham, USA
MAGPIX	Luminex Corporation, Austin, USA
Microscope Axioskop 40/ 40 C	Zeiss, Feldbach, Switzerland
Nanodrop Photometer	Peqlab, Erlangen, Germany
PowerSupply	Bio-Rad, Hercules, USA
Safety Workbench Class II (MSC-Advantage)	Thermo Fisher Scientific, Waltham, USA
Scale (CP2202S)	Sartorius, Göttingen, Germany
Thermoblock	Eppendorf, Hamburg, Germany
Thermocycler T3000	Biometra, Göttingen, Germany

4.5 Chemicals

Table 3 Chemicals

Chemical	Company
Agarose	Biozym, Oldendorf, Germany
Albumin bovine Fraction V (BSA)	Serva Electrophoresis GmbH, Heidelberg, Germany
Alsever‘s solution	Sigma Aldrich, St. Louis, USA
Boric acid	Carl Roth GmbH, Karlsruhe, Germany
Brefeldin A	Sigma Aldrich, St. Louis, USA
Deoxynucleoside Triphosphates (dNTPs)	Fermentas, St. Leon-Rot, Germany
Ethanol, absolute	Carl Roth GmbH, Karlsruhe, Germany
Ethylenediaminetetraacetic acid (EDTA)	Carl Roth GmbH, Karlsruhe, Germany
Fetal Calve Serum (FCS)	PAA Laboratories, Pasching, Austria
Fibronectin	Roche, Mannheim, Germany
Fixable viability dye eFluor780 (FvD)	eBioscience, San Diego, USA
Giemsa Azur Eosin-Methylenblue-solution	Merck, Darmstadt, Germany
Heparin-Sodium-25000-ratiopharm©	Merckle GmbH, Blaubeuren, Germany
HEPES 1M	Gibco, Life Technologies, Carlsbad, Germany
Hydrochloric acid [HCl]	Merck, Darmstadt, Germany
IGEPAL®CA-63	Sigma Aldrich, St. Louis, USA
Ionomycin	Sigma Aldrich, St. Louis, USA
Magnesium chloride [$MgCl_2$]	Promega, Mannheim, Germany
Methanol	Carl Roth GmbH, Karlsruhe, Germany
Na_2HPO_4 x 2 H_2O	Carl Roth GmbH, Karlsruhe, Germany
Paraformaldehyde	Carl Roth GmbH, Karlsruhe, Germany
Penicillin-Streptomycin	Sigma Aldrich, Hamburg, Germany
Percoll	Sigma Aldrich, Hamburg, Germany
Phorbol 12-myristate 13-acetate (PMA)	Sigma Aldrich, Hamburg, Germany
Potassium chloride [KCl]	Carl Roth GmbH, Karlsruhe, Germany
Potassium dihydrogen carbonate [$KHCO_3$]	Carl Roth GmbH, Karlsruhe, Germany

Potassium hydrogen phosphate [KH_2PO_4]	Carl Roth GmbH, Karlsruhe, Germany
RLT buffer	Qiagen, Hilden, Germany
SDS	Carl Roth GmbH, Karlsruhe, Germany
Sodium chloride [NaCl]	Carl Roth GmbH, Karlsruhe, Germany
Tris	Carl Roth GmbH, Karlsruhe, Germany
Trypan Blue Dye	Invitrogen, Karlsruhe, Germany
β-Mercaptoethanol	Carl Roth GmbH, Karlsruhe, Germany

4.6 Enzymes, DNA-Markers

Table 4 Enzymes and DNA markers

Enzyme/DNA Marker	Company
Gene Ruler 100 bp ladder Plus	Fermentas, St- Leon-Rot, Germany
GoTaq Hot Start Polymerase	Promega, Mannheim, Germany
Maxima SYBR Green/ROX qPCR Master Mix (2x)	Thermo Fisher Scientific, Waltham, USA
Midori Green Advance	Nippon Genetics Europe, Düren, Germany
M-MLV Reverse Transkriptase	Promega, Mannheim, Germany
OligodT primers	Invitrogen, Karlsruhe, Germany
Proteinase K	Sigma Aldrich, Hamburg, Germany
Random Hexamer Primer	Invitrogen, Karlsruhe, Germany

4.7 Primers

Table 5 Primers for qPCR

Gene	Sequence	Concen-tration	T_A
Nrp-1 5’	CGACAAATGTGGCGGGACCATAA	300 nM	55°C
Nrp-1 3’	CCGGAGCTTGGATTAGCCATTCAC	300 nM	
RPS9 5’	CTGGACGAGGGCAAGATGAAGC	900 nM	58°C
RPS9 3’	TGACGTTGGCGGATGAGCACA	50 nM	
VEGF-5'	ATCCGCATGATCTGCATGG	300 nM	58°C
VEGF-3'	AGTCCCATGAAGTGATCAAGTTCA	300 nM	

Table 6 Primers for mouse genotyping

Gene	Sequence	Concen-tration	T_A
Cre 5' Cre 3'	ACGACCAAGTGACAGCAATG CTCGACCAGTTTAGTTACCC	250 nM	60°C
FIC 5' FIC 3'	CTG CTT CCT TCA CGA CAT TCA AC AAG TGC TTT GTG CGA GTG GAG AGC	250 nM	61°C
Nrp-1 5' Nrp-1 3'	AGGCCAATCAAAGTCCTGAAAGACAGTCCC AAACCCCCTCAATTGATGTTAACACAGCCC	250 nM	63°C

4.8 Antibodies for flow cytometry

Table 7 Antibodies for flow cytometry

Epitope	Fluoro-chrome	Clone	Dilution	Company
αCD107a	PE	1D4B	1:200	BD Biosciences, Heidelberg, Germany
αCD11a	FITC	M17/4	1:600	BioLegend, San Diego, USA
αCD11b	AF488	M1/70	1:300	eBioscience, San Diego, USA
αCD11c	PE-Cy7	N418	1:1000	BioLegend, San Diego, USA
αCD138	BV421	281-2	1:400	BioLegend, San Diego, USA
αCD160	PE-Cy7	7H1	1:200	BioLegend, San Diego, USA
αCD19	PE-Cy7	1D3	1:1000	BD Biosciences, Heidelberg, Germany
αCD3	PE	145-2C11	1:200	BD Biosciences, Heidelberg, Germany
αCD4	PB	RM4-5	1:800	BD Biosciences, Heidelberg, Germany
	PE	H129.19	1:800	BD Biosciences, Heidelberg, Germany
	PerCP	RM4-5	1:1200	BD Biosciences, Heidelberg, Germany
αCD44	APC	IM7	1:500	BD Biosciences, Heidelberg, Germany
αCD45	PB	30-F11	1:2000	BioLegend, San Diego, USA
	PE-Cy7	30-F11	1:800	BioLegend, San Diego, USA
αCD49d	AF647	R1-2	1:400	BD Biosciences, Heidelberg, Germany
αCD62L	PE	MEL-14	1:1000	eBioscience, San Diego, USA
αCD69	FITC	H1.2F3	1:1000	eBioscience, San Diego, USA
αCD8	PB	53.6-7	1:200	BD Biosciences, Heidelberg, Germany
	FITC	53.6-7	1:800	BD Biosciences, Heidelberg, Germany

	PE-Cy7	53.6-7	1:200	eBioscience, San Diego, USA
αCTLA4	PE	UC10-4F10-11	1:100	BD Biosciences, Heidelberg, Germany
αCXCR3	PE	CXCR3-173	1:600	eBioscience, San Diego, USA
αF4/80	PB	BM8	1:400	Invitrogen, Karlsruhe, Germany
αFoxp3	FITC	FJK-16s	1:150	eBioscience, San Diego, USA
	PE	FJK-16s	1:150	eBioscience, San Diego, USA
	APC	FJK-16s	1:100	eBioscience, San Diego, USA
αGzm B	APC	GB12	1:100	Invitrogen, Karlsruhe, Germany
αKi-67	PE-Cy7	SolA15	1:1000	eBioscience, San Diego, USA
αKLRG-1	PE-Cy7	2F1	1:800	eBioscience, San Diego, USA
αIFN-γ	PE	XMG1.2	1:300	BD Biosciences, Heidelberg, Germany
	FITC	XMG1.2	1:150	BD Biosciences, Heidelberg, Germany
αLag-3	PE	C9B7W	1:100	BD Biosciences, Heidelberg, Germany
αNK1.1	FITC	PK136	1:300	BD Biosciences, Heidelberg, Germany
αNrp-1	APC	polyclonal	1:100	R&D Systems, Minneapolis, USA
	BV421	3DS304M	1:100	eBioscience, San Diego, USA
	FITC	polyclonal	1:200	R&D Systems, Minneapolis, USA
αPD-1	PE-Cy7	RMP1-30	1:200	BioLegend, San Diego, USA
αTer119	PE	TER-119	1:800	BioLegend, San Diego, USA
αTim-3	APC	215008	1:200	R&D Systems, Minneapolis, USA
αTNF-α	APC	MP6-XT22	1:400	eBioscience, San Diego, USA

4.9 Antibodies for T cell activation

Table 8 Antibodies for *in vitro* T cell activation

Epitope	Fluorchrome	Clone	Concentration	Company
αCD3	Purified	145-2C11	1 µg/mL	BD Biosciences, Heidelberg, Germany
αCD28	Purified	37.51	1 µg/mL	BD Biosciences, Heidelberg, Germany

4.10 Cell culture supplements

Table 9 Cell culture supplements

Chemokine	Species	Concentration	Company
IL-2	Human	250 U/mL	eBioscience, San Diego, USA
rCXCL10	Mouse	200 µg/mL	R&D Systems, Minneapolis, USA
rVEGF165	Human	100 ng/mL	Preprotech, Hamburg, Germany
SDF-1β	Human	100 ng/mL	Preprotech, Hamburg, Germany

4.11 Blocking peptide

Table 10 Blocking peptide

Epitope/Peptides	Company
A7R (H-ATWLPPR-OH)	Intavis, Cologne, Germany

4.12 Fluorochromes

Table 11 Fluorochromes

Fluorochrome	Abbreviation	Absorption	Emission
Alexa Fluor 488	AF488	495 nm	519 nm
Alexa Fluor 647	AF647	650 nm	665 nm
Allophycocyanin	APC	650 nm	660 nm
Brilliant Violet 421	BV421	405 nm	421 nm
eFluor780	eFluor780	633 nm	780 nm
Fluoresceinisothiocyanat	FITC	494 nm	519 nm
Pacific Blue	PB	401 nm	452 nm
Peridinin-Chlorophyll-protein	PerCP	482 nm	676 nm
Phycoerythrin	PE	496 nm	578 nm

Phycoerythrin-Cyanine 7	PE-Cy7	496 nm	786 nm

4.13 Kits

Table 12 Kits

Kit	Company
$CD4^+$ T Cell Isolation Kit, mouse	Miltenyi Biotec, Bergisch Gladbach, Germany
$CD8^+$ T Cell Isolation Kit, mouse	Miltenyi Biotec, Bergisch Gladbach, Germany
FoxP3 Staining Buffer Kit	eBioscience, San Diego, USA
Luminex Assay Mouse premixed Multi-analyte Kit	R&D Systems, Minneapolis, USA
RNeasy Mini Kit	Qiagen, Hilden, Germany
Single Cell Lysing Kit	Thermo Fisher Scientific, Waltham, USA

4.14 Software

Table 13 Software

Software	Company
7500 Fast System Software	Applied Biosystems, Waltham, USA
BD FACSDiva™ Software	BD Biosciences, Heidelberg, Germany
GraphPad Prism 7	GraphPad Software, La Jolla, USA
Luminex xPONENT Software	Luminex Corporation, Austin, USA
Microsoft Office 2016	Microsoft Corporation, Redmond, USA
OriginPro 2019b software	OriginLab, Northampton, USA

5 Methods

5.1 Cell biological methods

5.1.1 Animal perfusion

As peripheral immune cell numbers in the brain are usually proportionately low, the immune cell-rich blood needs to be removed from circulation and the brain. After sacrificing the experimental animal, blood from the right atrium was collected for serum analysis or collected in PBS supplemented with Heparin for immune cell analysis. The animal was then perfused with 20 mL ice cold PBS into the left ventricle. The spleen was removed before the skull was opened and the brain, together with the olfactory bulb and cerebellum, was collected in RPMI medium with 1 % HEPES addition and stored on ice until further processed.

5.1.2 Cell suspensions

5.1.2.1 Spleen

Freshly isolated spleens were rinsed or homogenised with 5 mL ACK lysis buffer, washed with FACS buffer and filtered through a 70 µm cell strainer. After centrifugation for 10 minutes at 300 g and 4°C, splenocytes were resuspended in FACS buffer.

5.1.2.2 Blood and serum

To isolate leukocytes from the blood, the blood in PBS/Heparin was incubated with 1 mL ACK lysis buffer for two minutes at room temperature. 10 minutes of centrifugation at 200 g and 4°C removed lysed erythrocytes. The supernatant was aspirated and this step was repeated before the cell pellet was resuspended in FACS buffer.

For the collection of serum, the blood without anti-coagulant was left at room temperature for at least 3 hours. After centrifugation for 10 minutes at 6,797 g, the supernatant was transferred into new tubes and stored at -80°C until further use.

5.1.2.3 Brain cells

The perfused and isolated brain was homogenised with 15 mL of RPMI supplemented with 1 % HEPES through a 70 µm cell strainer. After centrifugation for five minutes at 400 g and 18°C, the supernatant was aspirated and the pellet was resuspended in 5 mL of 37 % Percoll in 0.01 M HCl in PBS with a pH between 7.0 and 7.2. To remove the myelin, cells were centrifuged for 20 minutes at 2800 g and 18°C without

acceleration or break. The upper white ring containing the myelin was removed and the remaining supernatant was aspirated. The pellet at the bottom of the tube was rich in immune cells and microglia. The pellet was washed with FACS buffer and the cell pellet resuspended in FACS buffer.

5.1.3 Cell counts

To determine the absolute cell numbers of the generated cell suspensions, the cells were counted with a Neubauer counting chamber under a light microscope. Samples were diluted in Trypan blue, which only penetrates and stains dead cells, while intact cells remain unstained and therefore appear white under the light microscope. Cell numbers of X squares of the chamber were calculated according to the formula below:

$$Absolute\ cell\ number = \frac{counted\ cells}{X\ [squares]} \times Dilution\ \times Volume\ in\ mL\ \times 10^4$$

5.1.4 Flow cytometry

Flow cytometry is a method to detect and count cells, whereby the fluorescence-activated cell sorting (FACS) allows the separation of cell populations for their further procession and analysis. The scattered light caused by the individual cells passing a laser beam provides information about the size and the granularity of the cells. Additionally, mAbs coupled to fluorochromes can be used to specifically label surface or intracellular and soluble proteins on and in the cells. The lasers excite the fluorochromes and the emission correlates with the expression of the molecules [1].

5.1.4.1 Surface stainings

To analyse the expression of surface molecules, cells were transferred into a 96-well round-bottom plate, centrifuged for 5 minutes at 300 g and 4°C. The supernatant was discarded and the pellet was resuspended in FACS buffer containing fluorescence-labelled mAbs (Table 7). After an incubation period of 10 minutes or if the master mix contained αNrp-1 antibodies for 30 minutes at 4°C, the cells were washed with FACS buffer and measured at the FACS Canto (Balb/c mice) or LSR II (C57BL/6 mice). The analysis was conducted with DIVA software by BD. For cell sorting, a FACSAria II (BD) was used.

5.1.4.2 Intracellular stainings

To stain intracellular proteases like GzmB or transcription factors such as FoxP3, the cells were fixed and permealised after they were stained for surface molecules. For this purpose, the cells were incubated with 1:4 of the Fix/Perm concentrate and Fix/Perm Diluent of the FoxP3 Staining buffer kit (eBioscience) for 90 minutes at 4°C. The cells were washed with 1x Perm buffer (eBioscience) and stained with intracellular mAbs in 1x Perm buffer for 30 minutes at 4°C. Cells were washed and measured in FACS buffer.

5.1.4.3 Cytokine stainings

To detect intracellular cytokines like IFN-γ and TNF-α by flow cytometry, splenocytes were re-stimulated with 100 ng/mL Phorobol 12-myristate 13-acetate (PMA) and 1 µg/mL ionomycin in the presence of 5 µg/mL Brefeldin A for 4 hours at 37°C. The supplementation of Brefeldin A to the IMDMc Medium prevented the release of cytokines from the cell. The cells were washed twice with PBS and fixed in 2 % Paraformaldehyde (PFA) for 15 minutes at 4°C. Next, the cells were washed and permeabilised with 0.1 % IGEPAL®CA-63. The intracellular staining with flourochrome-coupled mAbs occurred in PBS for 30 minutes at 4°C, before cells were washed and measured by flow cytometry.

5.1.5 Magnetic activated cell sorting

Magnetic activated cell sorting (MACS) is a technique to enrich immune cell populations. According to the manufacturer's protocol (Miltenyi), cell suspensions were incubated with biotin-coupled antibodies binding to all non-target cells. These antibodies were bound by anti-biotin MicroBeads that were retained on the MACS column that was placed in the magnetic field of the AutoMACS (Miltenyi). Target cells passed the magnetic field untouched and were ready to use for further experiments.

5.1.6 *In vitro* stimulation

For T cell activation *in vitro*, spleen cells were isolated from naïve C57BL/6 or Nrp-1$^{fl/fl}$ x CD4cre^{tg} and Nrp-1$^{+/+}$ x CD4cre^{tg} mice as described in section 5.1.2.1. CD8$^+$ T cells were negatively selected by MACS technology (section 5.1.5). For *in vitro* stimulation, 96 well plates were pre-incubated with 1 µg/mL αCD3 for 90 minutes at 37°C. The wells were washed with PBS twice and 1.5 x 10^5 CD8$^+$ T cells were then incubated in 200 µL IMDM$_c$ with 1 µg/mL soluble αCD28. Unstimulated controls were incubated with

$IMDM_c$ without αCD3 or αCD28. TCR-independent stimulation was achieved by supplementation of 10 ng/mL Phorobol 12-myristate 13-acetate (PMA) and 1 µg/mL ionomycin. Cells were incubated for 24, 48, 72, 96 and 168 hours at 37°C and were then harvested, washed with PBS and stained for flow cytometry according to section 5.1.4.

5.1.7 Re-cultivation of *in vitro* stimulated $CD8^+$ T cells

For the analysis of the stability of Nrp-1 expression, 2.5 x 10^6 $CD8^+$ T cells from naïve C57BL/6 mice were stimulated in 2 mL volume per well in a 24 well plate according to section 5.1.6 for 48 hours. Cell were then harvested and washed with PBS. For FACS separation of Nrp-$1^{+/-}$ $CD8^+$ T cells, cells were stained with αCD8 PB and αNrp1 APC in FACS buffer for 30 minutes at 4°C. Cells were sorted and washed again and 1 x 10^5 Nrp-1^+ or Nrp-1^-CD8^+ T cells were incubated in 200 µL $IMDM_c$ per well of a 96 well plate. As a survival stimulus, 250 U IL-2 were added and cells were incubated at 37°C. For analysis, cells were harvested and washed after 24, 48, 72 and 96 hours and stained for flow cytometry analysis.

5.1.8 Migration assay

For the migration assay, spleen cells from naïve Nrp-$1^{fl/fl}$ x $CD4cre^{tg}$ or Nrp-$1^{+/+}$ x $CD4cre^{tg}$ mice were processed like in section 5.1.6 described. However, 2.5 x 10^6 $CD8^+$ T cells were stimulated in 2 mL volume and 24 well plates. Cells were then harvested and washed with RPMI medium. Transwell inserts of the 24 well plate were coated with 100 µL fibronectin diluted in PBS (6.5 µg Fibronectin/mL PBS) for 90 minutes at 37°C. Inserts were washed with PBS twice and dried at room temperature. 7.5 x 10^5 of the previously activated $CD8^+$ T cells were resuspended in 200 µL RPMI with 0.1 % BSA and transferred into the upper chamber of the transwell. In the bottom chamber 500 µL RPMI with 0.1 % BSA were supplemented with 100 ng/mL hSDF-1β as a positive control and 100 ng/mL rhVEGF or 200 ng/mL rmCXCL10 as chemoattractants. RPMI with 1 % BSA without supplementation was used as negative control. The transwell-inserts containing the cells were transferred into the bottom chamber. After 4 hours at 37°C, 10 µL of 0.5 M EDTA were added to the bottom chamber and incubated on a shaker for 10 minutes at 60 rpm at room temperature to stop migration and detach the cells from the membrane. Transwell-inserts were discarded and cells were collected from the bottom chamber. After centrifugation for 10 minutes at 500 g, the supernatant was aspirated and the pellet respuspended in 50

µL PBS. Cells were counted under the light microscope and the migration index calculated by dividing the number of the migrated cells by the numbers of cells in the negative control without chemoattractant.

5.1.9 Luminex

Cytokines from serum were quantified by Luminex technology with a kit of R&D Systems. This technology is based on a dual-laser flow system and involves colour-coded beads that are coated with cytokine-specific antibodies. After the beads captured the present cytokines in the 1:2 diluted serum, biotinylated detection antibodies were added and bound to the target cytokines. To quantify the concentration of cytokines, fluorescence-labelled Streptavidin was added and bound to the biotin of the detection antibodies that were in relation to the cytokine concentration. In a final step, the type of bead and therefore the type of cytokine as well as the amount of cytokine by PE-emission were detected. Samples were measured by the MAGPIX Luminex machine and the results were analysed by Sina Luppus with the xPONENT software by Luminex.

5.2 Molecular biological methods

5.2.1 RNA extraction from brain hemispheres

To extract RNA from brains, the left hemisphere was halved after perfusion. One fourth of the brain was transferred in Eppendorf tubes containing a ceramic ball and 1 mL of RLT buffer. The tissue was homogenised in a homogeniser at 4 m/s, twice. After spinning down the homogenates at 10,621 g for 5 minutes, the two suspensions were combined and again centrifuged at 20,817 g for 5 minutes. Aliquots of the supernatants were stored at -80°C until further use.

To isolate RNA from these homogenates, samples were thawed and centrifuged at 20,817 g for 5 minutes. 300µL of the supernatant was used and mixed 1:1 with 80 % Ethanol. The mixture was transferred onto RNeasy columns of the RNeasy Mini kit by Qiagen. RNA was extracted according to the manufacturer’s manual. In brief, columns were washed with RW1 buffer, an additional step including DNase was conducted. After washing with RPE twice, RNA was eluted in 21.5 µL RNAse-free water. Quality and quantity of the RNA was measured by Nanodrop.

5.2.2 cDNA synthesis

2 µg of purified RNA were diluted in 13 µL RNase-free water and were reverse-transcribed into cDNA. For this purpose, 0.25 µg OligodT primers and 1.5 µg random hexamer primers (Invitrogen) were added and the samples were heated for 10 minutes at 70°C in the PCR machine. On ice, 4 µL of Promega M-MLV-RT 5x buffer (Promega), 1 µL dNTPs (10 mM) and 1 µL M-MLV-RT (200 U/µL, Promega) were added to the sample. The PCR program was continued at 42°C for 60 minutes. The reaction was stopped during 5 minutes incubation at 95°C. Synthesised cDNA was diluted 1:1 in 1x TE buffer and stored at -20°C degrees until further use.

5.2.3 Semi-quantitative PCR

To check cDNA synthesis, *rps-9*, a housekeeping gene that is constitutively expressed in all cells, was amplified by PCR. Furthermore, semi-quantitative PCR was used to detect the presence of target genes. For this purpose, the following Go-Taq PCR protocol was used:

Table 14: Go-Taq PCR approach

Substance	**Volume [µL]**
RNase-free water	12.3
Go Taq 5x Flexi reaction buffer	4.0
dNTPs	0.4
$MgCl_2$	1.2
Primer Mix (forward/reverse)	1.0
GoTaq Polymerase	0.1
cDNA	1.0

PCRs were run according to the following standard program with the appropriate annealing temperature (T_A):

Table 15: Standard PCR program

Cycles [#]	1	10			27		
Temperature [°C]	95	95	T_A	72	95	T_A	72
Time [minutes]	10.00	0.30	1.30	1.30	0.15	0.45	1.30

5.2.4 Gel electrophoresis

Gel electrophoresis is a method that uses an electric field to separate DNA fragments by their size. 1 % agarose gels (1 g in 100 mL TBE buffer) were supplemented with Midori Green dye. Samples were applied to the gel, which was connected to 150 V for 30 minutes. The DNA intercalating dye was visualised by UV light and DNA ladders were included for size comparison.

5.2.5 Real-time PCR

In contrast to the semi-quantitative conventional PCR, real-time PCR (qPCR) is a method to monitor the PCR process in real time and thereby quantify the amplification of the PCR product relatively to a control gene. For this purpose, a fluorescent dye that binds to double-stranded DNA, here SYBR Green, is used. With every duplication of the DNA, the fluorescence intensity increases and can be quantified. For qPCR, the following qPCR protocol was used:

Table 16 SYBR Green PCR protocol

Substance	**Concentration in 20 µL H_2O ad.**
Mastermix SYBR Green (Fermentas)	10 µL
Rox (1:10 in H_2O)	0.04µL
Forward Primer	50-900 nM in 2.5 µL H_2O
Reverse Primer	50-900 nM in 2.5 µL H_2O
cDNA	5µL

As a housekeeping gene, *rps-9* was used. cDNA was pre-diluted 1:50 and further applied according to table 16. Primers were used according to table 5. The qPCRs program below was proceeded in a 7500 real-time PCR system with the appropriate annealing temperature (T_A) of 58°C:

Table 17 qPCR program

Cycles [#]	1	45			1			
Temperature [°C]	95	95	T_A	72	95	T_A	95	60
Time [minutes]	10.00	00.15	0.30	0.30	0.15	1.00	0.15	0.15

Relative mRNA levels were calculated in relation to the standard curve of *rps-9* and the target genes.

5.2.6 Genotyping

To determine the genotype of the mice, tail tips were digested in 90 µL tail buffer and 10 µL proteinase K (10 mg/mL) at 56°C over-night. The digestion was stopped by heating the solution for 10 minutes to 95°C. Supernatant was diluted 1:50 in water after centrifuging for 5 minutes at 20,817 g. PCRs were prepared according to table 14, including appropriate primers (Table 6). The following PCR programs were run:

Table 18 PCR program Nrp-1 and cre

Cycles [#]	1	9			26		
Temperature [°C]	95	95	T_A	72	95	T_A	72
Time [minutes]	10.00	0.30	1.30	1.30	0.15	0.45	1.30

Table 19 PCR program FoxP3cre

Cycles [#]	1	37			37			1
Temperature [°C]	94	94	61	72	94	61	72	72
Time [minutes]	10.00	0.30	0.30	0.30	0.30	0.30	0.30	5.00

PCR products were separated by gel electrophoresis as described in section 5.2.4.

5.2.7 Microarray

For Microarray analysis, spleens of PbA-infected C57BL/6 mice were isolated and single cell suspensions prepared as described in section 5.1.2.1. $CD8^+$ T cells were negatively selected by MACS (section 5.1.5) and cells were stained with αCD8 PECy7 and αNrp-1 APC for 30 minutes at 4°C. After washing, 2,000 Nrp-1^+ and Nrp-1^-CD8^+ T cells were sorted by FACS into Eppendorf tubes containing 4.5 L Single Cell Lysis Buffer and 0.5 µL DNase I of the single-cell lysis kit (Invitrogen, Karlsruhe, Germany). Cells were spun down and incubated for 2 minutes at room temperature. 0.5 µL Stop solution was added and samples were again incubated for 2 minutes at room temperature to stop cell lysis. Cells were then immediately put on ice and transferred to -20°C until they were sent to the Helmholtz Centre for Infection Research in Brunswick, where the samples were further processed and an Affymetrix Microarray was conducted by Robert Geffers.

5.3 Animal experimental methods

5.3.1 Blockade of Nrp-1/VEGF interaction

ATWLPPR, abbreviated A7R, is a peptide that is used to specifically block VEGF-Nrp-1 interaction. Here, 20 µg/g were applied in 200 µL PBS on d0, 2 and 4 post infection i.v. into PbA-infected C57BL/6 mice. The control group received PBS.

5.3.2 Parasitemia

5.3.2.1 P. yoelii

To quantify the parasite burden in the blood of *P. yoelii*-infected mice, blood smears were prepared: One drop of blood was collected from the tail vein of the mouse and was smeared onto a microscope slide. After air-drying, it was fixed in methanol for one minute and subsequently stained in Giemsa solution for 30 minutes. Slides were washed with Giemsa buffer and erythrocytes were analysed with the Axiovert 40 C (Zeiss) light microscope. Using immersion oil, a monolayer of erythrocytes was set in the 100-fold magnification. In an area of 10x10 mm the number of erythrocytes was determined. Then the iRBCs were counted in n regions of interest (ROIs). With the following formula, the blood parasitemia was calculated:

$$Parasitemia\ [\%] = \frac{iRBCs\ (of\ n\ ROIs) \times 100}{RBCs \times n}$$

5.3.2.2 P. berghei ANKA

The *P. berghei ANKA* strain used in this work constitutively expressed eGFP, which could be detected by FACS. One drop of blood was collected from the tail vein of PbA-infected mice and transferred into 100 µL of PBS with heparin (1:100). After antibody labelling of αTer119, which is expressed by erythrocytes, the percentage of iRBCs was quantified.

5.3.3 Production of blood stabilates

To stock up *Plasmodium*-infected erythrocytes, wildtype mice with blood parasitic levels between 1 and 10% were used. For this, blood from infected wildtype mice was collected from the heart and stored in heparin-coated tubes. 100 µL blood was mixed with 200 µL of Alsever's solution in cryo tubes and immediately frozen in liquid nitrogen.

5.3.4 Plasmodium infection

For *Plasmodium* infection, stabilates were injected i.p. into wildtype mice to increase viability of the previously frozen parasites. After 3 days (PY) or 4 days (PbA), when the mice had a parasite burden between 0.1 and 1.0 %, the mice were sacrificed and blood was collected with a heparin-coated syringe from the heart. The blood was diluted with RPMI medium to receive an infection dose of 1 x 10^5 iRBCs in 200 µL for PY as well as PbA infection. Experimental animals were infected i.v. without anaesthesia.

5.3.5 Pathology score

To monitor cerebral malaria manifestation and neurological symptoms during PbA infection, the rapid murine coma and behaviour scale (RMCBS) score described by Carroll and colleagues was used [171]: Coordination, exploratory behaviour, strength and muscle tone, reflexes, self-reservation as well as hygiene-related behaviour were tested in a fresh cage and scored with 0-2 per category. A maximal score of 20 could be reached, representing a completely healthy mouse. With manifestation of ECM, the score declined. Mice with a RMCBS score under 12 were considered to suffer from ECM with neurological deficits. Each mouse in the experiment was put into the upper right corner of a fresh cage. The fur, body position and gait was analysed and scored according to table 20 below. The mouse had 15 seconds to explore all four corners of the cage to achieve a score of 2 in this category, or 90 seconds to explore at least one corner for a score of 1. After these 90 seconds, the ear pinnar and touch escape reflex were tested by touching each ear or flank three times and waiting for reaction. Subsequently, the mouse was grabbed and moved near the grid of the cage. The strength of the grab and the toe pinch reflex were examined. The mouse was then put into a box to investigate its balance before the mouse was moved into an i.v. injection tube to see its rejection and aggression potential.

Table 20 RMCBS Score [171]

Label	Description (Score) – Total Score of 20
Grooming	(0) ruffled fur, with swaths of hair out of place – (1) dusty/piloerection – (2) normal/clean fur with sheen
Body Position	(0) on side – (1) hunched – (2) full extension
Gait	(0) none – (1) ataxic – (2) normal
Motor Performance (exploration of the cage)	(0) no corner of the cage explored in 90 seconds – (1) 1 or more corners explored in 90 seconds – (2) explores 4 corners in 15 seconds
Balance	(0) no body extension – (1) one paw on wall of cage/box – (2) both fore feet on wall of cage/box, entire body lift
Pinna Reflex (Ear)	(0) none – (1) unilateral – (2) instant and bilateral; in 3 attempts)
Touch Escape	(0) none – (1) unilateral – (2) instant and bilateral; in 3 attempts
Limb Strength on the grid	(0) hypotonic, no grasp – (1) grasp, weak pull-back – (2) strong pull-back
Toe Pinch	(0) none – (1) unilateral – (2) instant and bilateral; in 3 attempts
Aggression in the i.v. injection tube	(0) none – (1) retention – (2) bite attempt/noise

5.4 Statistics

Graphs and statistics were made with GraphPad Prism 7 (GraphPad Software, La Jolla, USA). Statistical tests are described in the figure legends. P-value were defined as < 0.05 (*), < 0.01 (**), < 0.001 (***) and < 0.0001 (****). Radar graphs were made with OriginPro 2019b software by OriginLab (Northampton, USA).

6 Results

6.1 Analysis of the role of T cell-expressed Nrp-1 during *P.yoelii* infection

Infection with *Plasmodium yoelii* (PY) is a common model to study blood-stage malaria in rodents. The immune response is based on pro-inflammatory cytokines and the priming of immune cells in the spleen. T_H1-differentiated $CD4^+$ T cells and antibody-producing plasma cells play an essential role in the clearance of high parasite loads within 21 days of infection.

Here, Balb/c mice were infected intravenously with 10^5 PY-infected RBCs to study and characterise Nrp-1 expression on various immune cells during blood-stage malaria. Nrp-1 is a co-receptor of semaphorin and VEGF, known to play a role in immune cell interaction and might therefore modulate immune responses. The T cell phenotype and course of blood-stage infection was analysed in Nrp-$1^{fl/fl}$ x CD4cre^{tg} and Nrp-$1^{fl/fl}$ x FoxP3cre^{tg} mice with a T cell- or Treg-specific ablation of Nrp-1, respectively.

6.1.1 Characterisation of Nrp-1 expression on immune cells during PY infection

To study Nrp-1 expression during PY infection, spleen cells were isolated from naïve or PY-infected Balb/c mice on day 7 and 14 post infection (p.i.) and analysed by flow cytometry. In the naïve state, Nrp-1 was primarily expressed on the surface of macrophages, DCs and $CD4^+$ T cells, especially on a high proportion of $CD4^+FoxP3^+$ Tregs (Figure 9B, white bars). Nrp-1 expression on macrophages was stable during PY infection and the frequencies of Nrp-1^+ DCs significantly rose in the early phase of infection (day 7 p.i.) compared to the naïve state (Figure 9B). NK cells, which have the ability to kill iRBCs and produce IFN-γ, showed an increase in Nrp-1 expression and elevated numbers of Nrp-1^+ B cells were detected on day 14 after infection (Figure 9B and C). The most significant alterations of Nrp-1 expression during PY infection were found in the T cell compartment: From the naïve status to the peak of infection on day 14, the percentage of Nrp-1-expressing conventional $CD4^+FoxP3^-$ T cells was elevated by 10 %, which was reflected by a significant increase of absolute $Nrp1^+CD4^+$ T cells. Blood-stage malaria decreased Nrp-1 expression on $CD4^+FoxP3^+$ Tregs, but led to a significant increase in absolute numbers of Nrp-1^+ Tregs. Merely a proportion of 1.3 % of $CD8^+$ T cells in the spleens of uninfected mice expressed Nrp-1 on their surface, which was elevated to 3.5 % during PY infection (Figure 9B).

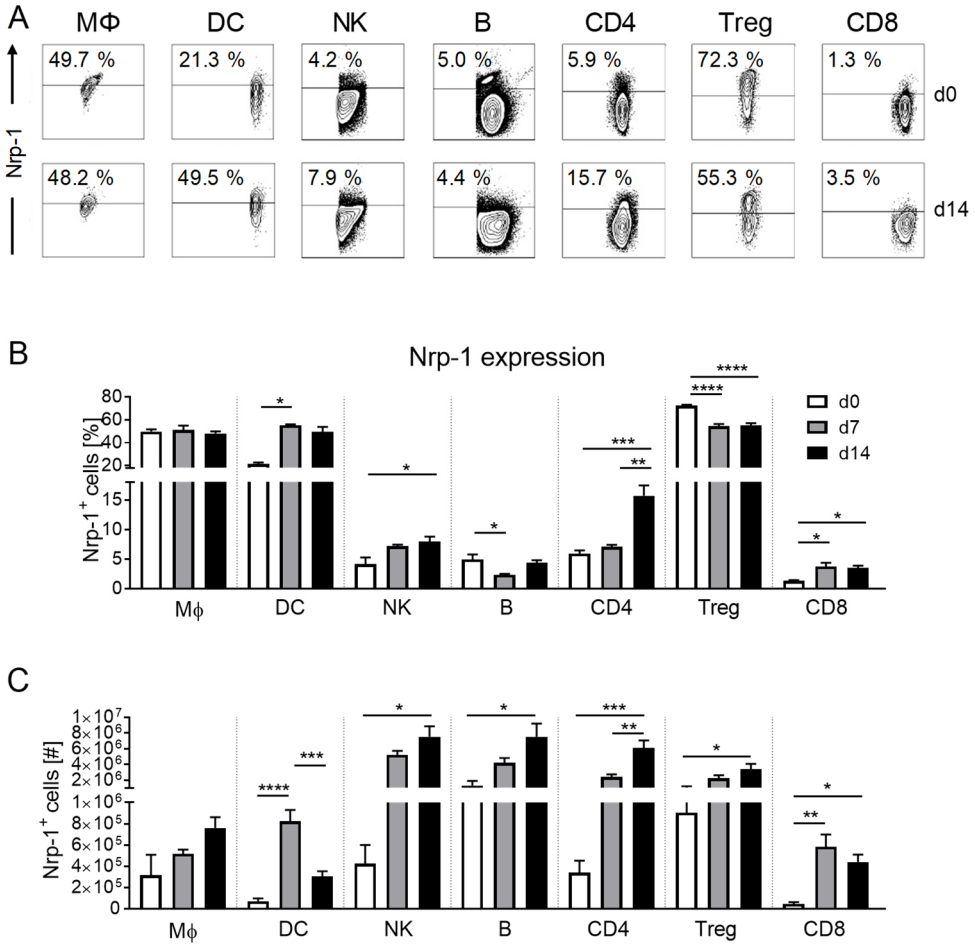

Figure 9: Nrp-1 expression on splenocytes from naïve and PY-infected Balb/c mice

Splenocytes were isolated from naïve (white bars) or PY-infected Balb/c mice on day 7 and 14 p. i. (grey and black bars, respectively). Nrp-1 expression on various immune cells was measured by flow cytometry. (**A**) Representative contour plots show Nrp-1 expression on F4/80^{+}CD11b^{high} macrophages (MΦ), CD11c^{high} dendritic cells (DC), NK1.1^{+}CD3^{-} natural killer (NK) cells, CD19^{+} B cells (B), CD3^{+}CD4^{+}FoxP3^{-} T cells (CD4), CD3^{+}CD4^{+}FoxP3^{+} regulatory T cells (Treg) and CD3^{+}CD8^{+} T cells (CD8) on day 0 or 14 after infection. Frequencies (**B**) and absolute numbers (**C**) of Nrp-1-expressing immune cells from n=4-5 mice per group are shown as means with SEM. To calculate statistical significance within the immune cell populations, one-way ANOVA or non-parametric Kruskal-Wallis test was used. (*p<0.05, **p<0.01, ***p<0.001, ****p<0.0001).

6.1.2 Analysis of the activation state of conventional CD4^{+} T cells during PY infection

As conventional CD4^{+} T cells, defined as CD4^{+}FoxP3^{-}, showed the most prominent alterations in Nrp-1 expression during blood-stage malaria and are at the same time known to play a major role in parasite clearance, we focused on T cells within the following experiments. In order to assess the activation state of CD4^{+} T cells and put it into context with Nrp-1 expression during the course of infection, CD4^{+} T cells of the spleen were analysed by flow cytometry for molecules known to be regulated during malaria. Conventional CD4^{+} T cells were activated and proliferated from the early phase of PY-infection, which was reflected in an increased proportion of CD69^{+} and Ki-67^{+} T cells (Figure 10A and B). On day 14, a significant elevation of antigen-

experienced CD11a$^+$CD49d$^+$ T cells was observed (Figure 10C), but at the same time, immune checkpoint molecules such as PD-1 and CTLA-4, associated with activation but also exhaustion were expressed by CD4$^+$ T cells (Figure 10D and E). Percentages of cytokine-producing CD4$^+$ T cells declined during the course of infection (Figure 10F, G). The increase of Nrp-1 expression on conventional CD4$^+$ T cells followed the pattern of the antigen-experienced CD4$^+$ T cells and was induced during the peak of infection on day 14 of blood-stage malaria (Figure 10H).

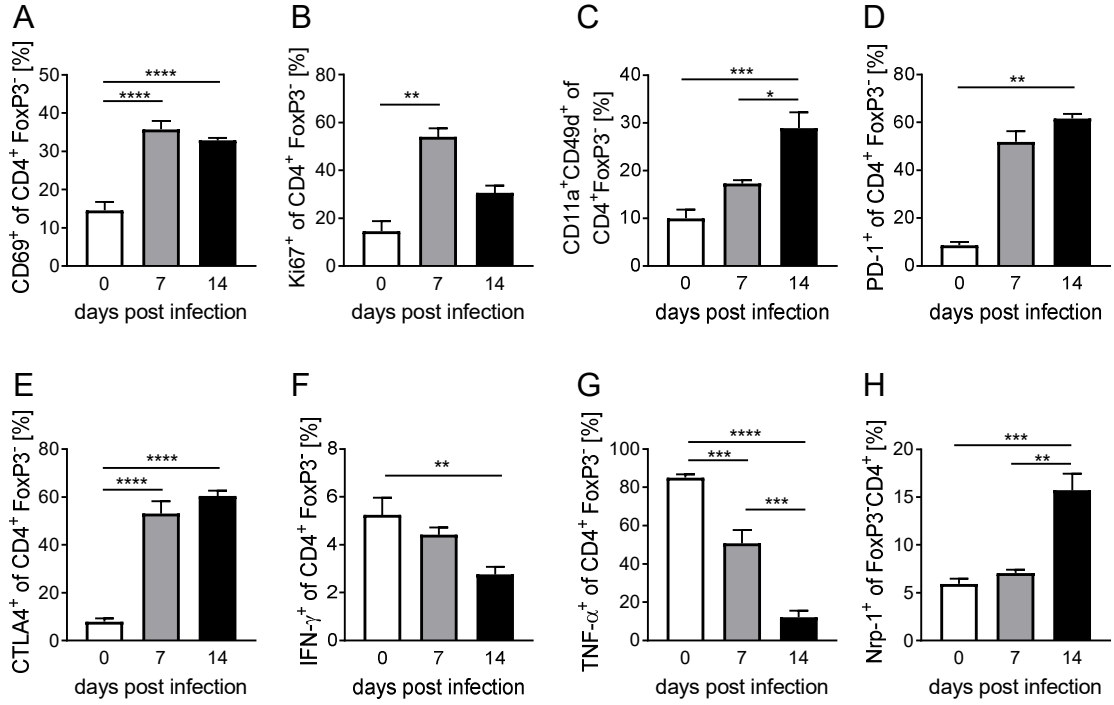

Figure 10: Characterisation of the activation phenotype of conventional CD4$^+$ T cells during PY infection

Immune cells were obtained from spleens of naïve (white bars) or PY-infected Balb/c mice on day 7 and 14 (grey and black bars, respectively). Frequencies of (**A**) CD69$^+$ (**B**) Ki-67$^+$ (**C**) CD11a$^+$CD49d$^+$ (**D**) PD-1$^+$ (**E**) CTLA-4$^+$ (**F**) IFN-γ$^+$ (**G**) TNF-α$^+$ and (**H**) Nrp-1$^+$ CD4$^+$FoxP3$^-$ T cells were measured by flow cytometry. Percentages from n= 4-5 mice per group are displayed as means with SEM. Statistical significance was calculated with one-way ANOVA or Kruskal-Wallis test for non-parametric populations. (*p<0.05, **p<0.01, ***p<0.001, ****p<0.0001).

6.1.3 Nrp-1$^+$ conventional CD4$^+$ T cells showed increased PY-characteristic effector functions

To examine the phenotype of Nrp-1$^+$CD4$^+$FoxP3$^-$ T cells in comparison to their Nrp-1$^-$ counterparts in naïve state and during PY infection, the expression of activation-associated proteins was analysed by flow cytometry in spleens of non-infected and PY-infected Balb/c mice. A detailed analysis of markers for acute PY-characteristic effector functions suggested that Nrp-1$^+$ conventional T cells (orange area in Figure 11) had a higher activation phenotype in the naïve state compared to the Nrp-1$^-$ counterparts (blue area in Figure 11A). Nrp-1$^+$ T cells showed elevated antigen-experience (CD11a$^+$CD49d$^+$), early activation (CD69) and proliferative capacity (Ki-67) in comparison to Nrp-1$^-$ conventional CD4$^+$ T cells.

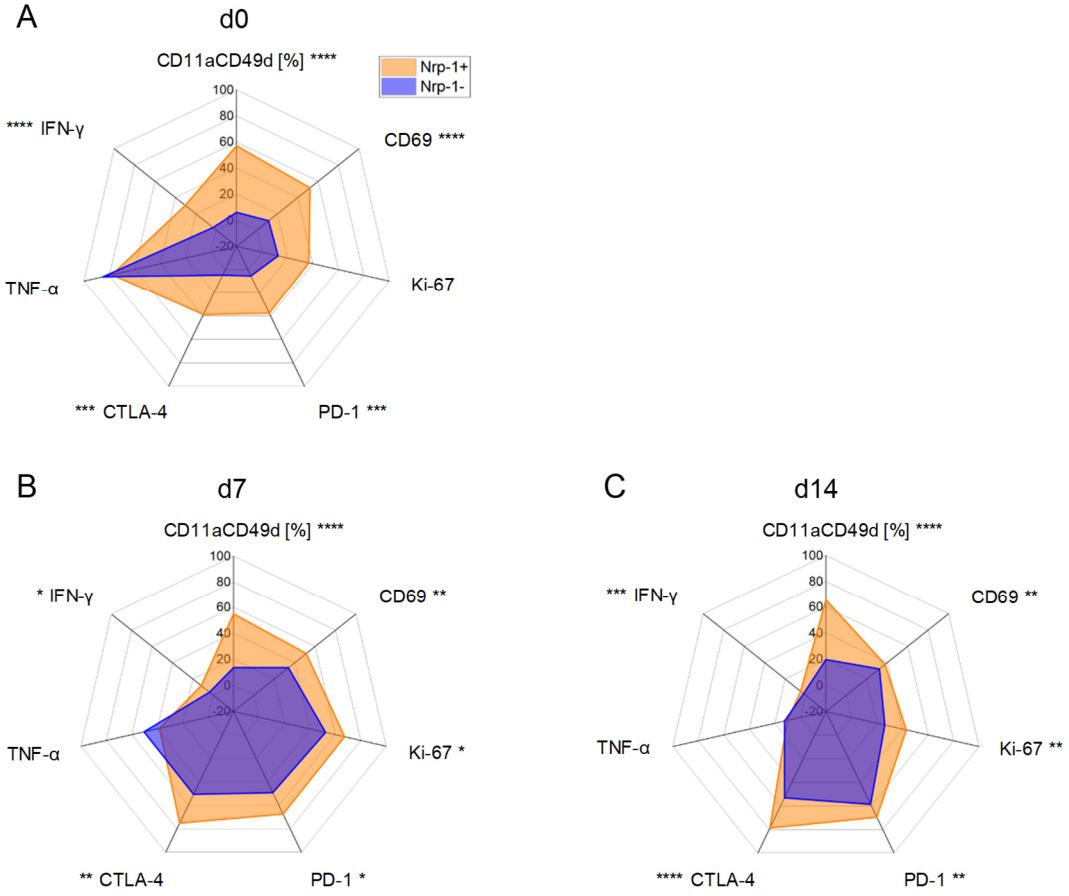

Figure 11: Analysis of the PY-characteristic phenotype of Nrp-1$^{-/+}$ conventional CD4$^+$ T cells in spleens of naive and PY-infected Balb/c mice

Splenocytes were isolated from Balb/c mice on day (**A**) 0, (**B**) 7 or (**C**) 14 post PY-infection. Comparison of Nrp-1$^-$ and Nrp-1$^+$ CD4$^+$FoxP3$^-$ conventional T cells for activation and effector functions was conducted by flow cytometry. (**A**-**C**) Radiation plots visualise mean expression of malaria-characteristic markers on Nrp-1$^-$ (blue area) and Nrp-1$^+$ (orange area) conventional CD4$^+$ T cells in percent. Graphs summarise data from n= 4-5 mice per group. Unpaired t-test or non-parametric Mann-Whitney test was used to test for significance. (*p<0.05, **p<0.01, ***p<0.001, ****p<0.0001).

Additionally, frequencies of PD-1$^+$ and CTLA-4$^+$CD4$^+$FoxP3$^-$ cells as well as the ability of IFN-y production was increased in presence of Nrp-1 expression. The percentage of TNF-α-producing cells was independent of Nrp-1 expression (Figure 11A).

PY infection enhanced the activated phenotype of Nrp-1$^+$CD4$^+$ T cells (Figure 11B and C). Interestingly, significant differences in activation state between Nrp-1$^+$ and Nrp-1$^-$ T cells of naïve mice were reduced upon PY infection, as Nrp-1$^-$CD4$^+$ T cells were also strongly activated in PY-infected Balb/c mice (Blue area in Figure 11B and C).

In summary, the experiments in Balb/c mice suggested that the most prominent alterations of Nrp-1 expression during *P. yoelii* infection occurred in the T cell-compartment, since frequencies and absolute number of Nrp-1$^+$CD4$^+$FoxP3$^-$ T cells were significantly elevated. Moreover, the activation status of Nrp-1$^+$ conventional CD4$^+$ T cells was significantly increased compared to Nrp-1$^-$ T cells. Therefore, the impact of T cell-derived Nrp-1 was analysed in more detail.

6.1.4 The course of *P. yoelii* infection was independent of Nrp-1 ablation on T cells

To investigate the influence of Nrp-1 expression on T cells during blood-stage malaria, Nrp-1$^{fl/fl}$ x CD4cre$^{wt/tg}$ mice were infected with 10^5 PY-infected RBCs. Nrp-1$^{fl/fl}$ mice have two loxP sites that flank exon 2 of the *nrp-1* gene [169]. When these mice were crossed with CD4cre mice, the cre recombinase under the control of the CD4 promoter eliminated the floxed exon 2 of the *nrp-1* gene resulting in an ablation of Nrp-1 expression specifically in T cells. In these mice, the T cell phenotype and parasitemia were analysed 7, 10 and 14 days p.i. (Figure 12A). As illustrated in Figure 12B and C, Nrp-1 expression was significantly reduced on conventional CD4$^+$ T cells as well as on Tregs from Nrp-1$^{fl/fl}$ x CD4cre^{tg} knockout mice (KO) compared to Nrp-1-expressing wildtype littermates (Nrp-1$^{fl/fl}$ x CD4cre^{wt}; WT). The development of T cells in spleens of naïve mice remained unaffected by the Nrp-1 ablation, since the T cell frequencies were constant between naive KO and WT mice. Interestingly, PY infection resulted in elevated percentages of Tregs and CD8$^+$ T cells in the spleens of KO mice at day 7 p.i. (Figure 12D).

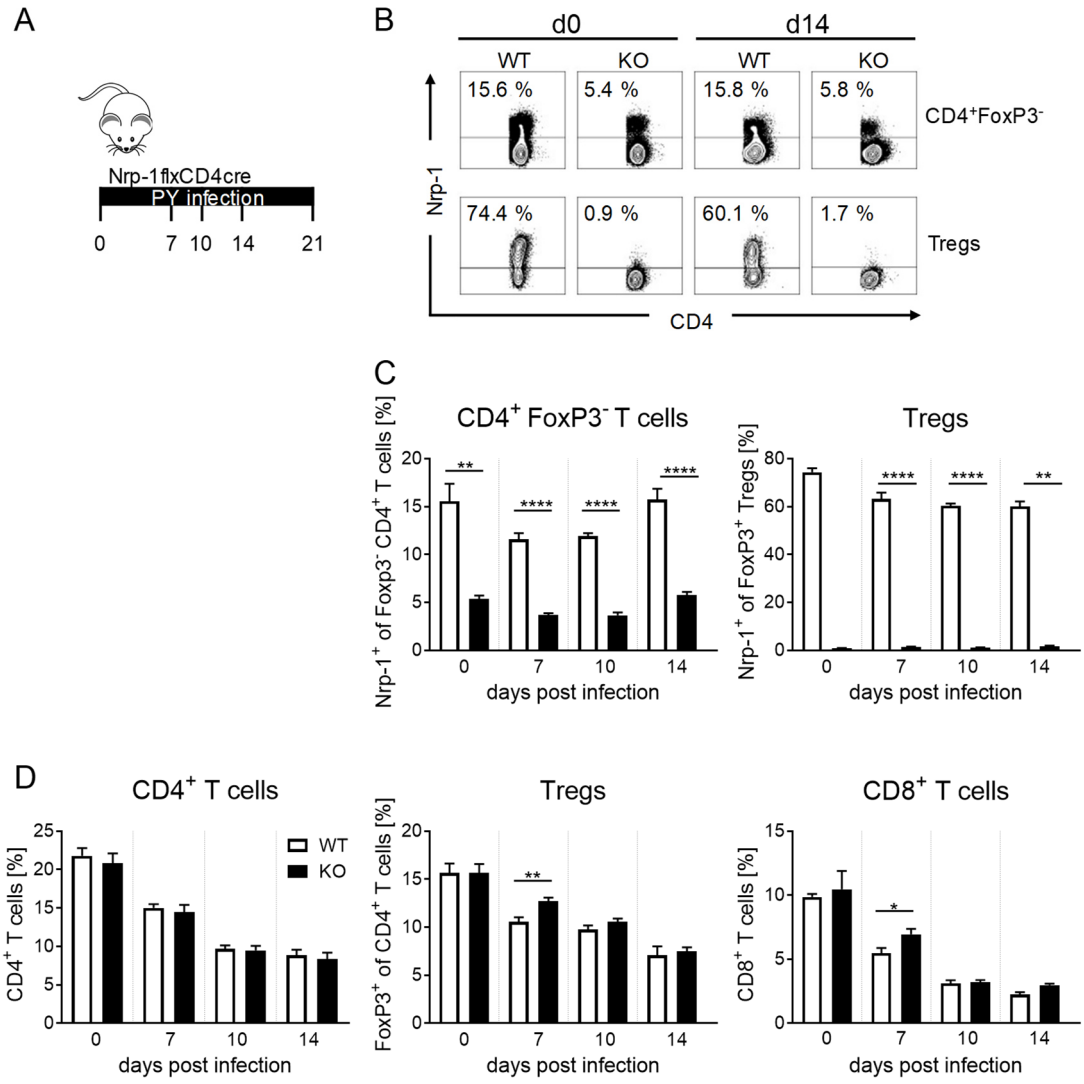

Figure 12 T cell-specific ablation of Nrp-1 increased splenic frequencies of Tregs and CD8⁺ T cells during PY infection

Nrp-1$^{fl/fl}$ x CD4cre$^{wt/tg}$ mice were used to study the influence of T cell-specific ablation of Nrp-1 during PY infection. For this purpose, KO (Nrp-1$^{fl/fl}$ x CD4cre^{tg}, black bars) mice and WT littermates (Nrp-1$^{fl/fl}$ x CD4cre^{wt}, white bars) were intravenously infected with 10^5 PY-infected RBCs. The T cell frequencies and Nrp-1 ablation was analysed in the spleen by flow cytometry 7, 10 and 14 days p.i. (**A**). (**B**) Exemplary contour plots of Nrp-1 expression on CD4⁺FoxP3⁻ conventional T cells (top row) and CD4⁺FoxP3⁺ Tregs (bottom row) analysed by flow cytometry are depicted for WT and KO mice on day 0 (left) and 14 (right) p.i.. (**C**) Nrp-1 expression on conventional CD4⁺ T cells (left) and Tregs (right) and overall T cell frequencies (**D**) were measured in the spleens of WT/KO mice during the course of PY infection. All graphs show mean values with SEM summarised from four independent experiments with n= 3-10 mice per group. Unpaired t-test or Mann-Whitney test was used to calculate significance between the groups within one time point during infection. (*p<0.05, **p<0.01, ****p<0.0001).

Moreover, the T cell-specific ablation in KO mice led to alterations in the activation state of CD4⁺ T cells: On day 7 post infection, WT mice showed an increase of antigen-experienced T cells, which was not observed in the absence of T cell-expressed Nrp-1 (Figure 13A). In the later stage of infection, the proportion of CD11⁺CD49d⁺CD4⁺ T cells in KO mice was elevated on day 14 post infection compared to WT littermates. The proliferative capacity of CD4⁺ T cells, identified by the expression of Ki-67, was

reduced in KO mice, but the frequencies of IFN-γ$^+$ and TNF-α$^+$CD4$^+$ T cells were elevated on day 7 p.i. (Figure 13B, C and D).

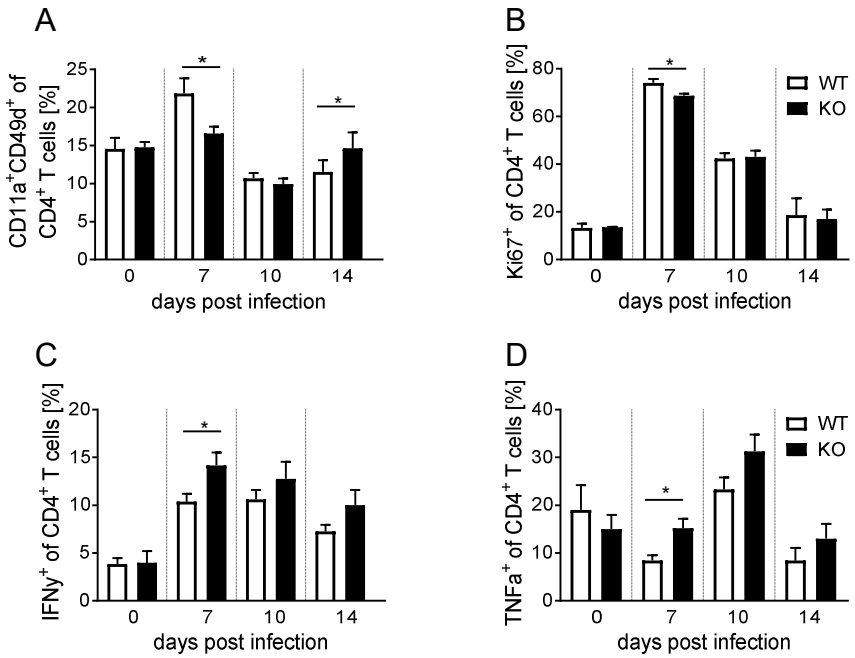

Figure 13 T cell-specific Nrp-1 ablation during PY infection impaired the activation state of splenic CD4$^+$ T cells

T cells were isolated from spleens of PY-infected Nrp-1$^{fl/fl}$ x CD4cre^{tg} knockout mice (KO, black bars) and Nrp-1$^{fl/fl}$ x CD4cre^{wt} littermates (WT, white bars) 0, 7, 10 and 14 days p.i.. The expression of malaria-characteristic activation markers on CD4$^+$FoxP3$^-$ T cells was analysed by flow cytometry. Percentages of (**A**) antigen-experienced (CD11aCD49d), (**B**) Ki-67, (**C**) IFN-γ and (**D**) TNF-α-positive cells are shown as means with SEM. Data are summarised from four independent experiments with n= 3-10 mice per group. Unpaired t-test or Mann-Whitney test was used to calculate significance between the groups within one time point during infection. (*p<0.05).

In summary, Nrp-1 ablation on T cells altered the malaria-characteristic phenotype of CD4$^+$ T cells during the early stage of infection (7 days p.i.). To determine the effect on the clearance of the parasites in the blood, blood smears were stained with Giemsa dye and levels of infected RBCs were counted under a light microscope. As displayed in Figure 14, parasitic loads in the blood were not affected by the altered T cell phenotype in KO mice. Moreover, differences in the enlargement of the spleen, which is associated with inflammation, were not detected between KO mice and WT littermates (Figure 14).

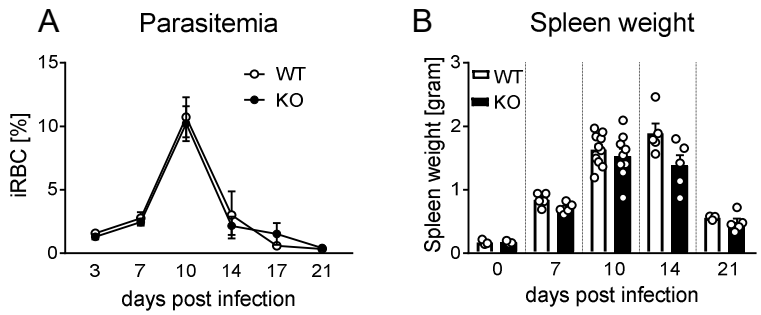

Figure 14 Nrp-1 expression on T cells did not affect the course of blood-stage malaria in Balb/c mice

Blood parasitemia and spleen weight were analysed in Nrp-1$^{fl/fl}$ x CD4cre$^{wt/tg}$ mice during PY infection. (**A**) Pecentages of PY-infected red blood cells (iRBC) were calculated from Giemsa-stained blood smears. Black circles represent Nrp-1$^{fl/fl}$ x CD4cre^{tg} (KO) mice and white circles are the respective Nrp-1$^{fl/fl}$ x CD4cre^{wt} (WT) littermates. (**B**) Spleen weights were determined on d0, d7, d10, d14 and d21 after PY infection. Circles and bars show means with SEM summarised from five independent experiments with n= 3-10 mice per group.

6.1.5 Nrp-1 expression on Tregs was dispensable during *P. yoelii* infection

Since results from previous experiments indicated that Nrp-1 expression was reduced on conventional CD4$^+$ T cells as well as on suppressive Tregs, the following experiments should exclude that the effects of Nrp-1 ablation on Tregs counteract those of Nrp-1-deficient conventional T cells. For this purpose, Nrp-1$^{fl/fl}$ mice were crossed with FoxP3cre mice that expressed the cre recombinase under the control of the FoxP3 promotor [170]. Consequently, Nrp1$^{fl/fl}$ x FoxP3cre^{tg} mice had a Nrp-1 ablation restricted to Tregs and not in conventional CD4$^+$FoxP3$^-$ T cells (Figure 15C and D). Nrp1$^{+/+}$ x FoxP3cre^{tg} littermates were used as wildtype (WT) controls. These mice were intravenously infected with 10^5 PY-infected RBCs and T cell frequencies were analysed on day 14 p.i. by flow cytometry (Figure 15A). In the naïve state, the distribution of T cell frequencies was independent of Nrp-1 expression on Tregs (Figure 15B). During PY-infection, percentages of T cells were equally reduced in mice with and without Treg-expressed Nrp-1. Additionally, the malaria-characteristic T cell phenotype was similar between PY-infected KO mice and WT littermates (data not shown).

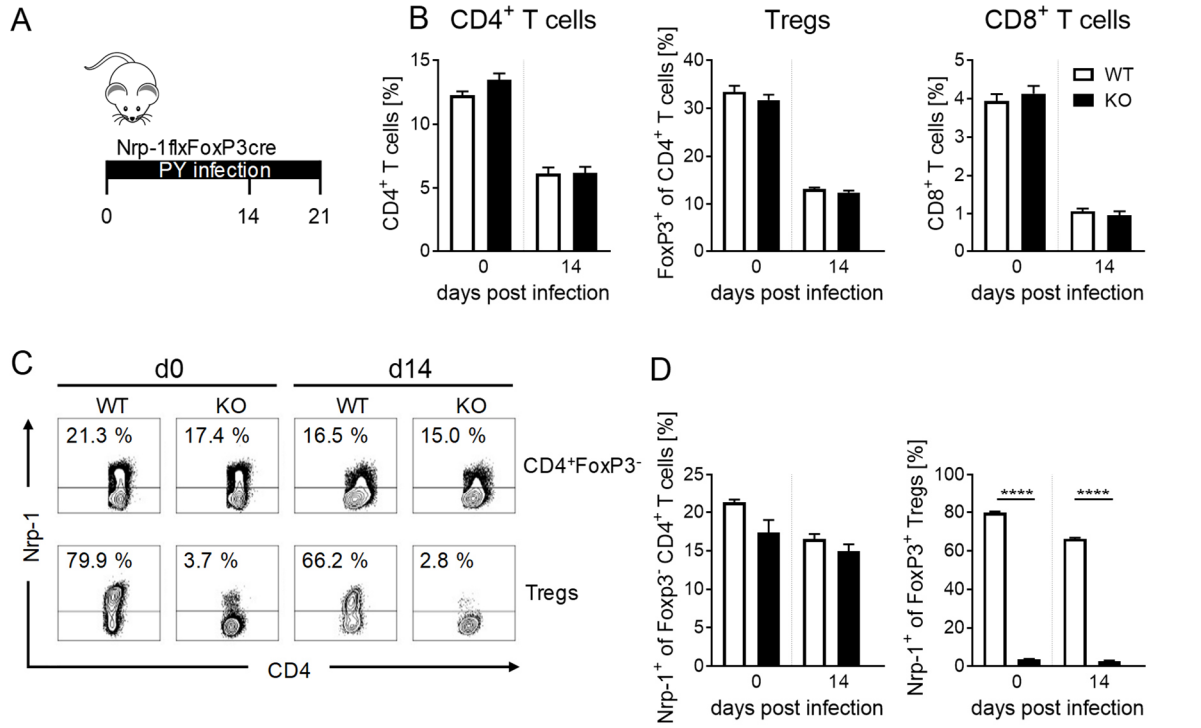

Figure 15 Splenic T cell frequencies were stable during PY infection in the absence of Nrp-1 expression on Tregs

The impact of Treg-expressed Nrp-1 ablation was studied in Nrp-$1^{fl/fl}$ x FoxP3cre^{tg} and Nrp-$1^{+/+}$ x FoxP3cre^{tg} mice during PY infection. Workflow is indicated in (**A**). (**B**) T cell frequencies in Nrp-$1^{fl/fl}$ x CD4cre^{tg} (KO, black bars) mice and Nrp-$1^{+/+}$ x CD4cre^{tg} (WT, white bars) littermates were determined in spleens of naïve or PY-infected mice 14 days p.i.. Representative contour plots (**C**) and summarised bar graphs (**D**) show Nrp-1 expression on conventional $CD4^+FoxP3^-$ T cells (top/ left) and Tregs (bottom/ right) in WT and KO mice on day 0 and 14 after PY infection analysed by flow cytometry. Data are collected from two independent experiments including n= 3 (d0) and n= 10 (PY d14) mice per group and are shown as means with SEM. Unpaired t-test or Mann-Whitney test was used to calculate significance. (****p<0.0001).

In accordance to a stable T cell phenotype, the parasite burden and the spleen weight during PY infection were not significantly altered in mice with Treg-specific Nrp-1 expression (KO) compared to WT littermates (Figure 16A and B). Therefore, Nrp-1 expression on Tregs seems to be negligible during blood-stage malaria.

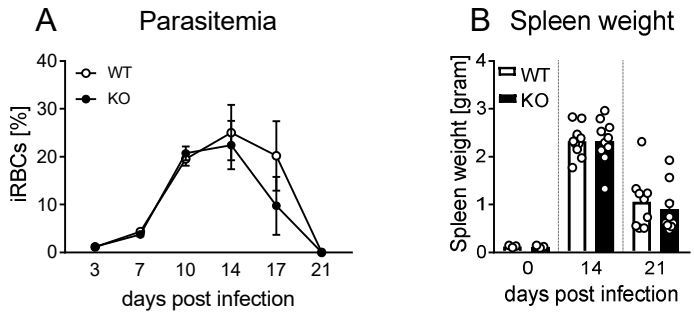

Figure 16 Blood-stage malaria was independent of Treg-specific ablation of Nrp-1

The course of blood-stage malaria was analysed in Nrp-1$^{fl/fl}$ x FoxP3cre^{tg} and Nrp-1$^{+/+}$ x FoxP3cre^{tg} littermates during PY infection. (**A**) Percentages of PY-infected RBCs were determined in Treg-specific Nrp-1-ablated mice (Nrp-1$^{fl/fl}$ x FoxP3cre^{tg}; KO, black circles/bars) on Giemsa-stained blood smears and compared to Nrp-1$^{+/+}$ x FoxP3cre^{tg} littermates (WT, white circles/bars). (**B**) Spleen weight was measured in naïve mice and on day 14 and 21 p.i.. Data was summarised from four independent experiments including n= 3 (uninfected) and n= 9-10 (PY-infected) mice per group and is shown as mean values with SEM.

In summary, PY infection of Balb/c mice resulted in significantly elevated Nrp-1 expression on splenic conventional CD4$^+$ T cells, important players of the parasite clearance during blood-stage malaria. Nrp-1 expression on CD4$^+$ T cells was associated with a highly activated phenotype in the naïve state and during PY infection. T cell-specific ablation of Nrp-1 decreased the proportion of antigen-experienced and proliferated CD4$^+$ T cells, but was associated with an increased cytokine production during PY infection. Nevertheless, the effects of the ablation of Nrp-1 expression on T cells or Tregs did not affect the parasite clearance in PY-infected Balb/c mice. Overall, these results provide evidence that, despite the upregulation of Nrp-1, T cell-expressed Nrp-1 plays only a minor role during blood-stage malaria.

6.2 Analysis of the influence of T cell-expressed Nrp-1 during experimental cerebral malaria

Experimental cerebral malaria (ECM) is an immune-driven disease induced by the rodent *Plasmodium berghei* ANKA parasite. CD8$^+$ T cells are known to migrate from the spleen into the brain, induce blood-brain barrier disruption and contribute to neuroinflammation. Nrp-1 is a molecule, which, besides its role in immune cell interaction, is important for cell migration. Tregs use Nrp-1 to invade tumour tissue and consequently affect anti-tumoural immune responses [32]. However, it is unclear, whether Nrp-1 expression is induced on T cells during ECM and whether this affects the migratory and/or functional properties of CD8$^+$ T cells. Therefore, Nrp-1 expression was characterised in C57BL/6 mice and ablated on T cells and/or Tregs during PbA infection.

6.2.1 Characterisation of Nrp-1 expression on immune cells during ECM

First, WT C57BL/6 mice were infected intravenously with 10^5 PbA-infected RBCs and Nrp-1 expression was examined in the spleen by flow cytometry on various immune cells on day 0 and 7 p.i. (Figure 17). The C57BL/6 background was important, as Balb/c mice are known to be resistant to ECM, which might be partly due to decreased percentages of CXCR3-expressing $CD8^+$ T cells [156].

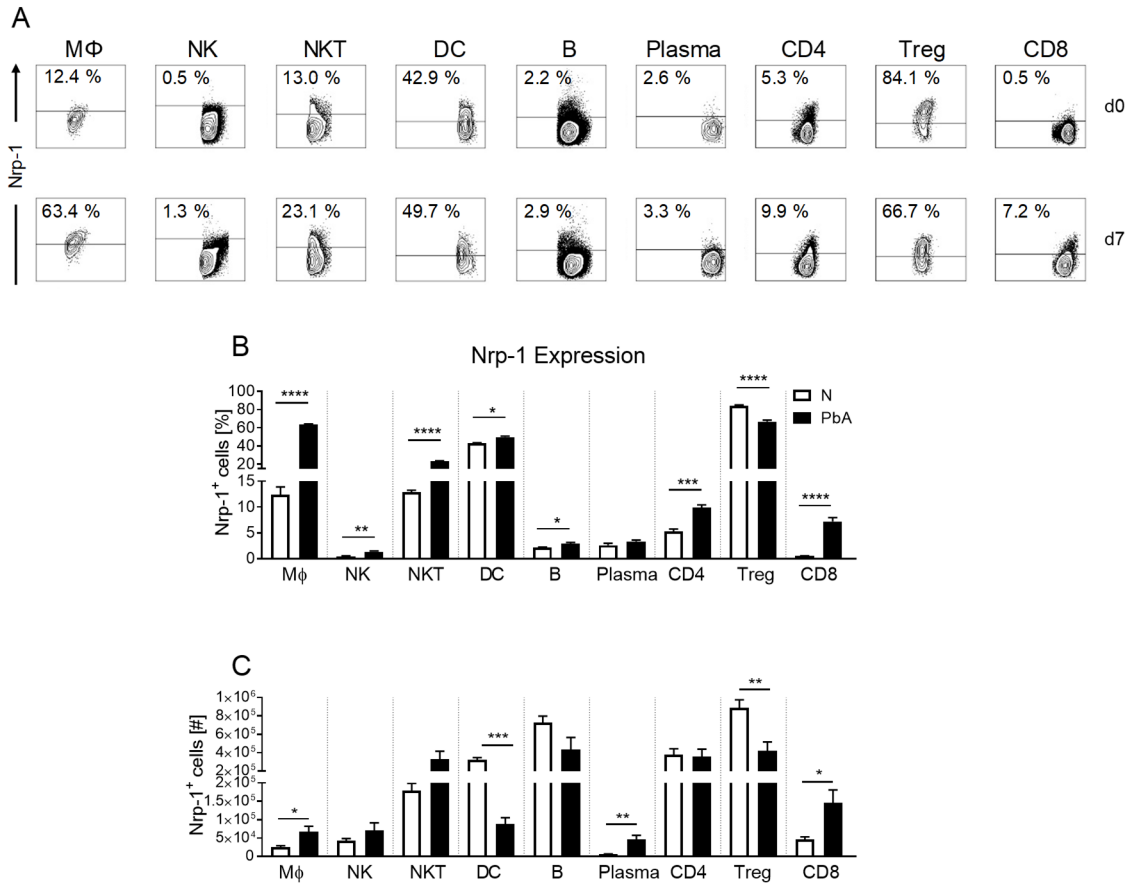

Figure 17 Nrp-1 expression on immune cells in naïve and PbA-infected mice

Spleen cells from naïve (white bars) or PbA-infected C57BL/6 mice (black bars) were isolated on day 7 post infection. Nrp-1 expression on various immune cells was measured by flow cytometry. (**A**) Representative contour plots show Nrp-1 expression on $F4/80^+CD11b^{high}$ macrophages (MΦ), $NK1.1^+CD3^-$ natural killer (NK) cells, $NK1.1^+CD3^+$ natural killer T (NKT) cells, $CD11c^{high}$ dendritic cells (DC), $CD19^+CD138^-$ B cells (B), $CD19^+CD138^+$ plasma cells (Plasma), $CD3^+CD4^+FoxP3^-$ T cells (CD4), $CD3^+CD4^+FoxP3^+$ regulatory T cells (Treg) and $CD3^+CD8^+$ T cells (CD8) on day 0 (top) and 7 p.i. (bottom). Frequencies (**B**) and absolute numbers (**C**) of Nrp-1-expressing immune cells from n= 4-5 mice per group are depicted as means with SEM. Unpaired t-test or Mann-Whitney test was used to calculate statistics between the two time points of infection within one immune cell population. (*p<0.05, **p<0.01, ***p<0.001, ****p<0.0001).

PbA infection in C57BL/6 mice led to an increase of Nrp-1 expression in every analysed immune cell population of the spleen, including innate immune cells like macrophages, NK, NKT and DCs as well as B cells (Figure 17B). Within the T cell compartment, the percentage of conventional $CD4^+FoxP3^-$ T cells that expressed Nrp-1 was doubled, whereas Tregs showed a decrease of Nrp-1 expression from 84 % in the naïve state to 67 % after seven days of PbA-infection. Whereas only 0.5 % of $CD8^+$ T cells

expressed Nrp-1 on their surface in naïve mice, the frequency was significantly elevated to 7 % during the manifestation of ECM. Strikingly, only the absolute numbers of Nrp-1$^+$ macrophages, plasma cells and Nrp-1$^+$CD8$^+$ T cells showed a significant increase during PbA-infection (Figure 17C).

6.2.2 Kinetics of the Nrp-1 expression on T cells in the spleen, blood and brain during PbA-infection

As PbA infection led to highly significant alterations in Nrp-1$^+$CD4$^+$ and especially CD8$^+$ T cells 7 days p.i., the time course of Nrp-1 expression was analysed in spleens of PbA-infected C57BL/6 mice. The frequencies of Nrp-1-expressing conventional CD4$^+$ T cells as well as CD8$^+$ T cells was increased in the spleen at day 5 p.i., which correlated with the time point of neurological deficits due to ECM manifestation (Figure 18A, left and right). Absolute numbers of Nrp-1$^+$CD8$^+$ T cells were doubled on day 6 compared to day 0 after infection (Figure 18B, right). In contrary, the progression of the disease led to significantly reduced Nrp-1 expression on FoxP3$^+$ Tregs (Figure 18A and B, centre).

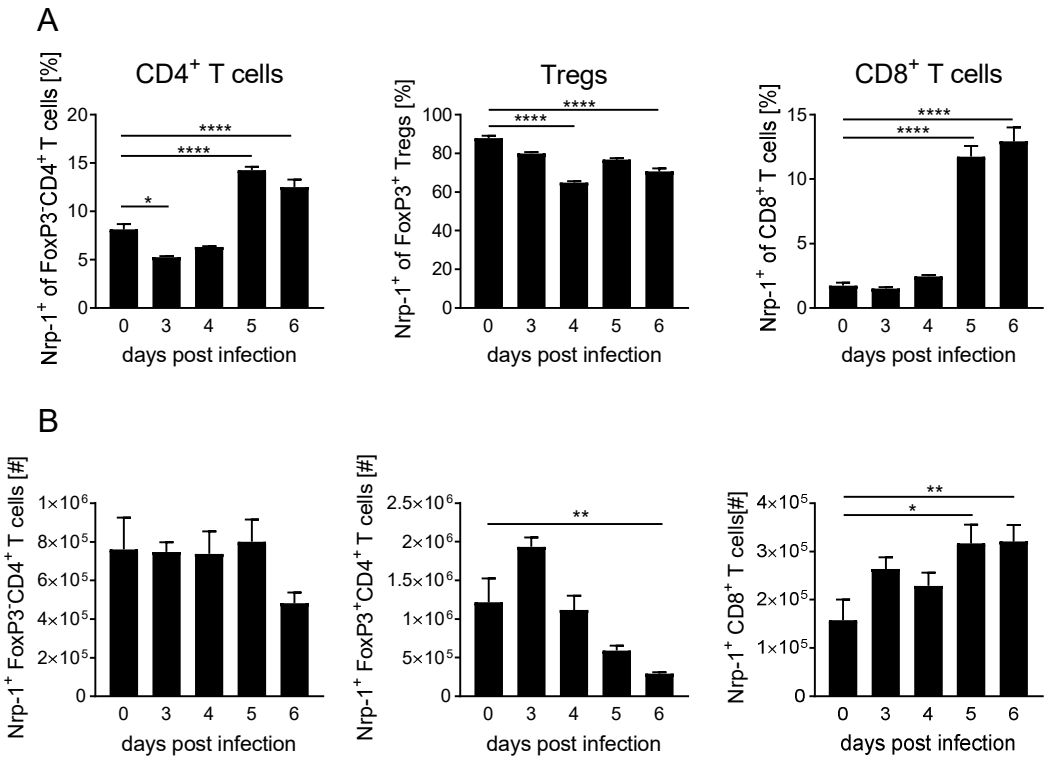

Figure 18 The manifestation of ECM resulted in increased Nrp-1 expression on conventional CD4$^+$ and CD8$^+$ T cells in the spleen of PbA-infected mice

T cells from spleens of naïve or PbA-infected C57BL/6 mice were analysed for Nrp-1 expression during the course of ECM. Frequencies (**A**) and absolute numbers (**B**) of CD4$^+$FoxP3$^-$ T cells (left), Tregs (centre) and CD8$^+$ T cells (right) were measured by flow cytometry. Data from five independent experiments with n= 5-11 mice per time-point are shown as means with SEM. Statistical significance was calculated with one-way ANOVA or non-parametric Kruskal-Wallis test. (*p<0.05, **p<0.01, ****p<0.0001).

After the priming of the T cells in the spleen, they are released into the blood stream. In the blood, the frequencies and absolute numbers of Nrp-1$^+$ Tregs decreased with the course of infection as observed in the spleen (Figure 19A and B, centre). With reduced frequencies of Nrp-1$^+$ suppressive Tregs, the frequencies of Nrp-1$^+$ conventional CD4$^+$ T cells increased significantly on day 5 and more prominently on day 6 p.i. (Figure 19A and B left). Nrp-1-positive CD8$^+$ T cells steadily increased in their frequencies and numbers by the factor of 10: From 10 Nrp-1$^+$CD8$^+$ T cells per µL blood in the naïve state, the numbers increased to approximately 50 on day 5 and 100 during the peak of PbA-infection on day 6 (Figure 19B, right).

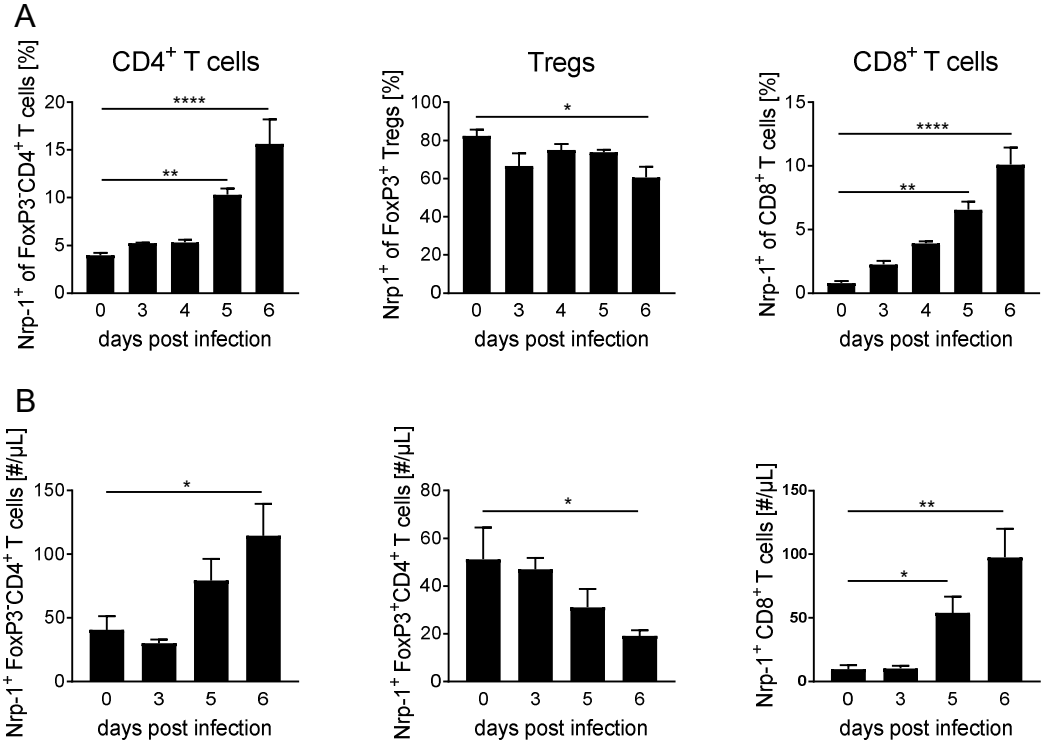

Figure 19 PbA infection led to elevated Nrp-1 expression on conventional CD4$^+$ and CD8$^+$ T cells in the blood

Immune cells were isolated from the blood of naïve and PbA-infected C57BL/6 mice. Nrp-1 expression on T cells was measured by flow cytometry. Frequencies (**A**) and absolute numbers (**B**) of Nrp-1$^+$CD4$^+$FoxP3$^-$ T cells (left), FoxP3$^+$ Tregs (centre) and CD8$^+$ T cells (right) are shown as means with SEM. Data from five independent experiments with n= 5-11 (A) and three independent experiments with n= 5-6 (B) mice per time point are summarised and statistics were calculated with one-way ANOVA or Kruskal-Wallis test. (*p<0.05, **p<0.01, ****p<0.0001).

During PbA infection, it is described that CD8$^+$ T cells actively migrate from the blood to the brain, recognise cross-presented antigens on endothelial cells and can induce blood-brain barrier disruption due to their cytotoxic activity. At this late phase of ECM, an influx of peripheral CD4$^+$ and CD8$^+$ T cells was measured by flow cytometry in the brain (data not shown). In the naïve brain, 12 % of peripheral CD4$^+$ T cells and 3 % of CD8$^+$ T cells expressed Nrp-1, corresponding to approximately 1100 Nrp1$^+$CD4$^+$ and

110 Nrp1^{+}CD8^{+} T cells (Figure 20B and C). The frequencies of Nrp-1^{+} T cells in the brain steadily increased with progression of ECM. Five days post infection, the percentage of Nrp-1^{+}CD4^{+} T cells was doubled and with ECM manifestation on day 6, the Nrp-1 expression of CD4^{+} as well as CD8^{+} T cells was significantly elevated: 45 % of CD4^{+} T cells and 40 % of CD8^{+} T cells present in the damaged brain expressed Nrp-1. In absolute numbers, approximately 30,000 Nrp-1^{+}CD4^{+} T cells were counted in the brain on day 6 after infection. Strikingly, the numbers of Nrp-1^{+}CD8^{+} T cells increased by the factor 1480 compared to the numbers in brains of naïve mice, which corresponds to approximately 160,000 Nrp-1^{+}CD8^{+} T cells in brains of mice suffering from ECM (Figure 20C).

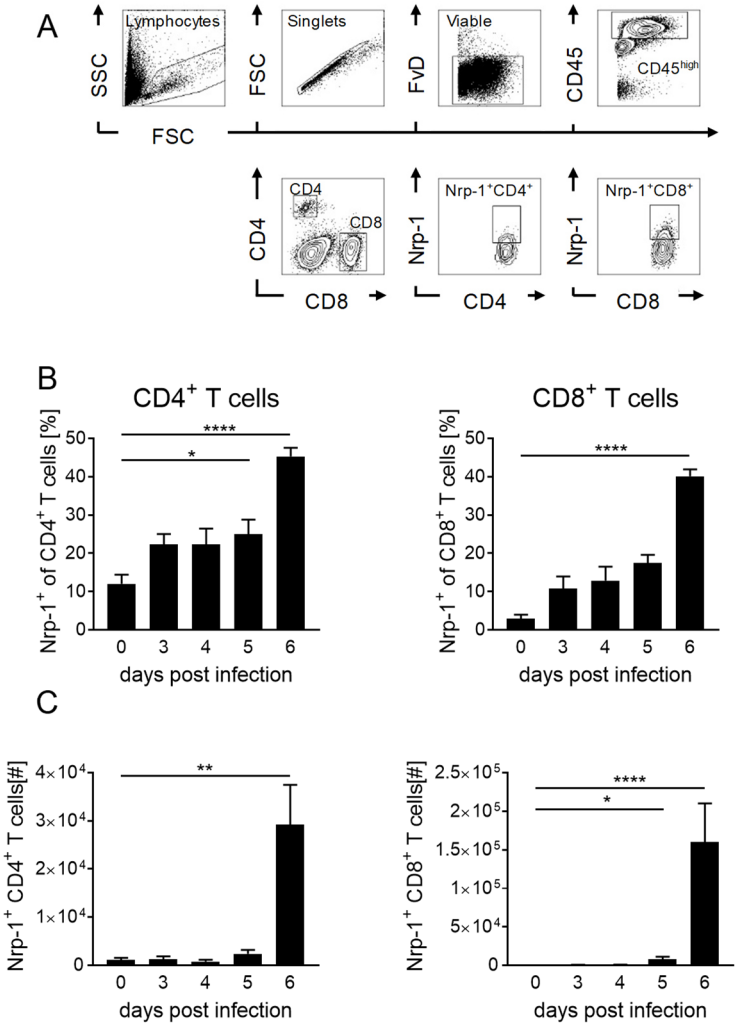

Figure 20 ECM was associated with a significant increase of Nrp-1-expressing CD4^{+} and CD8^{+} T cells in the brains of PbA-infected mice

Perfused brains were collected from PbA-infected C57BL/6 mice on day 0, 3, 4, 5 and 6 after infection. Peripheral immune cells were isolated by Percoll centrifugation and analysed by flow cytometry. (**A**) Representative contour plots show the gating strategy for the analysis of Nrp-1 expression on T cells on day 6 after infection. Infiltrated peripheral immune cells were characterised by CD45^{high} expression. (**B**) Percentages and (**C**) absolute numbers of peripheral Nrp-1-positive CD4^{+} (left) and CD8^{+} T cells (right) are shown as mean values. Error bars represent SEM. Data from five independent experiments including n= 5-11 mice per time point are summarised and significances were calculated with one-way ANOVA or non-parametric Kruskal-Wallis test. (*p<0.05, **p<0.01, ****p<0.0001).

6.2.3 Analysis of the malaria-characteristic phenotype of CD8⁺ T cells

In the following experiment, the activation phenotype of CD8⁺ T cells in the spleens of C57BL/6 mice was investigated in the context of ECM. In the early phase of infection on day 3, an immediate elevation of antigen-experienced CD11a⁺CD8⁺ T cells was observed, which steadily increased with the manifestation of disease (Figure 21A). From day 4 on, the activation marker CD69 was increasingly expressed and the percentages of proliferative (Ki-67⁺), IFN-γ-producing and cytotoxic CD8⁺ T cells (GzmB⁺) as well as PD-1 expressing CD8⁺ T cells were enhanced with the progression of the disease (Figure 21B-F). Starting from day 5, when the first neurological deficits appeared in the behaviour of the mice, CXCR3, a receptor essential for the migration of CD8⁺ T cells from the periphery into the ECM-damaged brain, was upregulated on the surface of CD8⁺ T cells (Figure 21G).

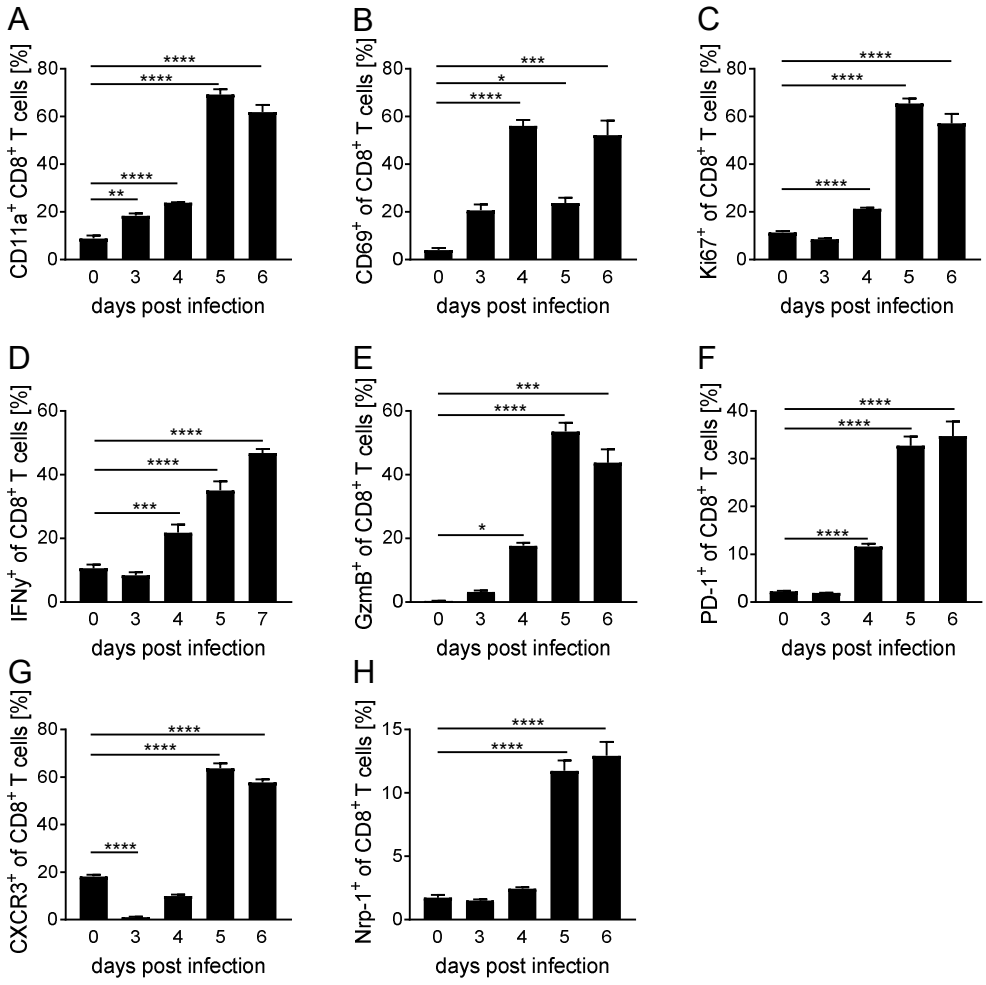

Figure 21 Characterisation of the malaria-characteristic activation phenotype of CD8⁺ T cells during PbA infection

Splenocytes from PbA-infected C57BL/6 mice were isolated 0, 3, 4, 5 and 6 or 7 days post PbA-infection. CD8⁺ T cell were analysed for their expression of (**A**) CD11a, (**B**) CD69, (**C**) Ki-67, (**D**) IFN-γ, (**E**) GzmB, (**F**) PD-1, (**G**) CXCR3 and (**H**) Nrp-1 by flow cytometry. Data from four independent experiments including n= 3-14 mice per time point are shown as means with SEM. One-way ANOVA or Kruskal-Wallis test were used to calculate significance. (*p<0.05, **p<0.01, ***p<0.001, ****p<0.0001).

Interestingly, the time point during ECM at which Nrp-1 expression was induced in $CD8^+$ T cells corresponded to the highest upregulation of molecules involved in T cell activation, proliferation and migration (Figure 21H).

6.2.4 Percentages of Nrp-1^+CD8^+ T cells correlated with ECM pathology

Since the increased frequencies of Nrp-1^+CD8^+ T cells occurred at the time of the first neurological deficits during ECM, the following experiments should clarify whether Nrp-1 expression correlated with the severity of disease in C57BL/6 mice. The RMCBS score was used to quantify the severity of ECM pathology considering different behavioural and neurological deficits on day 3, 4, 5, and 6 after PbA infection [171]. Healthy animals had a score of 18-20, while with progression of PbA-infection the score declined. A score under 12 defined mice with ECM manifestation. In the spleen of C57BL/6 mice, percentages of $CD8^+$ T cells were independent of the ECM pathology, but negatively correlated with the parasite load (Figure 22A and B, top).

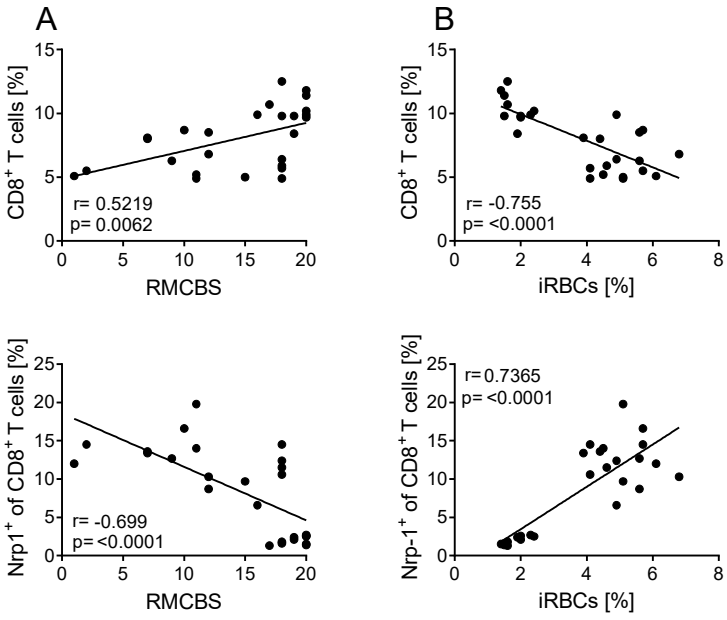

Figure 22 Frequencies of Nrp-1^+CD8^+ T cells in the spleen correlated with severity of ECM and parasitemia

The severity of ECM in PbA-infected C57BL/6 mice was quantified by the RMCBS score on day 3, 4, 5 and 6 post PbA-infection. The maximum score of 20 corresponded to healthy mice without any neurological abnormalities. With progression of PbA infection, increasing neurological deficits led to a decrease in the score. ECM manifestation with neurological deficits was characterised by a RMCBS score under 12. Parasitemia was determined in blood samples by detection of GFP-tagged parasites by flow cytometry. Percentages of $CD8^+$ and Nrp-1^+CD8^+ T cells were determined on day 3, 4, 5 and 6 post infection by FACS. Correlation of the frequencies of $CD8^+$ T cells (top) or Nrp-1^+CD8^+ T cells (bottom) in the spleen with the (**A**) severity of ECM, quantified by the RMCBS score, or (**B**) the levels of blood parasitemia are illustrated. Data from five independent experiments including n= 5-11 mice per time point are summarised. Pearson correlation coefficient or nonparametric Spearman correlation was used to test significance.

In contrast to that, the frequencies of splenic Nrp-1$^+$CD8$^+$ T cells analysed on day 3, 4, 5 and 6 p.i. showed a significant positive correlation with the severity of ECM, characterised by a decreased score, as well as with the increase of parasitemia (Figure 22A and B, bottom).

In contrast to the CD8$^+$ T cells in the spleen, the percentages of CD8$^+$ T cells in the blood and brain were independent of the severity of ECM (Figure 23 A and B, top). However, the presence of Nrp-1$^+$CD8$^+$ T cells in the blood and especially in the brain positively correlated with the pathology in PbA-infected C57BL/6 mice (Figure 23 A and B, bottom).

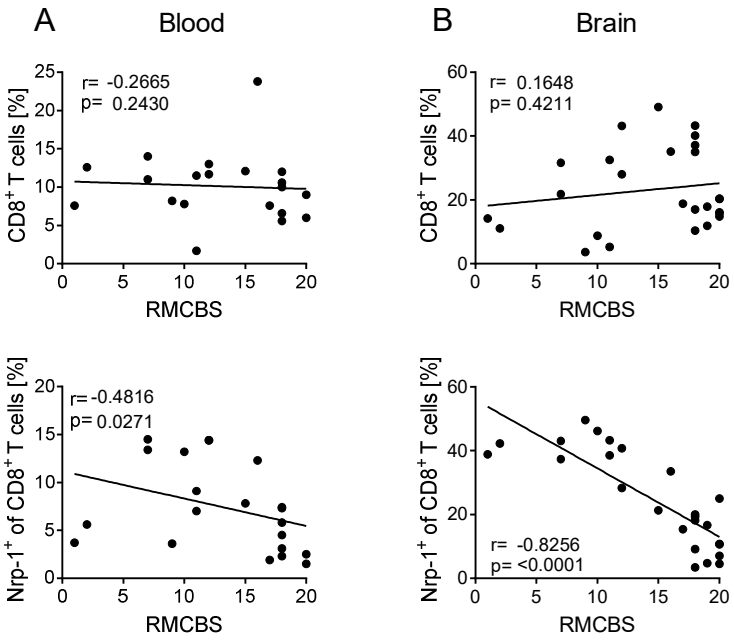

Figure 23 Frequencies of Nrp-1$^+$CD8$^+$ T cells in the blood and brain correlated with the severity of ECM

Pathology of ECM in C57BL/6 mice was measured by the RMCBS score on day 3, 4, 5 and 6 after PbA-infection. Manifestation of ECM with neurological deficits was associated with reduced scores. With flow cytometry, frequencies of CD8$^+$ and Nrp-1$^+$CD8$^+$ T cells were determined in the blood and brain of PbA-infected C57BL/6 mice. Correlation of the frequencies of CD8$^+$ T cells (top) or Nrp-1$^+$CD8$^+$ T cells (bottom) are shown in the blood (**A**) and brain (**B**). Data from four (blood) and five (brain) independent experiments including n= 5-11 mice per time point are shown. Pearson correlation coefficient or nonparametric Spearman correlation was used for statistics.

In summary, these results showed that CD8$^+$ T cells, the main players during the development of ECM, were activated during PbA-infection. Strikingly, the upregulation of Nrp-1 on the surface of CD8$^+$ T cells correlated with the time of CD8$^+$ T cell activation and more importantly with the appearance of neurological deficits and manifestation of ECM. Precisely, the severity of ECM and the parasitic burden of C57BL/6 mice positively correlated with the frequencies of Nrp-1$^+$CD8$^+$ T cells in the spleen, blood and brain, suggesting that Nrp-1 expression on CD8$^+$ T cells has an impact on the development of ECM.

6.2.5 Expression of genes involved in T cell activation was altered in Nrp-1^{+}CD8^{+} T cells

As elevated frequencies of Nrp-1^{+}CD8^{+} T cells were associated with an aggravated pathology during ECM, the molecular phenotype of Nrp-1^{+} and Nrp-1^{-}CD8^{+} T cells from PbA-infected mice was characterised in more detail. For this purpose, gene expression of 2,000 sorted Nrp-1^{+} or Nrp-1^{-}CD8^{+} T cells isolated from spleens of PbA-infected C57BL/6 mice on day 6 were analysed by Affymetrix Microarray by the Helmholtz Centre for Infection Research in Brunswick.

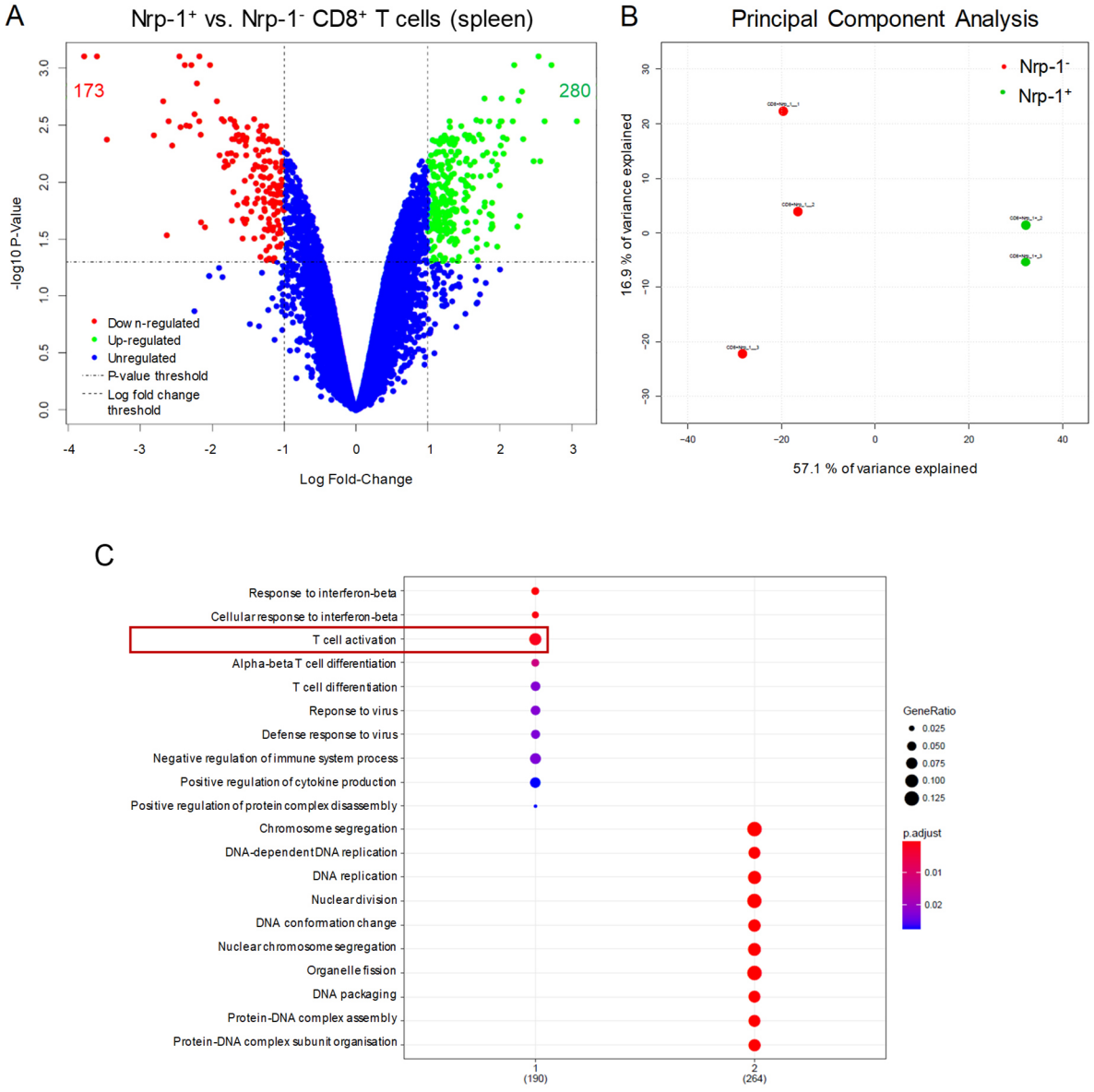

Figure 24 Gene expression profiling of Nrp-1^{+} and Nrp-1^{-}CD8^{+} T cells during ECM

Spleen cells of PbA-infected C57BL/6 mice were isolated 6 days p.i.. CD8^{+} T cells were sorted in 2,000 Nrp-1^{+} and Nrp-1^{-}CD8^{+} T cells and processed with the single-cell lysis kit (Invitrogen). Samples were further processed and Affymetrix Microarray and gene analyses kindly conducted by Robert Geffers at the Helmholtz Centre for Infection Research in Brunswick. (**A**) Results from Nrp-1^{+} compared to Nrp-1^{-}CD8^{+} T cells are shown as volcano plot. Unregulated genes are depicted as blue, down-regulated as red and upregulated genes as green dots. (**B**) Principle component analysis was calculated for Nrp-1^{-} (red) and Nrp-1^{+}CD8^{+} T cells (green). (**C**) Enriched Gene Ontology Analysis was conducted with GO-Term “Biological Process” with a qValue CutOff at 0.05.

The volcano plot in Figure 24A compared the magnitude of changes in gene expression (fold-change, x-axis) of the two populations of interest concerning statistical significance in form of the p-value on the y-axis. The analysis identified 173 genes that were significantly downregulated in Nrp-1^{+}CD8^{+} T cells compared to Nrp-1^{-} counterparts, whereas the expression of 280 genes was upregulated. The principal component analysis showed that Nrp-1^{+} and Nrp-1^{-}CD8^{+} T cells form two separate gene clusters (Figure 24B). Significant differences in gene expression were found i.e. in the cluster including genes that are involved in T cell activation (Figure 24C).

6.2.6 Nrp-1^{+}CD8^{+} T cells had a highly activated phenotype during ECM

As Microarray analysis revealed differences in T cell activation between Nrp-1^{+} and Nrp-1^{-}CD8^{+} T cells, a detailed characterisation of malaria-characteristic markers was conducted by flow cytometry. Nrp-1^{+}CD8^{+} T cells (orange area in Figure 25) isolated from spleens of PbA-infected C57BL/6 mice on day 6 or 7 p.i. showed a highly activated ECM-specific T cell phenotype compared to Nrp-1^{-}CD8^{+} T cells (blue area in Figure 25).

Nrp-1^{+}CD8^{+} T cells expressed elevated frequencies of proteins associated with activation and exhaustion such as PD-1, CTLA-4, Tim-3, Lag-3, CD160 and killer cell lectin-like receptor subfamily G member 1 (KLRG-1) compared to Nrp-1^{-}CD8^{+} T cells (Figure 25B). Additionally, percentages of malaria-characteristic proteins associated with antigen-experience (CD11a), migration (CXCR3), cytotoxicity (GzmB), proliferation (Ki-67), degranulation of toxic granules (CD107), early activation (CD69) and cytokines (IFN-γ and TNF-α) were significantly upregulated among the CD8^{+} T cells that expressed Nrp-1 on their surface (Figure 25C).

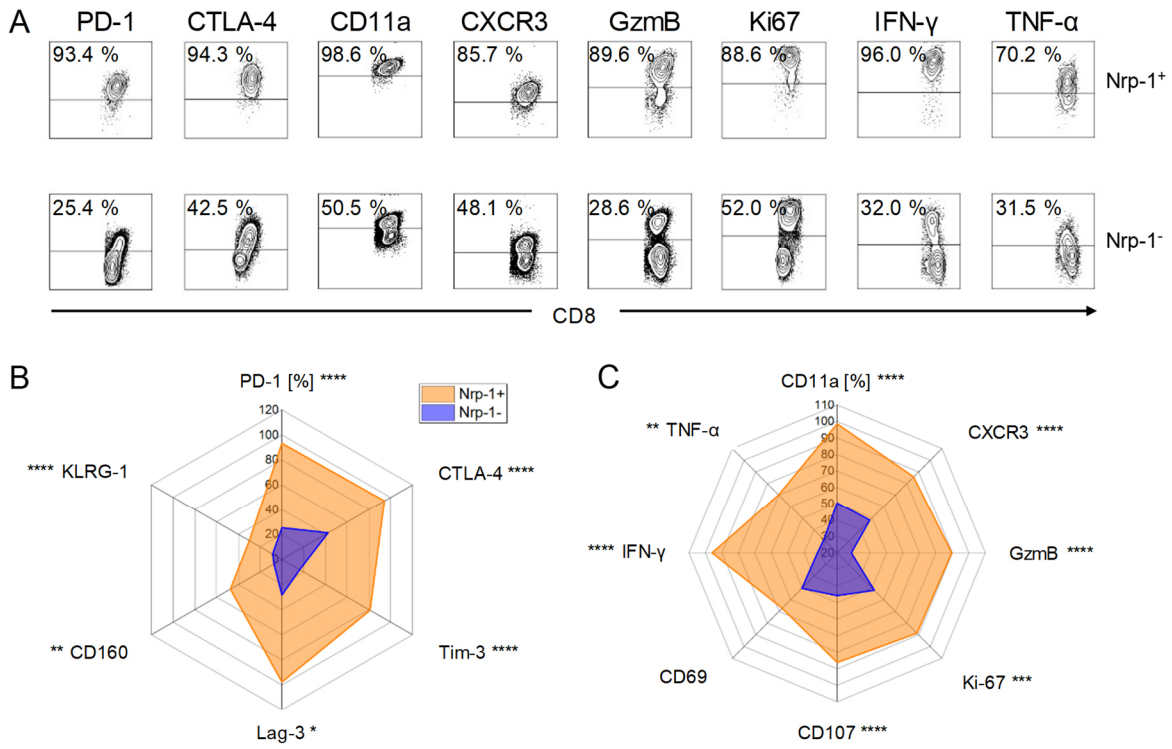

Figure 25 Nrp-1$^+$CD8$^+$ T cells had a highly activated malaria-characteristic phenotype

The activation state of splenic Nrp-1$^+$ and Nrp-1$^-$CD8$^+$ T cells from PbA-infected C57BL/6 were characterised by flow cytometry 6 or 7 days p.i.. (**A**) Representative contour plots show the expression of various malaria-characteristic markers on Nrp-1$^+$ (top) and Nrp-1$^-$ (bottom) CD8$^+$ T cells. (**B** and **C**) Radiation plots present mean values of these markers on Nrp-1$^+$ (orange area) and Nrp-1$^-$CD8$^+$ T cells (blue area) summarised from n= 3-5 mice. Unpaired t-test or non-parametric Mann-Whitney test was used to calculate statistics between the two immune cell populations. (*p<0.05, **p<0.01, ***p<0.001, ****p<0.0001).

In addition to the activated T cell phenotype, the presence or absence of Nrp-1 expression on CD8$^+$ T cells had an influence on the memory subset distribution: During acute PbA-infection, the majority of Nrp-1$^-$CD8$^+$ T cells were naïve T cells (T_N), characterised by high expression of CD62L and low expression of CD44. Only a minor percentage of Nrp-1$^-$ T cells were CD62L$^-$CD44$^+$ effector memory or CD62L$^+$CD44$^+$ central memory T cells (T_{EM} and T_{CM}, respectively). Within the Nrp-1$^+$CD8$^+$ T cell population, the majority of cells (61 %) were T_{CM} cells, while the T_N population was highly significantly decreased (Figure 26B).

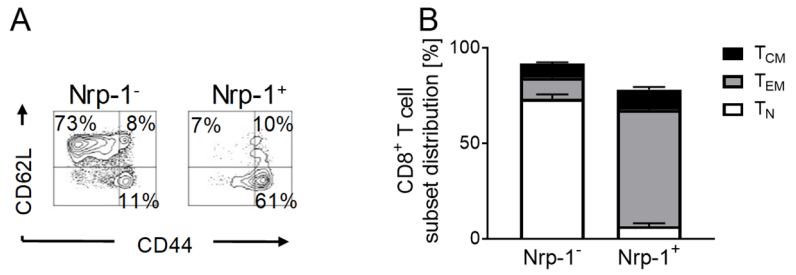

Figure 26 Nrp-1$^+$CD8$^+$ T cells were predominantly effector memory T cells

Spleen cells were isolated from naïve or PbA-infected C57BL/6 mice on day 7 post infection and were characterised by flow cytometry. (**A**) Representative contour plots show Nrp-1$^-$ (left) and Nrp-1$^+$ (right) CD8$^+$ T cells seven days post PbA infection. Expression of CD44 and CD62L was measured on the surface of these cells. (**B**) Distribution of naïve and memory T cell subsets are shown as mean values + SEM. Naïve T cells (T_N) were characterised by CD62L$^+$CD44$^-$ expression. Effector memory T cells (T_{EM}) were identified by their expression of CD62L$^-$CD44$^+$ and central memory T cells (T_{CM}) were CD62L$^+$CD44$^+$. Graphs include data from n= 3-4 mice.

In summary, frequencies of Nrp-1$^+$CD8$^+$ T cells not only correlated with ECM pathology and the parasite load in the blood, but also showed alterations in the expression of genes involved in T cell activation. Flow cytometry confirmed a highly activated ECM-characteristic T cell phenotype of Nrp-1$^+$CD8$^+$ T cells and high frequencies of effector memory T cells within this population.

6.2.7 T cell-specific ablation of Nrp-1 reduced peripheral immune cells in the brain and attenuated ECM severity

To further analyse the role of Nrp-1 expression on T cells in the course of ECM and the T cell phenotype during PbA-infection, Nrp-1$^{fl/fl}$ x CD4cre$^{wt/tg}$ mice with a C57BL/6 background were used in the following experiments. According to the Nrp-1$^{fl/fl}$ x CD4cre/c mice with Balb/c background that were used for studies in PY-infection (section 6.1.4), the Nrp-1$^{fl/fl}$ x CD4cre^{tg} (KO) mice had a loxP flanked exon two within the *nrp-1* gene that was removed by the cre recombinase in T cells [169]. Nrp-1$^{fl/fl}$ x CD4cre^{wt} littermates were used as WT control animals. These mice were infected with 10^5 PbA-infected RBCs intravenously. Spleen, blood and brain were analysed on day 6 or 7, when mice suffered from ECM, which corresponded to a RCMBS score under 12 (Figure 27A). First, CD4$^+$ and CD8$^+$ T cells were isolated by MACS and Nrp-1 expression was analysed on mRNA levels by qPCR (Figure 27B). Compared to WT littermates, Nrp-1 expression was successfully depleted in CD4$^+$ T cells and reduced in CD8$^+$ T cells of PbA-infected Nrp-1$^{fl/fl}$ x CD4cre^{tg} mice, which expressed CD4 as well as CD8 during the double-positive stage in the thymus and therefore had an active cre recombinase in both T cell subsets [1].

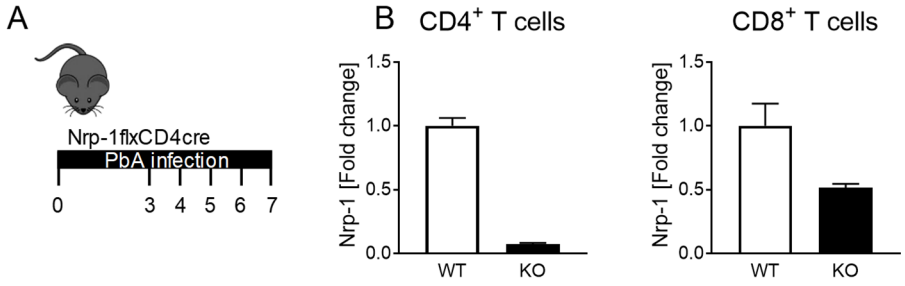

Figure 27 Nrp-1 ablation in Nrp-1$^{fl/fl}$ x CD4cre^{tg} mice during PbA-infection

Nrp-1$^{fl/fl}$ x CD4cre^{tg} (KO) mice and Nrp-1$^{fl/fl}$ x CD4cre^{wt} (WT) littermates were infected with 10^5 PbA-infected RBCs intravenously. Manifestation of ECM was monitored and severity of ECM was quantified by the RMCBS score on day 0, 3, 4, 5, 6 and 7 p.i. (**A**). (**B**) Nrp-1 ablation in KO mice (black bars) was confirmed on mRNA level by qPCR of sorted CD4$^+$ (left) and CD8$^+$ (right) T cells from spleens of PbA-infected Nrp-1$^{fl/fl}$ x CD4cre$^{wt/tg}$ mice on day 6. Nrp-1 expression was normalised to mRNA levels of PbA-infected WT littermates (white bars). RPS9 was used as a housekeeping gene. Data are summarised from n= 2 mice per group.

Flow cytometric analyses revealed that T cell frequencies in spleens of PbA-infected mice did not change upon T cell-specific Nrp-1 ablation (Figure 28A). In the blood, frequencies of CD4$^+$ T cells including conventional FoxP3$^-$ cells and Tregs were comparable between Nrp-1$^{fl/fl}$ x CD4cre^{tg} (KO) mice and Nrp-1$^{fl/fl}$ x CD4cre^{wt} (WT) littermates. However, ECM led to 4 % increase in the percentage of CD8$^+$ T cells in the blood of KO mice, compared to CD8$^+$ T cells in the blood of WT littermates (Figure 28B).

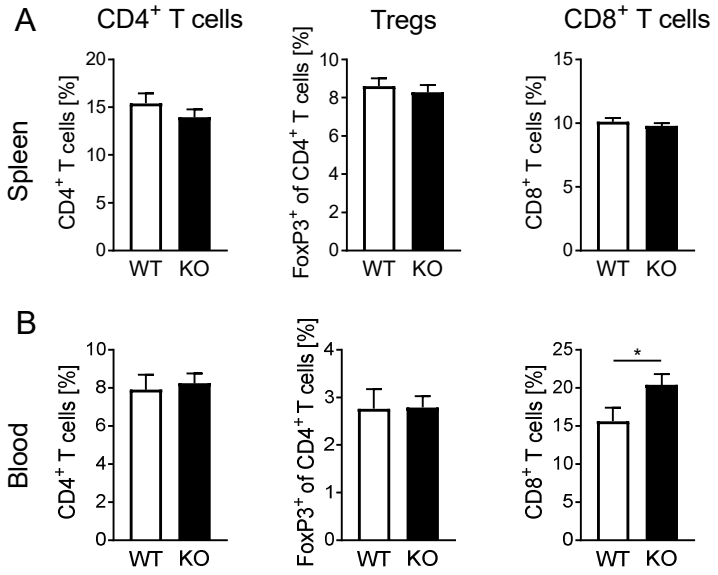

Figure 28 Percentages of CD8$^+$ T cells were increased in the blood of T cell-specific Nrp-1 ablated mice

T cell frequencies of Nrp-1$^{fl/fl}$ x CD4cre^{tg} (KO) mice and Nrp-1$^{fl/fl}$ x CD4cre^{wt} (WT) littermates were determined by flow cytometry 6 or 7 days post PbA infection. Percentages of CD4$^+$FoxP3$^-$ (left), Tregs (centre) and CD8$^+$ T cells (right) are shown in the spleen (**A**) and blood (**B**) of WT (white bars) and T cell-specific ablated KO mice (black bars). Data from five (spleen) or four (blood) independent experiments including n= 19-22 (spleen) and n= 13-17 (blood) mice per group are summarised and shown as mean with SEM. Mann-Whitney test was used to calculate statistics. (*p<0.05).

To analyse the influence of T cell-specific Nrp-1 ablation on the frequencies of peripheral immune cells that migrate into the brain during ECM, brains were isolated after intra-cardiac perfusion and peripheral immune cells were separated from brain-resident cells and myelin by a Percoll gradient centrifugation. PbA infection led to an infiltration of 54 % peripheral immune cells into the brain, which were separated from $CD45^{int}$ brain-resident microglia by $CD45^{high}$ expression. Figure 29A illustrates that a high proportion of infiltrated peripheral immune cells were $CD8^+$ T cells. In the brains of mice with T-cell-specific Nrp-1 ablation, frequencies of $CD45^{high}$ peripheral immune cells (41 %) tended to be decreased (Figure 29A, left). In absolute numbers, approximately 900,000 peripheral immune cells were identified in the brains of WT mice and only 500,000 in KO mice (Figure 29B, left). More precisely, ablation of Nrp-1 on T cells decreased the numbers of infiltrated $CD4^+$ T cells and $CD8^+$ T cells in the brains of PbA-infected KO mice compared to WT littermates (Figure 29B). The number of $CD8^+$ T cells, known to be involved in brain pathology upon PbA infection, was lowered by 75,000 $CD8^+$ T cells and thus tended to be reduced in comparison to PbA-infected WT mice (Figure 29B, right).

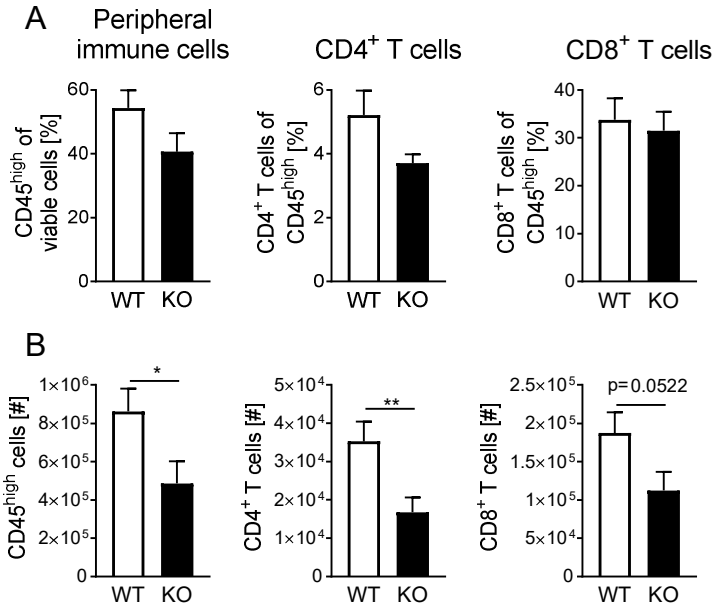

Figure 29 Ablation of Nrp-1 on T cells during PbA infection reduced the numbers of peripheral immune cells in the brain

Brains were collected after intra-cardiac perfusion from PbA-infected Nrp-$1^{fl/fl}$ x $CD4cre^{tg}$ (KO) mice and Nrp-$1^{fl/fl}$ x $CD4cre^{wt}$ (WT) littermates. Immune cells were isolated from brain tissue by density centrifugation via a Percoll gradient. Peripheral immune cells were identified as $CD45^{high}$ population in the brains of WT (white bars) or T cell-specific Nrp-1-ablated KO mice (black bars) by flow cytometry. Frequencies (**A**) and absolute numbers (**B**) of overall peripheral immune cells (left), $CD4^+$ (centre) and $CD8^+$ T cells (right), were analysed on day 6 or 7 post PbA-infection. Data from four independent experiments including n= 12-15 mice per group are depicted as mean with SEM. Unpaired t-test or Mann-Whitney test was used to calculate statistics. (*$p<0.05$, **$p<0.01$).

To further analyse, whether T cell-specific ablation of Nrp-1 expression not only influences the number of T cells within the brain of PbA-infected mice, but has also an effect on the functional phenotype, the expression of CD11a/CD49d and GzmB was determined by flow cytometry. Antigen-experienced $CD4^+$ and $CD8^+$ T cells were significantly diminished in the brains of KO mice compared to WT littermates (Figure 30A and B). Furthermore, the numbers of cytotoxic $GzmB^+$ T cells were significantly reduced in brains of PbA-infected mice with T cell-specific ablation of Nrp-1 (Figure 30C and D). Interestingly, the GzmB-positive T cells are known to be involved in blood-brain barrier disruption and neuronal damage during ECM, underlining the importance of this finding [160].

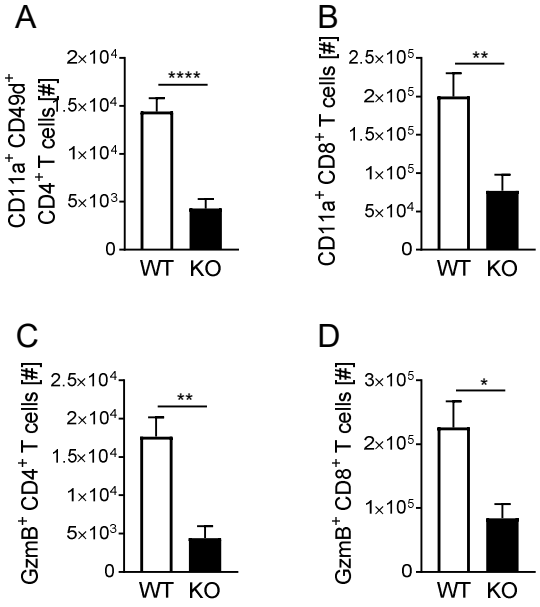

Figure 30 Antigen-specific and cytotoxic T cells were reduced in brains of PbA-infected Nrp-$1^{fl/fl}$ x $CD4cre^{tg}$ mice

Peripheral immune cells were isolated from perfused brains of PbA-infected Nrp-$1^{fl/fl}$ x $CD4cre^{tg}$ (KO) mice and Nrp-$1^{fl/fl}$ x $CD4cre^{wt}$ (WT) littermates by Percoll gradient centrifugation. Malaria-characteristic T cell phenotypes were analysed on day 6 or 7 post infection by flow cytometry. Numbers of antigen-specific $CD4^+$ (**A**) and $CD8^+$ T cells (**B**) were compared between WT (white bars) and KO mice (black bars). Cytotoxic capacities of $CD4^+$ (**C**) and $CD8^+$ (**D**) T cells were quantified by GzmB-expression. Data from three (A, and B) or two (C and D) independent experiments including n= 10 (A, B) and n= 5-6 (C, D) mice per group are depicted as mean values. Error bars represent SEM. Unpaired t-test was used to calculate statistics. (*p<0.05, **p<0.01, ****p<0.0001).

The reduced numbers of antigen-experienced and cytotoxic T cells in the brains of KO mice were reflected in alterations of ECM severity: while the mean score of WT mice was approximately 1 on day 7, the RMCBS score of mice depleted in T cell-expressed Nrp-1 was 8. In summary, the T cell-specific ablation of Nrp-1 significantly ameliorated ECM severity, while the parasite load in the blood was constant between the two groups (Figure 31A and B). The improved attenuated neurological symptoms were also

in line with decreased brain weight in the KO mice compared to WT littermates, which corresponds to reduced brain edema and is an indicator of diminished neuroinflammation (Figure 31C).

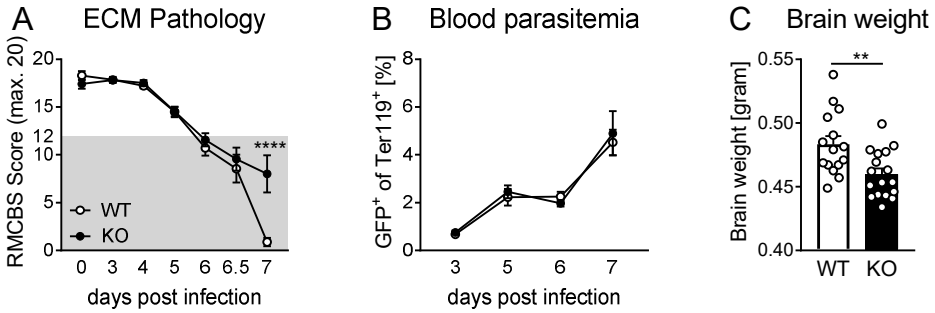

Figure 31 T cell-specific Nrp-1 ablation led to reduced severity of ECM and reduced brain weight

Nrp-1$^{fl/fl}$ x CD4cre$^{wt/tg}$ mice were infected with 10^5 PbA-infected RBCs intravenously. Severity of neurological deficits during the manifestation of ECM was quantified by the RMCBS score on day 0, 3, 4, 5, 6 and 7 p.i. in Nrp-1$^{fl/fl}$ x CD4cre^{tg} (KO, black circles/bars) and Nrp-1$^{fl/fl}$ x CD4cre^{wt} (WT, white circles/bars) littermates. Mice with a score under 12 (grey area) suffered from ECM (**A**). (**B**) Blood parasitemia was measured by flow cytometry and calculated by the percentage of GFP-expressing PbA parasites in Ter119$^+$ erythrocytes on day 3, 5, 6 and 7 post infection. Brain weight was measured on the day of sacrifice. Data are summarised from five independent experiments encompassing n= 23-24 mice per group (RMCBS and parasitemia). For brain weight, four independent experiments with n=15-17 mice are summarised. Means are shown with SEM. 2-way ANOVA (RMCBS and parasitemia) and unpaired t-test (brain weight) was used to calculate significance. (**p<0.01, ****p<0.0001).

6.2.8 Nrp-1 expression on Tregs was dispensable during ECM

The previous experiments suggested an alleviation of ECM in Nrp-1$^{fl/fl}$ x CD4cre^{tg} mice. Since the majority of murine CD4$^+$FoxP3$^+$ Tregs expresses Nrp-1 on their surface [67], Nrp-1$^{fl/fl}$ x FoxP3cre^{tg} were used to verify whether the observed effects during ECM are based on the ablation of Nrp-1 on effector T cells or Tregs. For this purpose, Nrp-1$^{fl/fl}$ x FoxP3cre^{tg} with a specific Nrp-1 knockout (KO) on Tregs and Nrp-1$^{+/+}$ x FoxP3cre^{tg} wildtype littermates (WT) were infected with 10^5 PbA-infected RBCs. T cell phenotypes were analysed on day 6 or 7 after infection and the manifestation of ECM was quantified by the RMCBS score (Figure 32A). The absence of Nrp-1 expression specifically on Tregs in KO mice had no impact on the frequencies and absolute numbers of peripheral CD45^{high} immune cells including CD4$^+$ and CD8$^+$ T cells of mice suffering from ECM (Figure 32B and C).

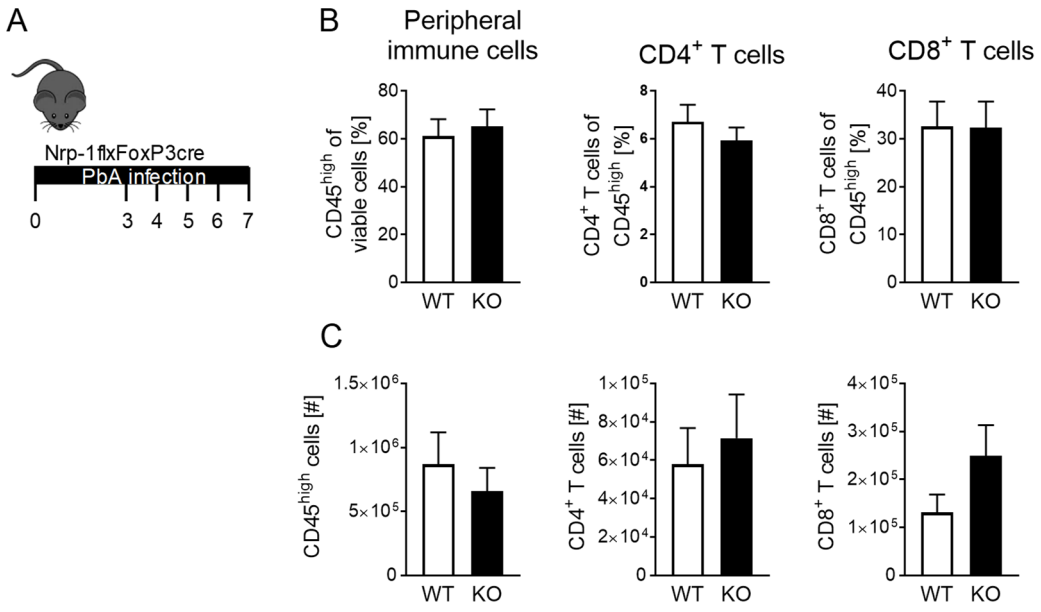

Figure 32 Peripheral immune cell frequencies in the brain of PbA-infected mice were independent of Treg-specific Nrp-1 ablation

Nrp-$1^{fl/fl}$ x FoxP3cre^{tg} (KO) mice and Nrp-$1^{+/+}$ x FoxP3cre^{tg} (WT) littermates were infected intravenously with 10^5 PbA-infected RBCs. Manifestation of ECM was monitored and severity of ECM was quantified by the RMCBS score on day 0, 3, 4, 5, 6 and 7 post infection (**A**). Peripheral immune cells were isolated by Percoll centrifugation and identified as CD45^{high} population in the brains of PbA-infected WT (white bars) or Treg-specific Nrp-1-ablated KO mice (black bars) by flow cytometry. Frequencies (**B**) and absolute numbers (**C**) of peripheral immune cells (left), CD4$^+$ (centre) and CD8$^+$ T cells (right), were analysed on day 6 or 7 post PbA-infection. Data from three independent experiments including n= 10-13 mice per group are depicted as mean with SEM.

In line with the similar T cell phenotypes, the course of ECM manifestation and the levels of parasite load in the blood were independent of Treg-specific ablation of Nrp-1 (Figure 33A and B). Additionally, the brain weight between PbA-infected WT and KO mice was comparable (Figure 33C).

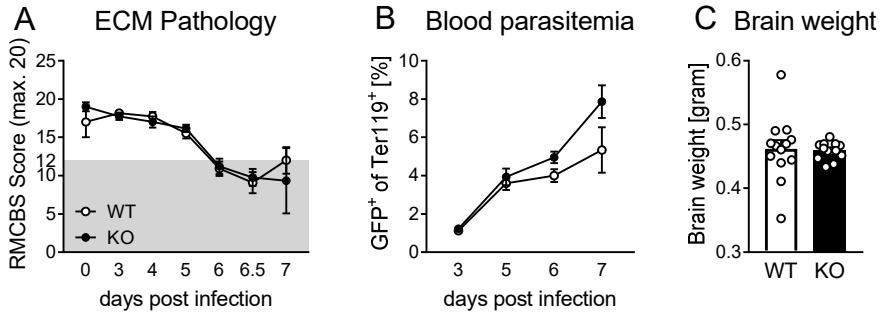

Figure 33 The presence of Nrp-1 on Tregs was dispensable for the manifestation of ECM

Manifestation of ECM in Nrp-$1^{fl/fl}$ x FoxP3cre^{tg} (KO, black circles/bars) mice and Nrp-$1^{+/+}$ x FoxP3cre^{tg} littermates (WT, white circles/bars) infected with PbA was monitored by the RMCBS score on day 0, 3, 4, 5, 6 and 7 post infection. Mice with a score under 12 (grey area) suffered from ECM (**A**). (**B**) Blood parasitemia is shown as GFP$^+$ PbA-parasites in Ter119$^+$ erythrocytes on day 3, 5, 6 and 7 p.i. and was analysed by flow cytometry. Brain weight was measured on the day of sacrifice. Data are summarised from three independent experiments encompassing n= 13 mice per group. Means are shown with SEM.

Consequently, these results suggest that the reduced immune cell frequencies in the brains and the attenuated ECM pathology of $Nrp1^{fl/fl}$ x $CD4cre^{tg}$ mice described in chapter 6.2.7 were likely due to the influence of Nrp-1 expression on conventional $CD4^+$ and/or $CD8^+$ T cells, rather than of Nrp-1^+ Tregs.

6.2.9 VEGF was increased in the serum of mice with ECM

The question of the underlying mechanism of how Nrp-1 expression of effector T cells alters cerebral immune cell frequencies and ECM pathology remained to be answered. One possibility might be that Nrp-1 expression directly alters the T cell function, since Nrp-1^-CD8^+ T cells showed an impaired activation status. Another mechanism, which is affected by Nrp-1, at least in Tregs, is the migratory activity in response to the vascular endothelial growth factor (VEGF). In the melanoma model, a VEGF gradient was described, which mediates Treg migration into the tumour [32]. To find out whether Nrp-1 might be involved in the migration of Nrp-1^+CD8^+ T cells from the spleen into the blood and due to blood-brain barrier disruption into the brains of ECM-suffering mice, the expression of the Nrp-1 ligand VEGF was measured in the brains by qPCR and in the serum by Luminex technology. VEGF showed a slight increase of expression on day 3, but a significant decrease during the late phase of infection on day 5 and 6 (Figure 34A). In contrast, Luminex-based analysis suggested a tendency of increased VEGF concentrations in the sera of PbA-infected C57BL/6 mice on day 6 or 7 compared to naïve mice (Figure 34B).

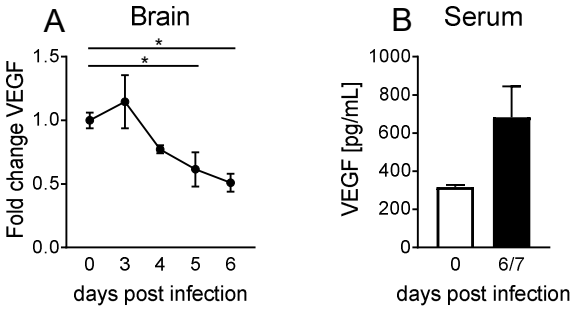

Figure 34 VEGF protein concentrations were increased in the sera of C57BL/6 mice during PbA-infection

(**A**) RNA was isolated from brains of PbA-infected C57BL/6 mice on day 0, 3, 4, 5 and 6 after infection. VEGF was determined on mRNA levels by qPCR. Fold change in expression levels of VEGF was normalised to the expression of VEGF in naïve mice, which was set to 1. Housekeeping gene was RPS-9. (**B**) Serum from PbA-infected C57BL/6 mice was collected from naïve mice (white bar) or on day 6 or 7 post infection (black bar). Serum levels of VEGF were measured by Luminex technology. Data was summarised from four independent experiments with n= 4-14 (A) and one experiment with n= 3-5 mice (B) and are shown as means ± SEM. Statistics were calculated with one-way ANOVA compared to naïve mice. (*$p<0.05$).

6.2.10 The Nrp-1/VEGF axis seemed to be dispensable during PbA-infection

To study whether the elevated sera concentrations of VEGF during ECM play a role in the trafficking of Nrp-1$^+$ T cells, the VEGF binding site (b1) of the Nrp-1 molecule was blocked by application of the blocking peptide A7R (Figure 35A, bottom) [172]. C57BL/6 mice were infected with PbA and treated with 20 µg/g A7R (ATWLPPR) or PBS as a control i.p. on day 0, 2 and 4 p.i. (Figure 35A, top). Interestingly, both the frequencies and absolute numbers of peripheral immune cells, including CD4$^+$ and CD8$^+$ T cells, were similar in the brains of PbA-infected A7R-treated and untreated mice (Figure 35B and C).

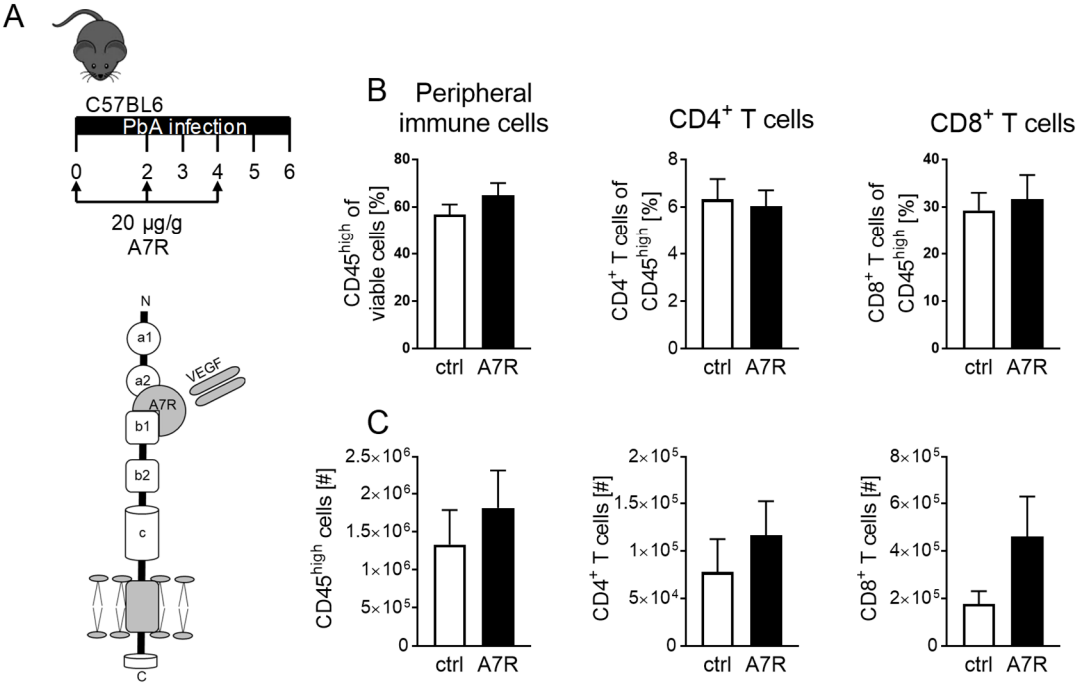

Figure 35 Numbers of peripheral immune cells in PbA-infected brains were independent of the Nrp-1-VEGF interaction

To study the impact of the Nrp-1/VEGF axis during ECM, C57BL/6 mice were infected with 10^5 PbA-infected RBCs intravenously. (**A, top**) Mice were treated with 20 µg/g A7R i.p. on day 0, 2 and 4 p.i.. Control mice received PBS. (**A, bottom**) A7R (ATWLPPR) is a peptide that binds to the b1 subunit of the Nrp-1 molecule and therefore blocks the interaction with VEGF. Frequencies (**B**) and absolute numbers (**C**) of peripheral CD45^{high} (left), CD4$^+$ (centre) and CD8$^+$ (right) T cells were analysed in brains by flow cytometry on day 6 post infection. Data from three independent experiments including n= 11-13 mice per group are depicted as means with SEM.

Similar immune cell frequencies in the brains of A7R-treated and control mice were accompanied by comparable severities of ECM as well as constant values of blood parasitemia and brain weights in both groups (Figure 36A-C). Thus, the numbers of peripheral immune cells in PbA-damaged brains and the manifestation of ECM seemed to be independent of the binding between Nrp-1 and VEGF.

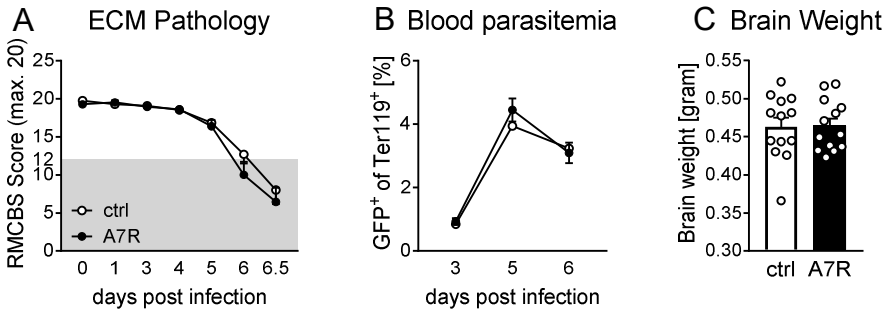

Figure 36 Interaction of Nrp-1 and VEGF was negligible for the severity of ECM

C57BL/6 mice were infected with 10^5 PbA-infected RBCs intravenously and were treated with 20 µg/g A7R (black circles/bars) i.p. on day 0, 2 and 4 post infection. Control mice received PBS (white circles/bars). (**A**) Development and severity of ECM was quantified by the RMCBS score. Mice with values under 12 (grey area) suffered from ECM. (**B**) Blood parasitemia was quantified by GFP^+ parasites in $Ter119^+$ RBCs in the blood by flow cytometry. (**C**) Brain weight was measured on the day of sacrifice, 6 days post infection. Data from three independent experiments including n= 13 mice per group are depicted as mean with SEM.

6.3 Impact of Nrp-1 expression on $CD8^+$ T cell migration and activation *in vitro*

Results from the present study indicate that PbA infection of Nrp-$1^{fl/fl}$ x $CD4cre^{tg}$ mice resulted in decreased numbers of cytotoxic T cells in the brain and therefore led to a better outcome of ECM compared to Nrp-$1^{fl/fl}$ x $CD4cre^{wt}$ littermates. However, the effects seemed to be independent of the Nrp-1/VEGF axis. To further identify potential underlying mechanisms responsible for these observations, the influence of Nrp-1 expression on $CD8^+$ T cells was analysed *in vitro*. First, the migration towards VEGF was examined in a transwell experiment and second, the activation status of Nrp-1-expressing and –deficient $CD8^+$ T cells was compared.

6.3.1 The migration capacity of $CD8^+$ T cells was independent of Nrp-1 expression

In the migration assay, the Nrp-1-dependent migration via the Nrp-1/VEGF axis as well as the Nrp-1-independent migration via CXCR3-CXCL10 interaction was analysed *in vitro*. For this purpose, $CD8^+$ T cells from spleens of non-infected, naïve Nrp-$1^{fl/fl}$ x $CD4cre^{tg}$ (KO) and Nrp-$1^{+/+}$ x $CD4cre^{tg}$ (WT) mice were isolated and stimulated in the presence of 1 µg/mL αCD3 and αCD28 for 48 hours. 7.5 x 10^5 of the stimulated Nrp-1-expressing $CD8^+$ T cells from WT or Nrp-1-deficient $CD8^+$ T cells from KO mice were transferred into the upper chamber of a transwell system. Cells had four hours to migrate from the upper chamber through the fibronectin-coated membrane into the lower chamber containing the chemoattractants VEGF and CXCL10. SDF-1β, the ligand of CXCR4, which is ubiquitously expressed on immune cells, was used as a

positive control, while only medium served as negative control. In general, the migratory potential of Nrp-1-expressing or –deficient CD8⁺ T cells towards the positive control SDF-1β was similar (Figure 37). Furthermore, T cells from WT and KO mice showed comparably low migratory potential towards the Nrp-1 ligand VEGF. The Nrp-1-independent migration towards CXCL10 via CXCR3-receptor expression was comparable between the two groups of CD8⁺ T cells.

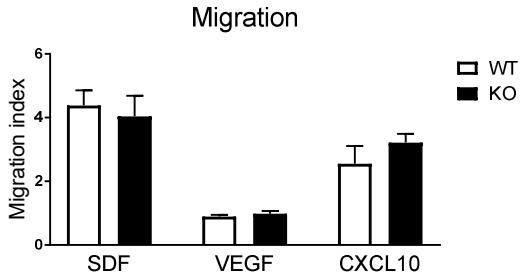

Figure 37 The migratory potential of CD8⁺ T cells was independent of Nrp-1 expression

CD8⁺ T cells were isolated from naïve Nrp-1$^{fl/fl}$ x CD4cre^{tg} (KO) and Nrp-1$^{+/+}$ x CD4cre^{tg} (WT) mice by MACS. They were stimulated *in vitro* with 1 µg/mL plate-bound αCD3 and 1 µg/mL soluble αCD28 for 48 hours. Migration was analysed in a transwell system with fibronectin-coated inserts. 7.5 x 10^5 WT (white bars) or KO CD8⁺ T cells (black bars) were transferred into the upper chamber of the 24-well transwell plate. In the lower chamber, 500 µL medium served as negative control, the supplementation of 100 ng/mL SDF-1β as positive control and 100 ng/mL rhVEGF and 200 ng/mL rmCXCL10 as chemoattractants. Cells that migrated to the lower chamber were collected after four hours and cell numbers were counted. Data from two independent experiments with n= 5-6 mice per group are summarised and shown as means with SEM.

Hence, an impact of Nrp-1 expression on the migratory capacity of CD8⁺ T cells during ECM seems to be rather unlikely. Therefore, the role of T cell expressed Nrp-1 on the activation was analysed in more detail *in vitro*.

6.3.2 Nrp-1 expression was induced on CD8⁺ T cells during *in vitro* stimulation

First of all, the expression of Nrp-1 was analysed on naïve and activated CD8⁺ T cells *in vitro*. For this purpose, isolated CD8⁺ T cells from spleens of naïve C57BL/6 mice were stimulated *in vitro* like previously described by TCR activation with the supplementation of 1 µg/mL αCD3 and αCD28. Strikingly, the proportion of Nrp-1⁺CD8⁺ T cells raised from 0.27 % to 16 % within 24 hours of stimulation (Figure 38A). The peak of Nrp-1 expression was reached after 48 hours of *in vitro* stimulation, where 42 % of CD8⁺ T cells were positive for Nrp-1 expression. After this time point the frequencies of Nrp-1⁺CD8⁺ T cells steadily decreased (Figure 38A). The expression of Nrp-1 on *in vitro* stimulated CD8⁺ T cells was independent of TCR stimulation, as activation with 10 ng/mL phorobol 12-myristate 13-acetate (PMA) and 1 µg/mL ionomycin also led to a significant induction of Nrp-1 expression on CD8⁺ T cells *in vitro* (Figure 38B).

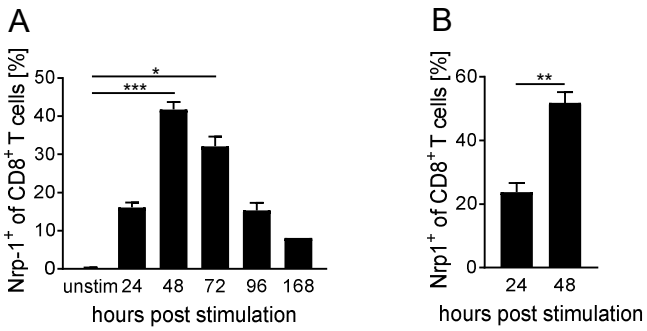

Figure 38 *In vitro* stimulation induced Nrp-1 expression on CD8⁺ T cells

Splenocytes were isolated from naïve C57BL/6 mice and CD8⁺ T cells were sorted by MACS. 1.5x10^5 CD8⁺ T cells were cultured *in vitro*. (**A**) Frequencies of Nrp-1-expressing CD8⁺ T cells were determined by flow cytometry after 24, 48, 72, 96 and 168 hours of incubation with 1 µg/mL plate-bound αCD3 and 1 µg/mL soluble αCD28. Unstimulated controls were incubated only with medium. (**B**) TCR-independent stimulation was achieved by supplementation of 10 ng/mL Phorobol 12-myristate 13-acetate (PMA) and 1 µg/mL ionomycin. Values are shown as means with SEM. Data are summarised from two (A) or one (B) independent experiments with n= 1-6 mice per group. Significance was calculated with non-parametric Kruskal-Wallis test (A) or unpaired t-test (B). (*p<0.05, **p<0.001, ***p<0.001).

As the frequencies of *in vitro* stimulated Nrp-1⁺CD8⁺ T cells peaked after 48 hours of stimulation and declined afterwards again, the following experiment analysed the stability of Nrp-1 expression on activated CD8⁺ T cells. For this purpose, *in vitro* induced Nrp-1-expressing CD8⁺ T cells were separated from Nrp-1⁻CD8⁺ T cell by FACS after 48 hours of stimulation and re-cultivated in presence of 250 U/mL IL-2. Exemplary contour plots in Figure 39 visualise that the Nrp-1⁺ cell population lost their Nrp-1 expression over time and became Nrp-1-negative. Consequently, Nrp-1 on CD8⁺ T cells was induced in a very early state of general activation and declined without re-stimulation during re-cultivation again.

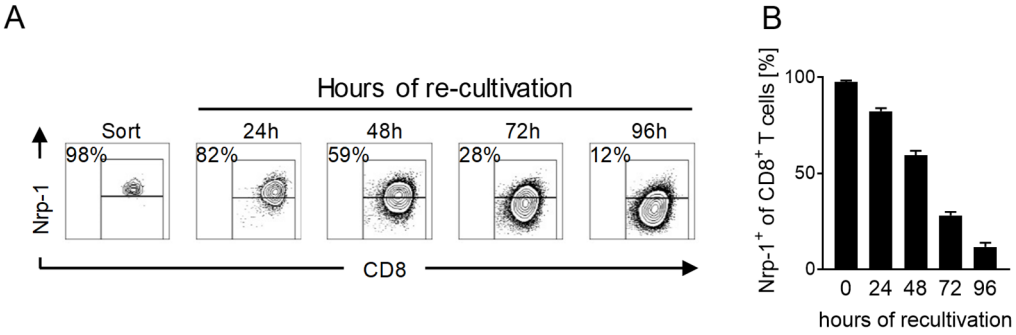

Figure 39 *In vitro* stimulated Nrp-1⁺CD8⁺ T cells downregulated Nrp-1 expression after re-cultivation

CD8⁺ T cells were sorted by MACS from spleens of naïve C57BL/6 mice and were cultured *in vitro* with 1 µg/mL plate-bound αCD3 and 1 µg/mL soluble αCD28 for 48 hours. Subsequently, Nrp-1⁺ and Nrp-1⁻CD8⁺ T cells were sorted by FACS and re-cultivated in the presence of 250 U/mL IL-2. Representative contour plots (**A**) and bars (**B**) show percentages of Nrp-1 expression on CD8⁺ T cells after re-cultivation. Bars represent mean values with SEM. Data are summarised from one experiment with n= 3 mice.

6.3.3 *In vitro* stimulated Nrp-1$^+$CD8$^+$ T cells had a highly activated phenotype

In the next step, the activation status of *in vitro* stimulated Nrp-1$^+$CD8$^+$ T cells was characterised by flow cytometry after 48 hours of stimulation. Nrp-1$^+$CD8$^+$ T cells were highly activated (CD69$^+$) and had an elevated proliferation potential (Ki-67$^+$) compared to Nrp-1$^-$CD8$^+$ T cells (Figure 40). In addition, the majority of Nrp-1$^+$CD8$^+$ T cells expressed CXCR3 on their surface, which was significantly decreased on Nrp-1$^-$CD8$^+$ T cells. Furthermore, the cytotoxic potential, characterised by GzmB expression, and the PD-1 expression were increased on Nrp-1-expressing CD8$^+$ T cells compared to CD8$^+$ T cells lacking Nrp-1 expression. In summary, *in vitro* induced Nrp-1$^+$CD8$^+$ T cells were highly activated and had elevated effector functions in comparison to Nrp-1$^-$CD8$^-$ T cells. Strikingly, these results were in line with the increased activation phenotype of Nrp-1$^+$CD8$^+$ T cells in PbA-infected mice, which was previously described in chapter 6.2.6.

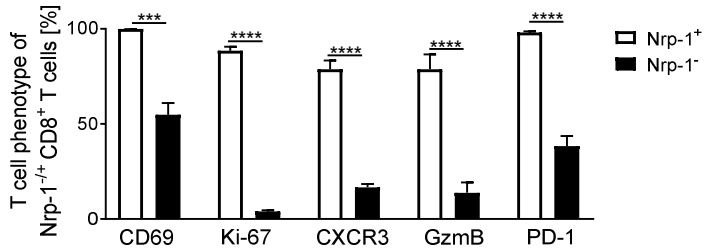

Figure 40 *In vitro* stimulated Nrp-1$^+$CD8$^+$ T cells showed a highly activated phenotype

CD8$^+$ T cells were sorted from naïve C57BL/6 mice by MACS technology and 1.5x10^5 cells per well were activated *in vitro* with 1 µg/mL plate-bound αCD3 and 1 µg/mL soluble αCD28 for 48 hours. Nrp-1$^+$ (white bars) and Nrp-1$^-$ CD8$^+$ T cells (black bars) were analysed for activation/effector functions by flow cytometry. Data from two independent experiments with n= 6 mice are shown as means with SEM. Statistical significance was calculated with paired t-test. (***p<0.001, ****p<0.0001).

6.3.4 Nrp-1 ablation on T cells reduced the activated phenotype of CD8$^+$ T cells

To analyse the impact of Nrp-1 on T cell activation in more detail, CD8$^+$ T cells were isolated from WT and T cell-specific Nrp-1-deficient mice by MACS technology. 1.5 x 10^5 CD8$^+$ T cells were activated with 1 µg/mL plate-bound αCD3 and 1 µg/mL soluble αCD28 for 48 hours *in vitro*. CXCR3 was increased and the cytotoxic potential as well as PD-1 expression was similar in the absence of Nrp-1 on *in vitro* stimulated CD8$^+$ T cells (Figure 41). A tendency of reduced CD69 and Ki-67 was observed in CD8$^+$ T cells from KO compared to WT mice. These results suggest that Nrp-1 expression directly promotes T cell activation and are, at least in tendency, in line with the reduced activation of CD8$^+$ T cells from brains of PbA-infected Nrp-1$^{fl/fl}$ x CD4cre^{tg} mice.

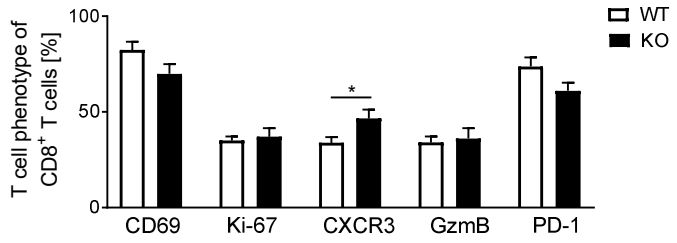

Figure 41 Reduced activation of Nrp-1-deficient CD8⁺ T cells *in vitro*

$CD8^+$ T cells were sorted from naïve $Nrp\text{-}1^{fl/fl}$ x $CD4cre^{tg}$ (KO) and $Nrp\text{-}1^{+/+}$ x $CD4cre^{tg}$ (WT) mice by MACS technology. $1.5x10^5$ $CD8^+$ T cells were stimulated *in vitro* with 1 µg/mL plate-bound αCD3 and 1 µg/mL soluble αCD28 for 48 hours. $CD8^+$ T cells from WT (white bars) and KO (black bars) mice were analysed for activation/effector functions by flow cytometry. Data from two independent experiments with n= 6 mice are summarised and shown as means with SEM. Statistical significance was calculated with unpaired t-test (*$p<0.05$).

In summary, the *in vitro* experiments showed that Nrp-1 expression was inducible on $CD8^+$ T cells and was independent of TCR stimulation. The peak of Nrp-1 expression was 48 hours after activation and declined afterwards, suggesting that $CD8^+$ T cells lose their Nrp-1 expression without continuous stimulus. Strikingly, $Nrp\text{-}1^+CD8^+$ T cells had increased effector functions and were highly activated in comparison to the $Nrp\text{-}1^-$ counterparts. *In vitro* stimulation of $CD8^+$ T cells from WT and KO mice showed a trend of decreased T cell activation in Nrp-1-deficient $CD8^+$ T cells, which was in line with less activated T cells in the brains of PbA-infected KO mice. Consequently, *in vitro* analyses not only suggested that Nrp-1 acts as an activation marker, but also had a direct impact on T cell activation.

Overall, during the peak of *Plasmodium* infections, Nrp-1 was highly upregulated on conventional $CD4^+$ T cells during PY-infection and on ECM pathology-driving $CD8^+$ T cells during PbA infection. Even though the influence of $Nrp\text{-}1^+CD4^+$ T cells was negligible during PY infection, the presence of Nrp-1 on $CD8^+$ T cells during PbA infection aggravated ECM pathology. $Nrp\text{-}1^+CD8^+$ T cells showed a significantly increased activation state and enhanced malaria-characteristic effector functions. Reduced peripheral immune cells in brains of PbA-infected $Nrp\text{-}1^{fl/fl}$ x $CD4cre^{tg}$ mice compared to WT littermates were associated with an improved ECM outcome. Further mechanistical analyses revealed that Nrp-1/VEGF-mediated migration is rather unlikely to be responsible for the observed phenotype in PbA-infected KO mice. In fact, analysis of $CD8^+$ T cells *in vitro* provide evidence for a direct effect of Nrp-1 on $CD8^+$ T cell activation, which is known to play a key role during ECM manifestation.

7 Discussion

Nrp-1 is a co-receptor for VEGF, semaphorins as well as TGF-β and is important for neuronal development and angiogenesis. Endothelial cells, tumour cells and immune cells express Nrp-1, whereby especially the function of Nrp-1 on Tregs has been investigated in more detail. Nrp-1 plays a role in DC/T cell interaction and thereby influences T cell activation. In addition, Nrp-1 on Tregs is known to be important for migration along a VEGF gradient into tumours, as published in a previous study by our group [32]. In the present study, the impact of Nrp-1 on $CD4^+$ T cell responses was analysed in blood-stage malaria, where immune cells are primed in the spleen. In the second part, the role of Nrp-1 expression on $CD8^+$ T cell migration and activation was studied in the context of ECM.

7.1 The role of Nrp-1 during blood-stage malaria

During blood-stage malaria, besides B cells, $CD4^+$ T cells and their differentiation into T_H1 cells are the key cells involved in pathogen clearance [136]. Strikingly, PY infection led to an increase of Nrp-1 expression on immune cells from spleens of Balb/c mice, which was most prominent on conventional $CD4^+FoxP3^-$ T cells.

Focusing on conventional $CD4^+$ T cells, 6 % expressed Nrp-1 in the naïve state. The characterisation of Nrp-1^+ and Nrp-1^- conventional T cells revealed a highly activated T cell phenotype in the presence of Nrp-1 (Figure 11). Upon PY infection, frequencies of Nrp-1^+CD4^+ T cells were increased and the expression of activation markers were kept at high levels. Unpublished data by our research group support these results and describe an upregulation of Nrp-1^+ on conventional $CD4^+$ T cells also in other diseases such as cancer as well as diabetes (manuscript in progress). Moreover, in atherosclerosis, Nrp-1^+ T cell frequencies were elevated and associated with increased proliferative capacity and an enhanced ability to produce IFN-γ [76].

In addition to the expression of activation-associated proteins, PY infection also resulted in an elevated expression of co-inhibitory receptors such as PD-1 and CTLA-4 on conventional $CD4^+$ T cells (Figure 11). The function of co-inhibitory receptors is controversially discussed as they are expressed upon activation, but can also be associated with exhaustion of T cells. The diminished production of cytokines such as TNF-α and IFN-γ during the progression of PY infection by both, the Nrp-1^+ as well as Nrp-1^- conventional $CD4^+$ T cells suggested an exhausted T cell phenotype. During

malaria, a general exhaustion of T cells is described to be a protective mechanism to prevent an excessive immune response due to the high numbers of parasites in the blood [173]. The malaria treatment with chloroquine is known to diminish the parasite load resulting in reduced T cell exhaustion [165]. Another option to enhance T cell activation during infection is the combinatory blockade of PD-L1 and Lag-3 by antibodies that clearly diminishes the parasitemia of PY-infected mice [165].

As the upregulation of Nrp-1 on $CD4^+$ T cells correlated with strong activation, but also significantly decreased cytokine production on day 14 p.i., the role of Nrp-1 during blood-stage malaria was analysed in Nrp-$1^{fl/fl}$ x $CD4cre^{wt/tg}$ mice. The loxP/cre system offered the opportunity to specifically ablate Nrp-1 on T cells and to analyse its impact on the course of malaria. Increased percentages of Tregs were detected in the spleens of KO mice compared to WT littermates (Figure 12). During blood-stage malaria, Tregs play an important role: their depletion in DEREG mice resulted in significantly increased T cell activation accompanied by diminished parasite loads in the blood [138]. In accordance, on day 7 post PY infection, the frequencies of antigen-experienced $CD4^+FoxP3^-$ T cells and proliferative Ki-67^+ conventional $CD4^+$ T cells was reduced in the KO mice compared to WT littermates, suggesting that Nrp-1 expression has an impact on Treg frequencies and $CD4^+$ T cell activation during blood-stage malaria (Figure 13). In contrast to that, the production of pro-inflammatory cytokines by conventional $CD4^+$ T cells was increased. Overacre-Delgoffe and colleagues suggest a connection between cytokines and Nrp-1 expression: The ablation of Nrp-1 on Tregs led to an increased IFN-γ production, which was the basis for an enhanced anti-tumoural immune response [174]. However, further experiments are necessary to clarify whether Nrp-1 expression of conventional $CD4^+$ T cells also directly affects the cytokine production during blood-stage malaria.

Overall, Nrp-1 ablation in all T cell subsets including conventional $CD4^+$ T cells and Tregs in Nrp-$1^{fl/fl}$ x $CD4cre^{tg}$ mice did not affect the course of blood-stage malaria in terms of the parasite load (Figure 14). One reason might be that the effects of Nrp-1 depletion on effector and suppressive T cells counteract each other.

Focusing on the Nrp-1 expression, the characterisation of immune cells during PY infection revealed a significantly decreased proportion of Nrp-1^+ Tregs with progression of the disease (Figure 9). Nrp-1 on Tregs is a surface marker for thymus- or naturally-derived nTregs [67] and was suggested to be essential for their ability to suppress the proliferation of effector T cells [31]. A previous study by our group

analysed whether the frequencies of Nrp-1$^+$ Tregs in *P. yoelii*-infected mice decreased due to induction of Nrp-1$^-$ iTregs in the periphery [175]. However, transfer of FoxP3$^-$ CD4$^+$ T cells did not result in the induction of FoxP3 and thus, one might speculate about a loss of Nrp-1 expression by Tregs in the blood-stage of malaria.

The effect of ablation of Nrp-1 expression on Tregs was studied in Nrp-1$^{fl/fl}$ x Foxp3cre^{tg} mice, in which Nrp-1 is specifically ablated in FoxP3$^+$ Tregs but not in conventional CD4$^+$ T cells. During blood-stage malaria, the phenotype of effector T cells and the parasitemia was independent of Nrp-1 ablation in Tregs (Figure 15 and 16). One reason might be that PY parasites cause such a strong systemic inflammation caused by parasite loads up to 25 % that the Nrp-1 ablation of Tregs is insufficient to have an impact on the strong expansion and function of conventional CD4$^+$ T cells and other immune cells.

In summary, results from the present study indicate that Nrp-1 expression on Tregs is dispensable for the T cell response and pathogen clearance during PY infection. However, on CD4$^+$ T conventional cells Nrp-1 expression is involved in the increase of T cell activation and is associated with reduced cytokine levels. Nevertheless, T cell-specific ablation of Nrp-1 was inefficient to affect the parasite clearance during blood-stage malaria.

7.2 The role of Nrp-1 during experimental cerebral malaria

The role of Nrp-1 expression on T cells was studied in another *Plasmodium* infection model, which ultimately targets the brain and induces experimental cerebral malaria (ECM). During *P. berghei ANKA* infection, the innate immune response is activated by the parasites in the blood. Subsequently, between day 3 and 5 after infection, DCs present PbA-antigens and produce cytokines, resulting in the induction of the adaptive immune response [126]. In this model, CD8$^+$ T cells are responsible for the loss of blood-brain barrier stability and cause neuroinflammation due to their cytotoxic potential [159, 161]. Strikingly, CD8$^+$ T cells were the immune cells that most significantly increased their Nrp-1 expression upon PbA-infection (Figure 17). The time point of Nrp-1 upregulation in the spleen correlated with the first neurological deficits on day 5 post infection. Simultaneously with Nrp-1, proteins associated with proliferation (Ki-67), cytotoxicity (GzmB) and migration (CXCR3) were upregulated on CD8$^+$ T cells when they start to migrate from the spleen into the blood and subsequently into the brain (Figure 21).

The characterisation of $CD8^+$ T cells from spleens of PbA-infected C57BL/6 mice revealed a highly activated T cell phenotype in the presence of Nrp-1 (Figure 24 and 25). Microarray analysis provided evidence for increased T cell activation on mRNA level, which was confirmed for protein expression by flow cytometric analysis. Co-inhibitory molecules associated with exhaustion such as PD-1, CTLA-4 and CD160 were significantly increased on $Nrp\text{-}1^+CD8^+$ T cells compared to the $Nrp\text{-}1^-$ counterparts. Additionally, several molecules associated with effector functions important during malaria were elevated on these cells. These included antigen-experience, migration, cytotoxicity, proliferation, activation and the production of pro-inflammatory cytokines (Figure 25). It is therefore reasonable that all these functions lead to a correlation between Nrp-1 expression and the severity of cerebral malaria pathology (Figure 22 and 23). This is supported by the fact that also the percentages of $CD160^+CD8^+$ T cells, which have been described to have a comparable phenotype to $Nrp\text{-}1^+CD8^+$ T cells correlate with the severity of ECM [176]. Muscate and colleagues further analysed the function of the $CD160^+CD8^+$ T cells, which were high in Ki-67, GzmB, CD107a, KLRG1 and PD-1 expression, to exclude exhaustion of these cells. As $CD160^+CD8^+$ T cells were still cytotoxic and produced IFN-γ, they suggested T cells that express inhibitory receptors like PD-1 have a rather activated phenotype during murine ECM [176].

In accordance, elevated frequencies of $PD\text{-}1^+CD8^+$ T cells were measured in the blood of *P. falciparum*-infected patients compared to healthy controls [177]. Strikingly, the activation as well as the $PD\text{-}1^+$ frequencies of T cells was consistent between severe and uncomplicated malaria, further underlining an activated instead of exhausted $CD8^+$ T cell phenotype. Kaminski and colleagues suggested that the functionality and cytotoxicity of $CD8^+$ T cells is decisive for the course of malaria. They described that the percentages of GzmB-expressing $CD8^+$ T cells correlated with the severity of disease as they found lower levels of these cells in patients with uncomplicated malaria compared to severe disease outcomes [177]. This highlights our finding that not the absolute number of $CD8^+$ T cells correlates with the parasite load or severity of ECM, but rather the increased activation status of $Nrp\text{-}1^+CD8^+$ T cells (Figure 22 and 23).

The induction of Nrp-1 expression on $CD8^+$ T cells is not restricted to malaria, but is also reported in cancer. High percentages of Nrp-1-expressing tumour-infiltrating $CD8^+$ T cells have been described to co-express PD-1, Lag-3, Tim-3 and CTLA-4 [77, 80]. Liu and colleagues reported further, that $Nrp\text{-}1^+CD8^+$ T cells in murine tumours are

also associated with increased expression of activation markers, proliferation and lower levels of CD62L, CD127 and KLRG1 expression compared to Nrp-1$^-$CD8$^+$ T cells [80]. Therefore, we hypothesise that Nrp-1 might be associated with T cell activation and thus a potential therapeutic target in various CD8$^+$ T cell-driven diseases.

Not only the effector, but also the memory CD8$^+$ T cell subset was influenced by Nrp-1 expression. In naïve mice, the majority of T cells express CD62L and low frequencies of CD44. Upon antigen-contact, T cell are activated, differentiate and develop into long-lived memory T cells that alter their expression of adhesion molecules to migrate into lymphoid organs. Two main types of memory T cells are known: CD62L$^-$CD44$^+$ effector memory T cells (T_{EM}) and CD62L$^+$CD44$^+$ central memory cells (T_{CM}) [178]. T_{EM} are predominantly located in peripheral tissues and can directly target pathogens at the site of inflammation after re-infection by exerting effector functions, including the production of IFN-γ [179]. T_{CM} express homing molecules to enter lymph nodes where they persist as antigen-experienced cells. Upon re-infection, they induce DCs and effector cells as well as provide B cell help, supporting a rapid secondary immune response [179, 180].

On day 7 post PbA infection, the majority of Nrp-1$^+$CD8$^+$ T cells expressed CD62L$^-$CD44$^+$ and therefore had a T_{EM} phenotype, which allows them to act rapidly upon re-infection (Figure 26). This memory phenotype of Nrp-1-expressing CD8$^+$ T cells is independent of malaria, as Leclerc and colleagues identified 98 % of Nrp-1$^+$ tumour-infiltrating lymphocytes from mice bearing B16F10 tumours as effector memory cells [77]. Liu and colleagues, who studied the impact of Nrp-1 on CD8$^+$ T cells in long-lived memory T cells during cancer, described contradicting results. The removal of primary tumours from mice and the placing of a second tumour revealed that Nrp-1 expression interferes with the formation of memory T cells. Mice with Nrp-1-deficient CD8$^+$ T cells were more effective in eliciting a secondary immune response against the tumour than WT littermates [80]. Whether Nrp-1 expression on CD8$^+$ T cells plays a role upon *Plasmodium* re-infection is unclear. However, one might investigate this aspect by infection of mice with *P. chabaudi*, which leads to chronic recurrent blood-stage malaria [113].

To further analyse the influence of Nrp-1 expression on T cells during acute ECM, we infected Nrp-1$^{fl/fl}$ x CD4cre$^{wt/tg}$ mice with PbA. Manifestation of ECM resulted in decreased numbers of peripheral immune cells in the brains of Nrp-1$^{fl/fl}$ x CD4cre^{tg} (KO) mice compared to Nrp-1$^{fl/fl}$ x CD4cre^{wt} (WT) littermates (Figure 29). Strikingly, not only

the total numbers of T cells, but also the numbers of antigen-experienced and cytotoxic T cells were reduced in the brains of T cell-specific Nrp-1-ablated mice (Figure 30). Consequently, the severity as well as the inflammatory brain weight were decreased in PbA-infected KO mice (Figure 31). The parasite load was not affected by T cell-specific Nrp-1 ablation, which is in line with observations in human *P. falciparum* infection. The frequencies of cytotoxic $CD8^+$ T cells correlated with the parasite burden, but were inefficient to reduce the parasite load during CM, which was referred to the lack of antigen-presentation by erythrocytes [177].

In Nrp-$1^{fl/fl}$ x CD4cre^{tg} mice, Nrp-1 expression was ablated on conventional $CD4^+$ and $CD8^+$ T cells as well as on Tregs. During ECM, very low numbers of Tregs were detected in the brains of PbA-infected C57BL/6 mice [181]. Although the depletion of Tregs by the administration of αCD25 antibody led to a better outcome of ECM, it has to be considered that CD25 is also an activation marker for conventional T cells. Hence, the depleting antibody not only depleted Tregs but also recently activated T cells and therefore it was not surprising that the severity of ECM was reduced [182]. The specific depletion of Tregs was later analysed in the DEREG mouse model, which expresses a diphterin toxin (DT) receptor under the control of the *foxp3* locus [183]. The depletion of Tregs by administration of DT resulted in insignificant alterations of the T cell phenotype and did not influence the severity or course of PbA-infection, suggesting that Tregs play a minor role during ECM [181].

To confirm that Nrp-1 expression on conventional $CD4^+$ and $CD8^+$ T cells, rather than on Tregs plays a crucial role during ECM development, Treg-specific Nrp-1-deficient Nrp-$1^{fl/fl}$ x FoxP3cre^{tg} mice were infected with PbA. Indeed, the ablation of Nrp-1 expression on Tregs did not affect the activation status of effector or cytotoxic T cells in the periphery (data not shown). Moreover, the numbers of peripheral immune cells in the brains of Treg-specific Nrp-1-depleted mice and wildtype littermates were similar. Therefore, the ablation of Nrp-1 on Tregs was negligible for the immune response and severity of ECM pathology during PbA infection (Figure 33).

Consequently, the reduced numbers of peripheral immune cells in the brains of Nrp-$1^{fl/fl}$ x CD4cre^{tg} mice compared to Nrp-$1^{fl/fl}$ x CD4cre^{wt} littermates and the associated reduced severity of ECM is rather attributed to the Nrp-1 expression on conventional $CD4^+$ and/or $CD8^+$ T cells than on Tregs. One might speculate about two different underlying mechanisms: Either T cells that lack Nrp-1 on their surface are limited in their migratory function and are therefore less prominent in the brain. This hypothesis

could be supported by the fact that increased frequencies of $CD8^+$ T cells were detected in the blood of KO mice during ECM compared to WT mice (Figure 28). The second possibility might be the enhanced activation status of $CD8^+$ T cells that express Nrp-1 and therefore, the WT $CD8^+$ T cells might be more cytotoxic than $CD8^+$ T cells from KO mice. In consequence, activated Nrp-1^+CD8^+ T cells could damage the blood-brain barrier more seriously and subsequently enhance cell infiltration into the brain.

To identify the mechanism that leads to reduced peripheral immune cells in the brains of PbA-infected KO mice, the migratory potential and activation status in presence and absence of T cell-expressed Nrp-1 was analysed. Brain damage during human CM is known to be induced by the accumulation of iRBCs in the brain vessels. Due to the erythrocytic aggregates, oxygen in the surrounding tissue is scarce, which might result in the induction of VEGF [184]. Hence, one might speculate that VEGF is increased in brains of patients with cerebral malaria and subsequently Nrp-1^+ T cells migrate via the VEGF gradient from the periphery into the brain, like it was previously described for Nrp-1^+ Tregs in the melanoma mouse model by our research group [32]. However, human studies reported stable concentrations of VEGF between *P. falciparum*-infected patients and healthy control individuals [184]. Nevertheless, a redistribution of VEGF concentrations within different regions of the brain during CM was suggested [184]. In our study, one whole hemisphere including all brain regions was used for RNA extraction. Hence, relocation and potentially local upregulation of VEGF could not be detected by qPCR. However, during the peak of ECM on day 6 or 7, a tendency of elevated concentration of VEGF was measured in the sera of PbA-infected mice compared to naïve control C57BL/6 mice (Figure 34).

Therefore, the influence of the Nrp-1/VEGF axis during ECM was studied by administration of the A7R peptide on day 0, 2 and 4 post infection. A7R binds to Nrp-1 and blocks the binding site of VEGF [172]. Previous studies showed a successful treatment of nude mice suffering from breast cancer with A7R peptide leading to significantly reduced tumour sizes [172]. The blockade of the Nrp-1/VEGF axis during ECM was negligible with regard to the activation status of T cells (data not shown) and the numbers of peripheral immune cells that invaded the brain of PbA-infected C57BL/6 mice were similar between the A7R-treated and control group (Figure 35). Hence, the presence of the Nrp-1 ligand VEGF seems to be dispensable during ECM in terms of the migration of immune cells into the brain.

7.3 *In vitro* analysis of the influence of Nrp-1 expression on T cell migration and activation

To confirm that the migration of $CD8^+$ T cells via the Nrp-1/VEGF axis was rather unlikely to be involved during ECM, a migration assay was performed *in vitro*. Previously stimulated $CD8^+$ T cells from spleens of naïve WT mice that upregulated Nrp-1 or from Nrp-1-deficient mice were transferred into the upper chamber of a transwell system. Within 4 hours, the cells actively migrated towards the ligands VEGF or CXCL10, which were present in the bottom chamber, separated by a membrane. The positive control was SDF-1β, the ligand of the ubiquitously expressed receptor CXCR4 on T cells. In general, Nrp-1-expressing and Nrp-1-deficient $CD8^+$ T cells had the same migration ability (Figure 37). The migration towards VEGF was comparable between the two different $CD8^+$ types, but in general very low. This was surprising, as it was described by our research group that Nrp-1^+CD4^+ Tregs migrate towards VEGF, in contrast to Nrp-1-deficient Tregs [32]. However, results from the application of the A7R blocking peptide as well as from the migration assay highlights again the difference between the Nrp-1 expression on $CD8^+$ T cells and $CD4^+$ T cells, which seems to be at least partly dependent on VEGF-mediated migration. In accordance, VEGF concentrations are reported to be increased in the brain during EAE [185]. EAE is the murine model of multiple sclerosis, in which peripheral $CD4^+$ T_H17 cells are the main players and migrate into the brain to drive demyelination of neurons [186]. Histological analyses revealed that immune cell infiltration was accompanied by enhanced VEGF expression in the brain, which might therefore play a role during neurological EAE pathology [185]. Moreover, blocking the Nrp-1/VEGF axis by the treatment with the VEGFR2 inhibitor Semaxinib reduced the infiltration of immune cells into the brain and ameliorated the severity of EAE [185]. Solomon and colleagues showed significantly aggravated neurological inflammation in Nrp-$1^{fl/fl}$ x CD4cre^{tg} mice compared to C57BL/6 mice [31]. They claim that an increased T_H17 differentiation as well as impaired Treg function and therefore enhanced proliferation of conventional $CD4^+$ T cells occur due to the lack of Nrp-1 expression in T cells [31]. This underlines the hypothesis that Nrp-1 expression on $CD4^+$ T cells might have different effects and underlying mechanisms than Nrp-1 expression of $CD8^+$ T cells. Hence, Nrp-1 expression seems to be important for the migration of $CD4^+$ T cells. However, the similar migratory capacity of Nrp-1-expressing and Nrp-1-deficient $CD8^+$ T cells suggests that during ECM Nrp-1 might be dispensable for the migration of peripheral

immune cells into the brain, but might rather be important for the activation of $CD8^+$ T cells.

To study the impact of Nrp-1 expression on the activation of $CD8^+$ T cells, $CD8^+$ T cells from spleens of naïve C57BL/6 mice were sorted by negative selection, stimulated with αCD3 and αCD28 and Nrp-1 expression was measured by flow cytometry. At early time points of stimulation, Nrp-1 expression was strongly induced on $CD8^+$ T cells and peaked after 48 hours. Strikingly, this induction was TCR-independent, as Ca^{2+}-dependent stimulation with PMA and ionomycin also resulted in Nrp-1 induction (Figure 38). This provides evidence that the upregulation of Nrp-1 upon activation might be independent of antigen. Moreover, it highlights the potential of Nrp-1 as a valuable therapeutic target, as it might be involved in pathological effector functions of $CD8^+$ T cells in various diseases.

After 48 hours of stimulation, the Nrp-1 expression of $CD8^+$ T cells decreased again, which might be due to the fact that Nrp-1^+CD8^+ T cells either die or lose their Nrp-1 expression again. To study this in more detail, Nrp-1^+CD8^+ T cells were sorted 48 hours after activation and cultured in the presence of IL-2. Flow cytometric analysis revealed that Nrp-1^+ cells lose their Nrp-1 expression on the surface with time and become Nrp-1-negative (Figure 39). Liu and colleagues showed that re-stimulation of $CD8^+$ T cells with renewed supplementation of αCD3 and αCD28 results in the re-induction of Nrp-1 expression suggesting that $CD8^+$ T cells need a recurring stimulus to steadily express Nrp-1 [80]. Hence, downregulation of Nrp-1 on $CD8^+$ T cells after 48 hours stimulation *in vitro* seems to be more likely than dying of recently activated Nrp-1^+CD8^+ T cells.

The characterisation of *in vitro* induced Nrp-1^+CD8^+ T cells showed a significantly enhanced activation status compared to Nrp-1^-CD8^+ T cells (Figure 40), which was in line with the phenotype of Nrp-1^+CD8^+ T cells during PbA-infection (Figure 25). This gave rise to the question whether Nrp-1 is an activation marker or whether it has a direct influence on T cell activation.

To study this, $CD8^+$ T cells were isolated from spleens of naïve Nrp-$1^{fl/fl}$ x $CD4cre^{tg}$ or Nrp-$1^{+/+}$ x $CD4cre^{tg}$ mice and stimulated *in vitro* in the presence of αCD3 and αCD28. Nrp-1-deficient $CD8^+$ T cells of Nrp-$1^{fl/fl}$ x $CD4cre^{tg}$ mice expressed slightly reduced frequencies of CD69 and PD-1 (Figure 41). This might endorse the hypothesis that Nrp-1 is directly involved in the activation of $CD8^+$ T cells. In accordance, absence of Nrp-1 expression on T cells resulted in reduced T cell activation in the brain and was

accompanied by less severe pathologies during PbA infection (Figure 30 and 31). However, to gain further insights into the underlying mechanism of Nrp-1-mediated activation of $CD8^+$ T cells, further experiments are needed to identify the Nrp-1 ligand involved in elevated T cell activation in the context of ECM.

As we showed that the Nrp-1/VEGF axis is not important in ECM, sema3A, sema4A and TGF-β might be possible ligands involved. Human T cells stimulated *in vitro* with αCD3 and αCD28 in the presence of recombinant sema3A proliferated less and produced reduced concentrations of cytokines [42, 187]. Another study hypothesised that sema3A might be partly responsible for the suppression of T cells and reduced cytotoxicity within tumours as well as diminished migratory potential *in vitro* [77, 187]. Lepelletier and colleagues claimed that the reorganisation of the cytoskeleton is inhibited by sema3A and therefore the receptor rearrangement within the immunological synapse is altered, leading to impaired proliferation of T cells [42]. Hence, sema3A seems to be rather suppressive and unlikely to be involved in Nrp-1-mediated T cell activation during ECM.

The presence of the Nrp-1 ligand TGF-β is described to be suppressive and used as an escape mechanism by tumour cells. Precisely, TGF-β binds to transcription factors like Smad and inhibits the $CD8^+$ T cell-mediated killing [188]. During LCMV infection, $CD8^+$ T cells lacking the TGF-β receptor were more activated than the wildtype controls, but were also more apoptotic and showed decreased memory differentiation. In general, the presence of TGF-β led to reduced activation of $CD8^+$ T cells, but memory T cells needed TGF-β to survive and produce cytokines [189]. Consequently, also TGF-β seems not to be involved in Nrp-1-dependent T cell activation during *Plasmodium* infection.

One promising candidate that could be involved in the enhanced activation of $Nrp\text{-}1^+CD8^+$ T cells might be sema4A. Sema4A is not expressed by naïve unstimulated $CD8^+$ T cells *in vitro*, but is upregulated upon αCD3 and αCD28 stimulation (own data not shown) [46]. Upon *in vitro* activation, sema4A-deficient $CD8^+$ T cells expressed reduced percentages of perforin or GzmB and produced decreased levels of IFN-γ compared to sema4A WT cells [190]. Furthermore, sema4A expressed by DCs plays a role in the activation of T cells, which subsequently upregulate sema4A to differentiate into effector T cells [191]. Infection of sema4A-deficient mice with ovalbumin-expressing *Listeria monocytogenes* led to a reduced formation of antigen-specific $CD8^+$ T cells in sema4A-KO mice [190]. In summary, sema4A is likely to play

an important in the activation of $CD8^+$ T cells. Further experiments are needed to verify the role of the Nrp-1/sema4A axis during ECM.

In summary, this current work highlights the influence of Nrp-1 expression on conventional $CD4^+$ T cells and $CD8^+$ T cells. Conventional $CD4^+$ T cells express Nrp-1 in the naïve state and Nrp-1 expression was associated with a highly activated phenotype. However, T cell-specific ablation of Nrp-1 was not efficient to improve parasite clearance during blood-stage malaria in PY-infected Balb/c mice. Nrp-1 expression on $CD8^+$ T cells was very low in the naïve state, but was significantly upregulated upon PbA infection. Nrp-1^+CD8^+ T cells were strongly activated and T cell-specific ablation of Nrp-1 resulted in decreased severity of ECM. Unlike described for $CD4^+$ T cell-mediated diseases, the migration of $CD8^+$ T cells along a VEGF gradient seems to be not the underlying mechanism of ameliorated ECM severity in T cell-specific Nrp-1-deficient mice. We rather hypothesise, that Nrp-1 is an early activation marker that is actively involved in the activation of $CD8^+$ T cells. Since the frequencies of Nrp-1^+CD8^+ T cells correlated with the severity of neurological deficits during PbA infection and there is increasing evidence that $CD8^+$ T cells also play an important role in human CM [177], Nrp-1 might be a suitable therapeutic target for the treatment of severe malaria. In addition, future studies are necessary to investigate a potential role of Nrp-1 in other $CD8^+$ T cell-mediated diseases like virus infections and tumours. Vice versa, the identification of the Nrp-1 ligand that binds to Nrp-1 on activated $CD8^+$ T cells resulting in enhanced T cell activation and therefore boosts protective $CD8^+$ T cell-responses in other diseases might offer new immunotherapy treatment options.

8 References

1. Murphy, K.W.C., *Janeway's Immunobiology 9th edition.* New York, NY: Garland Science/Taylor & Francis Group, LLC, 2016.
2. Nesargikar, P.N., B. Spiller, and R. Chavez, *The complement system: history, pathways, cascade and inhibitors.* European journal of microbiology & immunology, 2012. **2**(2): p. 103-111.
3. Zhou, H., et al., *Activation of Both TLR and NOD Signaling Confers Host Innate Immunity-Mediated Protection Against Microbial Infection.* Frontiers in immunology, 2019. **9**: p. 3082-3082.
4. Harwood, N.E. and F.D. Batista, *New Insights into the Early Molecular Events Underlying B Cell Activation.* Immunity, 2008. **28**(5): p. 609-619.
5. Bröker B., S.C.a.F.B., *Grundwissen Immunologie.* Springer Spectrum, 2019.
6. Jung, S., et al., *In Vivo Depletion of CD11c+ Dendritic Cells Abrogates Priming of CD8+ T Cells by Exogenous Cell-Associated Antigens.* Immunity, 2002. **17**(2): p. 211-220.
7. Joffre, O.P., et al., *Cross-presentation by dendritic cells.* Nature Reviews Immunology, 2012. **12**(8): p. 557-569.
8. Dustin, M.L., *The immunological synapse.* Arthritis research, 2002. **4 Suppl 3**(Suppl 3): p. S119-S125.
9. Fontenot, J.D., M.A. Gavin, and A.Y. Rudensky, *Foxp3 programs the development and function of CD4+CD25+ regulatory T cells.* Nature Immunology, 2003. **4**(4): p. 330-336.
10. Workman, C.J., et al., *The development and function of regulatory T cells.* Cellular and molecular life sciences : CMLS, 2009. **66**(16): p. 2603-2622.
11. Strauss, L., et al., *A Unique Subset of CD4⁺CD25^{high}Foxp3⁺ T Cells Secreting Interleukin-10 and Transforming Growth Factor-β1 Mediates Suppression in the Tumor Microenvironment.* 2007. **13**(15): p. 4345-4354.
12. Huang, C.-T., et al., *Role of LAG-3 in Regulatory T Cells.* Immunity, 2004. **21**(4): p. 503-513.
13. Takahashi, T., et al., *Immunologic self-tolerance maintained by CD25(+)CD4(+) regulatory T cells constitutively expressing cytotoxic T lymphocyte-associated antigen 4.* The Journal of experimental medicine, 2000. **192**(2): p. 303-310.
14. Thornton, A.M. and E.M. Shevach, *CD4+CD25+ immunoregulatory T cells suppress polyclonal T cell activation in vitro by inhibiting interleukin 2 production.* The Journal of experimental medicine, 1998. **188**(2): p. 287-296.
15. Gondek, D.C., et al., *Cutting Edge: Contact-Mediated Suppression by CD4⁺CD25⁺ Regulatory Cells Involves a Granzyme B-Dependent, Perforin-Independent Mechanism.* 2005. **174**(4): p. 1783-1786.
16. Andersen, M.H., et al., *Cytotoxic T Cells.* Journal of Investigative Dermatology, 2006. **126**(1): p. 32-41.
17. Zhao, Z., et al., *Establishment and Dysfunction of the Blood-Brain Barrier.* Cell, 2015. **163**(5): p. 1064-1078.
18. Ballabh, P., A. Braun, and M. Nedergaard, *The blood–brain barrier: an overview: Structure, regulation, and clinical implications.* Neurobiology of Disease, 2004. **16**(1): p. 1-13.
19. Rosenberg, G.A., *Neurological diseases in relation to the blood-brain barrier.* Journal of cerebral blood flow and metabolism : official journal of the International Society of Cerebral Blood Flow and Metabolism, 2012. **32**(7): p. 1139-1151.
20. Abbott, N.J., L. Ronnback, and E. Hansson, *Astrocyte-endothelial interactions at the blood-brain barrier.* Nat Rev Neurosci, 2006. **7**(1): p. 41-53.
21. Forrester, J.V., P.G. McMenamin, and S.J. Dando, *CNS infection and immune privilege.* Nature Reviews Neuroscience, 2018. **19**(11): p. 655-671.
22. Ransohoff, R.M., P. Kivisäkk, and G. Kidd, *Three or more routes for leukocyte migration into the central nervous system.* Nature Reviews Immunology, 2003. **3**(7): p. 569-581.

23. Fujisawa, H., S. Takagi, and T. Hirata, *Growth-Associated Expression of a Membrane Protein, Neuropilin, in Xenopus Optic NerveFibers.* Developmental Neuroscience, 1995. **17**(5-6): p. 343-349.
24. Kitsukawa, T., et al., *Neuropilin–Semaphorin III/D-Mediated Chemorepulsive Signals Play a Crucial Role in Peripheral Nerve Projection in Mice.* Neuron, 1997. **19**(5): p. 995-1005.
25. Tordjman, R., et al., *A neuronal receptor, neuropilin-1, is essential for the initiation of the primary immune response.* Nat Immunol, 2002. **3**(5): p. 477-82.
26. Sarris, M., et al., *Neuropilin-1 expression on regulatory T cells enhances their interactions with dendritic cells during antigen recognition.* Immunity, 2008. **28**(3): p. 402-13.
27. Kawasaki, T., et al., *A requirement for neuropilin-1 in embryonic vessel formation.* 1999. **126**(21): p. 4895-4902.
28. Jones, E.A.V., et al., *Separating genetic and hemodynamic defects in neuropilin 1 knockout embryos.* 2008. **135**(14): p. 2479-2488.
29. Soker, S., et al., *Neuropilin-1 Is Expressed by Endothelial and Tumor Cells as an Isoform-Specific Receptor for Vascular Endothelial Growth Factor.* Cell, 1998. **92**(6): p. 735-745.
30. Kitsukawa, T., et al., *Overexpression of a membrane protein, neuropilin, in chimeric mice causes anomalies in the cardiovascular system, nervous system and limbs.* 1995. **121**(12): p. 4309-4318.
31. Solomon, B.D., et al., *Neuropilin-1 attenuates autoreactivity in experimental autoimmune encephalomyelitis.* Proc Natl Acad Sci U S A, 2011. **108**(5): p. 2040-5.
32. Hansen, W., et al., *Neuropilin 1 deficiency on CD4+Foxp3+ regulatory T cells impairs mouse melanoma growth.* J Exp Med, 2012. **209**(11): p. 2001-16.
33. Delgoffe, G.M., et al., *Stability and function of regulatory T cells is maintained by a neuropilin-1-semaphorin-4a axis.* Nature, 2013. **501**(7466): p. 252-6.
34. Rossignol, M., M.L. Gagnon, and M. Klagsbrun, *Genomic Organization of Human Neuropilin-1 and Neuropilin-2 Genes: Identification and Distribution of Splice Variants and Soluble Isoforms.* Genomics, 2000. **70**(2): p. 211-222.
35. Fujisawa, H., et al., *Roles of a neuronal cell-surface molecule, neuropilin, in nerve fiber fasciculation and guidance.* Cell Tissue Res, 1997. **290**(2): p. 465-70.
36. Gu, C., et al., *Characterization of Neuropilin-1 Structural Features That Confer Binding to Semaphorin 3A and Vascular Endothelial Growth Factor 165.* 2002. **277**(20): p. 18069-18076.
37. Zondag, G.C., et al., *Homophilic interactions mediated by receptor tyrosine phosphatases mu and kappa. A critical role for the novel extracellular MAM domain.* J Biol Chem, 1995. **270**(24): p. 14247-50.
38. Cai, H. and R.R. Reed, *Cloning and Characterization of Neuropilin-1-Interacting Protein: A PSD-95/Dlg/ZO-1 Domain-Containing Protein That Interacts with the Cytoplasmic Domain of Neuropilin-1.* 1999. **19**(15): p. 6519-6527.
39. Ellis, L.M., *The role of neuropilins in cancer.* 2006. **5**(5): p. 1099-1107.
40. Roy, S., et al., *Multifaceted Role of Neuropilins in the Immune System: Potential Targets for Immunotherapy.* Front Immunol, 2017. **8**: p. 1228.
41. Takahashi, T., et al., *Plexin-Neuropilin-1 Complexes Form Functional Semaphorin-3A Receptors.* Cell, 1999. **99**(1): p. 59-69.
42. Lepelletier, Y., et al., *Immunosuppressive role of semaphorin-3A on T cell proliferation is mediated by inhibition of actin cytoskeleton reorganization.* 2006. **36**(7): p. 1782-1793.
43. Guttmann-Raviv, N., et al., *Semaphorin-3A and Semaphorin-3F Work Together to Repel Endothelial Cells and to Inhibit Their Survival by Induction of Apoptosis.* 2007. **282**(36): p. 26294-26305.
44. Miao, H.Q., et al., *Neuropilin-1 mediates collapsin-1/semaphorin III inhibition of endothelial cell motility: functional competition of collapsin-1 and vascular endothelial growth factor-165.* The Journal of cell biology, 1999. **146**(1): p. 233-242.
45. Behar, O., et al., *Semaphorin III is needed for normal patterning and growth of nerves, bones and heart.* Nature, 1996. **383**(6600): p. 525-8.

46. Kumanogoh, A., et al., *Class IV semaphorin Sema4A enhances T-cell activation and interacts with Tim-2.* Nature, 2002. **419**(6907): p. 629-33.
47. Millauer, B., et al., *High affinity VEGF binding and developmental expression suggest Flk-1 as a major regulator of vasculogenesis and angiogenesis.* Cell, 1993. **72**(6): p. 835-46.
48. Plate, K.H., et al., *Vascular endothelial growth factor is a potential tumour angiogenesis factor in human gliomas in vivo.* Nature, 1992. **359**(6398): p. 845-848.
49. Dvorak, H.F., et al., *Distribution of vascular permeability factor (vascular endothelial growth factor) in tumors: concentration in tumor blood vessels.* J Exp Med, 1991. **174**(5): p. 1275-8.
50. Olofsson, B., et al., *Vascular endothelial growth factor B, a novel growth factor for endothelial cells.* Proceedings of the National Academy of Sciences of the United States of America, 1996. **93**(6): p. 2576-2581.
51. Joukov, V., et al., *A novel vascular endothelial growth factor, VEGF-C, is a ligand for the Flt4 (VEGFR-3) and KDR (VEGFR-2) receptor tyrosine kinases.* The EMBO journal, 1996. **15**(2): p. 290-298.
52. Achen, M.G., et al., *Vascular endothelial growth factor D (VEGF-D) is a ligand for the tyrosine kinases VEGF receptor 2 (Flk1) and VEGF receptor 3 (Flt4).* Proceedings of the National Academy of Sciences of the United States of America, 1998. **95**(2): p. 548-553.
53. Maglione, D., et al., *Isolation of a human placenta cDNA coding for a protein related to the vascular permeability factor.* Proceedings of the National Academy of Sciences of the United States of America, 1991. **88**(20): p. 9267-9271.
54. Ogawa, S., et al., *A Novel Type of Vascular Endothelial Growth Factor, VEGF-E (NZ-7 VEGF), Preferentially Utilizes KDR/Flk-1 Receptor and Carries a Potent Mitotic Activity without Heparin-binding Domain.* 1998. **273**(47): p. 31273-31282.
55. Takahashi, H., et al., *A Novel Snake Venom Vascular Endothelial Growth Factor (VEGF) Predominantly Induces Vascular Permeability through Preferential Signaling via VEGF Receptor-1.* 2004. **279**(44): p. 46304-46314.
56. Chen, C., et al., *Roles of neuropilins in neuronal development, angiogenesis, and cancers.* World J Surg, 2005. **29**(3): p. 271-5.
57. Namiki, A., et al., *Hypoxia induces vascular endothelial growth factor in cultured human endothelial cells.* J Biol Chem, 1995. **270**(52): p. 31189-95.
58. Whitaker, G.B., B.J. Limberg, and J.S. Rosenbaum, *Vascular Endothelial Growth Factor Receptor-2 and Neuropilin-1 Form a Receptor Complex That Is Responsible for the Differential Signaling Potency of VEGF165 and VEGF121.* 2001. **276**(27): p. 25520-25531.
59. Fuh, G., K.C. Garcia, and A.M. de Vos, *The interaction of Neuropilin-1 with Vascular Endothelial Growth Factor and its receptor Flt-1.* 2000.
60. Binétruy-Tournaire, R., et al., *Identification of a peptide blocking vascular endothelial growth factor (VEGF)-mediated angiogenesis.* The EMBO journal, 2000. **19**(7): p. 1525-1533.
61. Tirand, L., et al., *A peptide competing with VEGF165 binding on neuropilin-1 mediates targeting of a chlorin-type photosensitizer and potentiates its photodynamic activity in human endothelial cells.* Journal of Controlled Release, 2006. **111**(1): p. 153-164.
62. Massagué, J., *TGFβ in Cancer.* Cell, 2008. **134**(2): p. 215-230.
63. Glinka, Y., et al., *Neuropilin-1 exerts co-receptor function for TGF-beta-1 on the membrane of cancer cells and enhances responses to both latent and active TGF-beta.* Carcinogenesis, 2010. **32**(4): p. 613-621.
64. Glinka, Y. and G.J. Prud'homme, *Neuropilin-1 is a receptor for transforming growth factor β-1, activates its latent form, and promotes regulatory T cell activity.* 2008. **84**(1): p. 302-310.
65. Chaudhary, B., et al., *Neuropilin 1: function and therapeutic potential in cancer.* Cancer Immunol Immunother, 2014. **63**(2): p. 81-99.
66. Battin, C., et al., *Neuropilin-1 Acts as a Receptor for Complement Split Products.* Front Immunol, 2019. **10**: p. 2209.

67. Bruder, D., et al., *Neuropilin-1: a surface marker of regulatory T cells.* Eur J Immunol, 2004. **34**(3): p. 623-630.
68. Mizui, M. and H. Kikutani, *Neuropilin-1: The Glue between Regulatory T Cells and Dendritic Cells?* Immunity, 2008. **28**(3): p. 302-303.
69. Milpied, P., et al., *Neuropilin-1 is not a marker of human Foxp3+ Treg.* 2009. **39**(6): p. 1466-1471.
70. Weiss, J.M., et al., *Neuropilin 1 is expressed on thymus-derived natural regulatory T cells, but not mucosa-generated induced Foxp3+ T reg cells.* Journal of Experimental Medicine, 2012. **209**(10): p. 1723-1742.
71. Akimova, T., et al., *Helios Expression Is a Marker of T Cell Activation and Proliferation.* PLOS ONE, 2011. **6**(8): p. e24226.
72. Bourbié-Vaudaine, S., et al., *Dendritic Cells Can Turn CD4⁺ T Lymphocytes into Vascular Endothelial Growth Factor-Carrying Cells by Intercellular Neuropilin-1 Transfer.* 2006. **177**(3): p. 1460-1469.
73. Nishikawa, H. and S. Sakaguchi, *Regulatory T cells in tumor immunity.* Int J Cancer, 2010. **127**(4): p. 759-67.
74. Terme, M., et al., *VEGFA-VEGFR Pathway Blockade Inhibits Tumor-Induced Regulatory T-cell Proliferation in Colorectal Cancer.* 2013. **73**(2): p. 539-549.
75. Proescholdt, M.A., et al., *Vascular endothelial growth factor is expressed in multiple sclerosis plaques and can induce inflammatory lesions in experimental allergic encephalomyelitis rats.* J Neuropathol Exp Neurol, 2002. **61**(10): p. 914-25.
76. Gaddis, D.E., et al., *Neuropilin-1 Expression on CD4 T Cells Is Atherogenic and Facilitates T Cell Migration to the Aorta in Atherosclerosis.* J Immunol, 2019. **203**(12): p. 3237-3246.
77. Leclerc, M., et al., *Regulation of antitumour CD8 T-cell immunity and checkpoint blockade immunotherapy by Neuropilin-1.* Nat Commun, 2019. **10**(1): p. 3345.
78. Jackson, S.R., et al., *Neuropilin-1 expression is induced on tolerant self-reactive CD8+ T cells but is dispensable for the tolerant phenotype.* PLoS One, 2014. **9**(10): p. e110707.
79. Hwang, J.Y., et al., *Neuropilin-1 Regulates the Secondary CD8 T Cell Response to Virus Infection.* mSphere, 2019. **4**(3).
80. Liu, C., et al., *Neuropilin-1 is a T cell memory checkpoint limiting long-term antitumor immunity.* Nature Immunology, 2020. **21**(9): p. 1010-1021.
81. Kawakami, T., et al., *Neuropilin 1 and neuropilin 2 co-expression is significantly correlated with increased vascularity and poor prognosis in nonsmall cell lung carcinoma.* Cancer, 2002. **95**(10): p. 2196-201.
82. Li, L., et al., *Neuropilin-1 is associated with clinicopathology of gastric cancer and contributes to cell proliferation and migration as multifunctional co-receptors.* J Exp Clin Cancer Res, 2016. **35**: p. 16.
83. Liang, W.-C., et al., *Function Blocking Antibodies to Neuropilin-1 Generated from a Designed Human Synthetic Antibody Phage Library.* Journal of Molecular Biology, 2007. **366**(3): p. 815-829.
84. Pan, Q., et al., *Blocking Neuropilin-1 Function Has an Additive Effect with Anti-VEGF to Inhibit Tumor Growth.* Cancer Cell, 2007. **11**(1): p. 53-67.
85. Patnaik, A., et al., *A Phase Ib study evaluating MNRP1685A, a fully human anti-NRP1 monoclonal antibody, in combination with bevacizumab and paclitaxel in patients with advanced solid tumors.* Cancer Chemother Pharmacol, 2014. **73**(5): p. 951-60.
86. Ding, N., et al., *iRGD synergizes with PD-1 knockout immunotherapy by enhancing lymphocyte infiltration in gastric cancer.* Nature Communications, 2019. **10**(1): p. 1336.
87. Cox, F.E., *History of the discovery of the malaria parasites and their vectors.* Parasit Vectors, 2010. **3**(1): p. 5.
88. Capanna, E., *Grassi versus Ross: who solved the riddle of malaria?* Int Microbiol, 2006. **9**(1): p. 69-74.
89. *World malaria report 2019.* Geneva: World Health Organization, 2019.
90. WHO, *First malaria vaccine in Africa: A potential new tool for child health and improved malaria control.* 2018.
91. White, N.J., *The Treatment of Malaria.* 1996. **335**(11): p. 800-806.

92. *Global Health Estimates 2016: Deaths by Cause, Age, Sex, by Country and by Region, 2000-2016.* Geneva, World Health Organization, 2018.
93. Phillips, M.A., et al., *Malaria.* Nat Rev Dis Primers, 2017. **3**: p. 17050.
94. Tizifa, T.A., et al., *Prevention Efforts for Malaria.* Current tropical medicine reports, 2018. **5**(1): p. 41-50.
95. WHO, *Larval source management – a supplementary measure for malaria vector control. An operational manual.* 2013.
96. Gantz, V.M., et al., *Highly efficient Cas9-mediated gene drive for population modification of the malaria vector mosquito Anopheles stephensi.* 2015. **112**(49): p. E6736-E6743.
97. Tse, E.G., M. Korsik, and M.H. Todd, *The past, present and future of anti-malarial medicines.* Malaria Journal, 2019. **18**(1): p. 93.
98. Wang, J., et al., *Haem-activated promiscuous targeting of artemisinin in Plasmodium falciparum.* Nature Communications, 2015. **6**(1): p. 10111.
99. Meshnick, S.R., *Artemisinin: mechanisms of action, resistance and toxicity.* International Journal for Parasitology, 2002. **32**(13): p. 1655-1660.
100. Amato, R., et al., *Origins of the current outbreak of multidrug-resistant malaria in southeast Asia: a retrospective genetic study.* The Lancet. Infectious diseases, 2018. **18**(3): p. 337-345.
101. Antinori, S., et al., *Biology of human malaria plasmodia including Plasmodium knowlesi.* Mediterranean journal of hematology and infectious diseases, 2012. **4**(1): p. e2012013-e2012013.
102. Hafalla, J.C., O. Silvie, and K. Matuschewski, *Cell biology and immunology of malaria.* Immunol Rev, 2011. **240**(1): p. 297-316.
103. Silvie, O., et al., *Interactions of the malaria parasite and its mammalian host.* Curr Opin Microbiol, 2008. **11**(4): p. 352-9.
104. Kappe, S.H.I., et al., *That Was Then But This Is Now: Malaria Research in the Time of an Eradication Agenda.* 2010. **328**(5980): p. 862-866.
105. Cowman, A.F., et al., *Malaria: Biology and Disease.* Cell, 2016. **167**(3): p. 610-624.
106. Aly, A.S.I., A.M. Vaughan, and S.H.I. Kappe, *Malaria parasite development in the mosquito and infection of the mammalian host.* Annual review of microbiology, 2009. **63**: p. 195-221.
107. WHO, *Climate change and human health - risks and responses. Summary.* 2003.
108. Dayananda, K.K., R.N. Achur, and D.C. Gowda, *Epidemiology, drug resistance, and pathophysiology of Plasmodium vivax malaria.* Journal of vector borne diseases, 2018. **55**(1): p. 1-8.
109. Mendes, C., et al., *Duffy negative antigen is no longer a barrier to Plasmodium vivax--molecular evidences from the African West Coast (Angola and Equatorial Guinea).* PLoS neglected tropical diseases, 2011. **5**(6): p. e1192-e1192.
110. Cox-Singh, J., et al., *Plasmodium knowlesi malaria in humans is widely distributed and potentially life threatening.* Clin Infect Dis, 2008. **46**(2): p. 165-71.
111. Marchand, R.P., et al., *Co-infections of Plasmodium knowlesi, P. falciparum, and P. vivax among Humans and Anopheles dirus Mosquitoes, Southern Vietnam.* Emerging infectious diseases, 2011. **17**(7): p. 1232-1239.
112. Jiang, N., et al., *Co-infections with Plasmodium knowlesi and other malaria parasites, Myanmar.* Emerging infectious diseases, 2010. **16**(9): p. 1476-1478.
113. Otto, T.D., et al., *A comprehensive evaluation of rodent malaria parasite genomes and gene expression.* BMC biology, 2014. **12**: p. 86-86.
114. Stevenson, M.M. and E.M. Riley, *Innate immunity to malaria.* Nat Rev Immunol, 2004. **4**(3): p. 169-80.
115. Amino, R., et al., *Host Cell Traversal Is Important for Progression of the Malaria Parasite through the Dermis to the Liver.* Cell Host & Microbe, 2008. **3**(2): p. 88-96.
116. Torgler, R., et al., *Sporozoite-Mediated Hepatocyte Wounding Limits Plasmodium Parasite Development via MyD88-Mediated NF-κB Activation and Inducible NO Synthase Expression.* 2008. **180**(6): p. 3990-3999.

117. Seguin, M.C., et al., *Induction of nitric oxide synthase protects against malaria in mice exposed to irradiated Plasmodium berghei infected mosquitoes: involvement of interferon gamma and CD8+ T cells.* J Exp Med, 1994. **180**(1): p. 353-8.
118. Singh, A.P., et al., *Plasmodium circumsporozoite protein promotes the development of the liver stages of the parasite.* Cell, 2007. **131**(3): p. 492-504.
119. Cohen, J., et al., *From the circumsporozoite protein to the RTS,S/AS candidate vaccine.* Human Vaccines, 2010. **6**(1): p. 90-96.
120. Winau, F., et al., *Ito cells are liver-resident antigen-presenting cells for activating T cell responses.* Immunity, 2007. **26**(1): p. 117-29.
121. Miller, Jessica L., et al., *Interferon-Mediated Innate Immune Responses against Malaria Parasite Liver Stages.* Cell Reports, 2014. **7**(2): p. 436-447.
122. Doolan, D.L. and S.L. Hoffman, *IL-12 and NK cells are required for antigen-specific adaptive immunity against malaria initiated by CD8+ T cells in the Plasmodium yoelii model.* J Immunol, 1999. **163**(2): p. 884-92.
123. Oakley, M.S., et al., *Clinical and molecular aspects of malaria fever.* Trends in Parasitology, 2011. **27**(10): p. 442-449.
124. Mebius, R.E. and G. Kraal, *Structure and function of the spleen.* Nat Rev Immunol, 2005. **5**(8): p. 606-16.
125. Engwerda, C.R., L. Beattie, and F.H. Amante, *The importance of the spleen in malaria.* Trends in Parasitology, 2005. **21**(2): p. 75-80.
126. Lau, L.S., et al., *CD8+ T Cells from a Novel T Cell Receptor Transgenic Mouse Induce Liver-Stage Immunity That Can Be Boosted by Blood-Stage Infection in Rodent Malaria.* PLOS Pathogens, 2014. **10**(5): p. e1004135.
127. Krishnegowda, G., et al., *Induction of proinflammatory responses in macrophages by the glycosylphosphatidylinositols of Plasmodium falciparum: cell signaling receptors, glycosylphosphatidylinositol (GPI) structural requirement, and regulation of GPI activity.* The Journal of biological chemistry, 2005. **280**(9): p. 8606-8616.
128. Coban, C., et al., *Toll-like receptor 9 mediates innate immune activation by the malaria pigment hemozoin.* The Journal of experimental medicine, 2005. **201**(1): p. 19-25.
129. Gowda, D.C. and X. Wu, *Parasite Recognition and Signaling Mechanisms in Innate Immune Responses to Malaria.* Frontiers in immunology, 2018. **9**: p. 3006-3006.
130. Gilson, P.R., et al., *Identification and stoichiometry of glycosylphosphatidylinositol-anchored membrane proteins of the human malaria parasite Plasmodium falciparum.* Mol Cell Proteomics, 2006. **5**(7): p. 1286-99.
131. Ueffing, K., et al., *Conventional CD11c(high) Dendritic Cells Are Important for T Cell Priming during the Initial Phase of Plasmodium yoelii Infection, but Are Dispensable at Later Time Points.* Front Immunol, 2017. **8**: p. 1333.
132. Perry, J.A., et al., *Dendritic Cells from Malaria-Infected Mice Are Fully Functional APC.* 2004. **172**(1): p. 475-482.
133. Villegas-Mendez, A., et al., *IFN-γ-producing CD4+ T cells promote experimental cerebral malaria by modulating CD8+ T cell accumulation within the brain.* Journal of immunology (Baltimore, Md. : 1950), 2012. **189**(2): p. 968-979.
134. Orago, A.S. and C.A. Facer, *Cytotoxicity of human natural killer (NK) cell subsets for Plasmodium falciparum erythrocytic schizonts: stimulation by cytokines and inhibition by neomycin.* Clin Exp Immunol, 1991. **86**(1): p. 22-9.
135. Artavanis-Tsakonas, K., et al., *Activation of a Subset of Human NK Cells upon Contact with Plasmodium falciparum-Infected Erythrocytes.* 2003. **171**(10): p. 5396-5405.
136. Kumar, R., et al., *The regulation of CD4(+) T cells during malaria.* Immunol Rev, 2020. **293**(1): p. 70-87.
137. Su, Z. and M.M. Stevenson, *IL-12 is required for antibody-mediated protective immunity against blood-stage Plasmodium chabaudi AS malaria infection in mice.* J Immunol, 2002. **168**(3): p. 1348-55.
138. Abel, S., et al., *Strong impact of CD4+ Foxp3+ regulatory T cells and limited effect of T cell-derived IL-10 on pathogen clearance during Plasmodium yoelii infection.* J Immunol, 2012. **188**(11): p. 5467-77.

139. Montes de Oca, M., et al., *The Impact of Established Immunoregulatory Networks on Vaccine Efficacy and the Development of Immunity to Malaria.* J Immunol, 2016. **197**(12): p. 4518-4526.
140. Loevenich, K., et al., *DC-Derived IL-10 Modulates Pro-inflammatory Cytokine Production and Promotes Induction of CD4(+)IL-10(+) Regulatory T Cells during Plasmodium yoelii Infection.* Front Immunol, 2017. **8**: p. 152.
141. Zander, R.A., et al., *Type I Interferons Induce T Regulatory 1 Responses and Restrict Humoral Immunity during Experimental Malaria.* PLoS Pathog, 2016. **12**(10): p. e1005945.
142. Freitas do Rosario, A.P., et al., *IL-27 promotes IL-10 production by effector Th1 CD4+ T cells: a critical mechanism for protection from severe immunopathology during malaria infection.* J Immunol, 2012. **188**(3): p. 1178-90.
143. Lundie, R.J., et al., *Blood-stage Plasmodium berghei infection leads to short-lived parasite-associated antigen presentation by dendritic cells.* 2010. **40**(6): p. 1674-1681.
144. Piva, L., et al., *Cutting Edge: Clec9A⁺ Dendritic Cells Mediate the Development of Experimental Cerebral Malaria.* 2012. **189**(3): p. 1128-1132.
145. Dunst, J., F. Kamena, and K. Matuschewski, *Cytokines and Chemokines in Cerebral Malaria Pathogenesis.* Front Cell Infect Microbiol, 2017. **7**: p. 324.
146. Medana, I.M. and G.D.H. Turner, *Human cerebral malaria and the blood–brain barrier.* International Journal for Parasitology, 2006. **36**(5): p. 555-568.
147. BAUER, P.R., et al., *Regulation of Endothelial Cell Adhesion Molecule Expression in an Experimental Model of Cerebral Malaria.* 2002. **9**(6): p. 463-470.
148. Turner, G.D., et al., *An immunohistochemical study of the pathology of fatal malaria. Evidence for widespread endothelial activation and a potential role for intercellular adhesion molecule-1 in cerebral sequestration.* Am J Pathol, 1994. **145**(5): p. 1057-69.
149. Ockenhouse, C.F., et al., *Human vascular endothelial cell adhesion receptors for Plasmodium falciparum-infected erythrocytes: roles for endothelial leukocyte adhesion molecule 1 and vascular cell adhesion molecule 1.* Journal of Experimental Medicine, 1992. **176**(4): p. 1183-1189.
150. Amani, V., et al., *Involvement of IFN-γ receptor-mediated signaling in pathology and anti-malarial immunity induced by Plasmodium berghei infection.* 2000. **30**(6): p. 1646-1655.
151. Swanson, P.A., II, et al., *CD8+ T Cells Induce Fatal Brainstem Pathology during Cerebral Malaria via Luminal Antigen-Specific Engagement of Brain Vasculature.* PLOS Pathogens, 2016. **12**(12): p. e1006022.
152. Favre, N., et al., *Role of ICAM-1 (CD54) in the development of murine cerebral malaria.* Microbes and Infection, 1999. **1**(12): p. 961-968.
153. Prakash, D., et al., *Clusters of Cytokines Determine Malaria Severity in Plasmodium falciparum–Infected Patients from Endemic Areas of Central India.* The Journal of Infectious Diseases, 2006. **194**(2): p. 198-207.
154. Wilson, N.O., et al., *CXCL4 and CXCL10 Predict Risk of Fatal Cerebral Malaria.* Disease Markers, 2011. **30**: p. 828256.
155. Campanella, G.S., et al., *Chemokine receptor CXCR3 and its ligands CXCL9 and CXCL10 are required for the development of murine cerebral malaria.* Proc Natl Acad Sci U S A, 2008. **105**(12): p. 4814-9.
156. Van den Steen, P.E., et al., *CXCR3 determines strain susceptibility to murine cerebral malaria by mediating T lymphocyte migration toward IFN-γ-induced chemokines.* 2008. **38**(4): p. 1082-1095.
157. Belnoue, E., et al., *Control of pathogenic CD8+ T cell migration to the brain by IFN-gamma during experimental cerebral malaria.* Parasite Immunol, 2008. **30**(10): p. 544-53.
158. Srivastava, K., et al., *Platelet Factor 4 Mediates Inflammation in Experimental Cerebral Malaria.* Cell Host & Microbe, 2008. **4**(2): p. 179-187.
159. Howland, S.W., et al., *Pathogenic CD8+ T cells in experimental cerebral malaria.* Semin Immunopathol, 2015. **37**(3): p. 221-31.
160. Howland, S.W., et al., *Brain microvessel cross-presentation is a hallmark of experimental cerebral malaria.* 2013. **5**(7): p. 984-999.

161. El-Assaad, F., et al., *Cytoadherence of Plasmodium berghei-infected red blood cells to murine brain and lung microvascular endothelial cells in vitro.* Infect Immun, 2013. **81**(11): p. 3984-91.
162. Hunt, N.H., et al., *Immunopathogenesis of cerebral malaria.* International Journal for Parasitology, 2006. **36**(5): p. 569-582.
163. Jacobs, T., et al., *Murine Malaria Is Exacerbated by CTLA-4 Blockade.* 2002. **169**(5): p. 2323-2329.
164. Hafalla, J.C.R., et al., *The CTLA-4 and PD-1/PD-L1 Inhibitory Pathways Independently Regulate Host Resistance to Plasmodium-induced Acute Immune Pathology.* PLOS Pathogens, 2012. **8**(2): p. e1002504.
165. Butler, N.S., et al., *Therapeutic blockade of PD-L1 and LAG-3 rapidly clears established blood-stage Plasmodium infection.* Nat Immunol, 2011. **13**(2): p. 188-95.
166. Mackroth, M.S., et al., *Acute Malaria Induces PD1+CTLA4+ Effector T Cells with Cell-Extrinsic Suppressor Function.* PLoS Pathog, 2016. **12**(11): p. e1005909.
167. Hou, N., et al., *T-Cell Immunoglobulin- and Mucin-Domain-Containing Molecule 3 Signaling Blockade Improves Cell-Mediated Immunity Against Malaria.* J Infect Dis, 2016. **214**(10): p. 1547-1556.
168. Ribas, A. and J.D. Wolchok, *Cancer immunotherapy using checkpoint blockade.* 2018. **359**(6382): p. 1350-1355.
169. Gu, C., et al., *Neuropilin-1 Conveys Semaphorin and VEGF Signaling during Neural and Cardiovascular Development.* Developmental Cell, 2003. **5**(1): p. 45-57.
170. Wing, K., et al., *CTLA-4 Control over Foxp3⁺ Regulatory T Cell Function.* Science, 2008. **322**(5899): p. 271-275.
171. Carroll, R.W., et al., *A Rapid Murine Coma and Behavior Scale for Quantitative Assessment of Murine Cerebral Malaria.* PLOS ONE, 2010. **5**(10): p. e13124.
172. Starzec, A., et al., *Antiangiogenic and antitumor activities of peptide inhibiting the vascular endothelial growth factor binding to neuropilin-1.* Life Sci, 2006. **79**(25): p. 2370-81.
173. Frimpong, A., et al., *Phenotypic Evidence of T Cell Exhaustion and Senescence During Symptomatic Plasmodium falciparum Malaria.* Frontiers in immunology, 2019. **10**: p. 1345-1345.
174. Overacre-Delgoffe, A.E., et al., *Interferon-gamma Drives Treg Fragility to Promote Anti-tumor Immunity.* Cell, 2017. **169**(6): p. 1130-1141 e11.
175. Abel, S., et al., *Plasmodium yoelii infection of BALB/c mice results in expansion rather than induction of CD4(+) Foxp3(+) regulatory T cells.* Immunology, 2016. **148**(2): p. 197-205.
176. Muscate, F., et al., *HVEM and CD160: Regulators of Immunopathology During Malaria Blood-Stage.* Frontiers in immunology, 2018. **9**: p. 2611-2611.
177. Kaminski, L.C., et al., *Cytotoxic T Cell-Derived Granzyme B Is Increased in Severe Plasmodium Falciparum Malaria.* Front Immunol, 2019. **10**: p. 2917.
178. Oehen, S. and K. Brduscha-Riem, *Differentiation of Naive CTL to Effector and Memory CTL: Correlation of Effector Function with Phenotype and Cell Division.* The Journal of Immunology, 1998. **161**(10): p. 5338-5346.
179. Sallusto, F., et al., *Two subsets of memory T lymphocytes with distinct homing potentials and effector functions.* Nature, 1999. **401**(6754): p. 708-712.
180. Lanzavecchia, A. and F. Sallusto, *Dynamics of T Lymphocyte Responses: Intermediates, Effectors, and Memory Cells.* Science, 2000. **290**(5489): p. 92-97.
181. Steeg, C., et al., *Limited Role of CD4⁺Foxp3⁺ Regulatory T Cells in the Control of Experimental Cerebral Malaria.* The Journal of Immunology, 2009. **183**(11): p. 7014-7022.
182. Amante, F.H., et al., *A role for natural regulatory T cells in the pathogenesis of experimental cerebral malaria.* Am J Pathol, 2007. **171**(2): p. 548-59.
183. Lahl, K., et al., *Selective depletion of Foxp3+ regulatory T cells induces a scurfy-like disease.* J Exp Med, 2007. **204**(1): p. 57-63.
184. Medana, I.M., et al., *Induction of the vascular endothelial growth factor pathway in the brain of adults with fatal falciparum malaria is a non-specific response to severe disease.* Histopathology, 2010. **57**(2): p. 282-294.

185. Roscoe, W.A., et al., *VEGF and angiogenesis in acute and chronic MOG(35–55) peptide induced EAE.* Journal of Neuroimmunology, 2009. **209**(1): p. 6-15.
186. Kurschus, F.C., *T cell mediated pathogenesis in EAE: Molecular mechanisms.* Biomed J, 2015. **38**(3): p. 183-93.
187. Catalano, A., et al., *Semaphorin-3A is expressed by tumor cells and alters T-cell signal transduction and function.* Blood, 2006. **107**(8): p. 3321-9.
188. Thomas, D.A. and J. Massagué, *TGF-β directly targets cytotoxic T cell functions during tumor evasion of immune surveillance.* Cancer Cell, 2005. **8**(5): p. 369-380.
189. Filippi, C.M., et al., *Transforming growth factor-beta suppresses the activation of CD8+ T-cells when naive but promotes their survival and function once antigen experienced: a two-faced impact on autoimmunity.* Diabetes, 2008. **57**(10): p. 2684-2692.
190. Ito, D., et al., *mTOR Complex Signaling through the SEMA4A-Plexin B2 Axis Is Required for Optimal Activation and Differentiation of CD8+ T Cells.* Journal of immunology (Baltimore, Md. : 1950), 2015. **195**(3): p. 934-943.
191. Kumanogoh, A., et al., *Nonredundant Roles of Sema4A in the Immune System: Defective T Cell Priming and Th1/Th2 Regulation in Sema4A-Deficient Mice.* Immunity, 2005. **22**(3): p. 305-316.

9 Abbreviations

Abbreviation	Meaning
APCs	Antigen presenting cells
BBB	Blood-brain barrier
Bcl	B cell lymphoma
BCR	B cell receptor
BSA	Bovine serum albumin V
CLRs	C-type lectin receptors
CM	Cerebral malaria
CNS	Central nervous system
CPPs	Cell-penetrating peptides
CRISPR/cas9	clustered regularly interspaced short palindromic repeats/CRIPR-associated protein 9
CSP	circumsporozoite protein
CTLA-4	Cytotoxic T lymphocyte antigen 4
CTLs	Cytotoxic T lymphocytes
CUB	complement binding factors C1r/C1s, sea urchin epidermal growth factor, bone morphogenetic protein 1
CXCL	Chemokine ligand
CXCR	Chemokine receptor
DAMPs	Damage-associated molecular patterns
DCs	Dendritic cells
dNTPs	Deoxynucleoside Triphosphates
DT	Diphtheria toxin
EAE	Experimental autoimmune encephalomyelitis
ECM	Experimental cerebral malaria
EDTA	Ethylenediaminetetraacetic acid
FACS	Fluorescence-associated cell sorting
Fas-L	Fas ligand
FoxP3	Forkhead box P3
FV/VIII	Factor V/VIII coagulation factor homology domains
FvD	Fixable viable dye
G-CSF	Granulocyte-colony stimulating factor

GPI	Glycosylphosphatidylinositol
Gzm	Granzyme
ICAM-1	Intercellular adhesion molecule 1
ICOS	Inducible T-cell costimulator
IFNR	Interferon receptor
IFN-γ	Interferon γ
Igs	Immunoglobulins
IL	Interleukin
iRBCs	Infected red blood cells
iTregs	Induced regulatory T cells
KLRG-1	Killer cell lectin-like receptor subfamily G member 1
KO	Knockout
Lag-3	lymphocyte activation gene 3
LAP	Latency-associated peptide
LFA-1	Lymphocyte function-associated antigen 1
mAbs	Monoclonal antibodies
MACS	Magnetic activated cell sorting
MAM	meprin, A5 protein, protein tyrosine phosphatase μ
MHC	Major histocompatibility complex
MyD88	Myeloid differentiation gene 88
MΦ	Macrophages
NF-κB	Nuclear factor κ-light-chain-enhancer of activated B cells
NK	Natural killer
NKT	Natural killer T cell
NLRs	Nucleotide-binding oligomerisation domain-like receptors
NO	Nitric oxide
NOD	Nucleotide-binding oligomerisation domain
Nrp-1	Neuropilin-1
nTregs	Natural regulatory T cells
P.	Plasmodium
p.i.	Post infection
PAMPs	Pathogen-associated molecular patterns
PbA	Plasmodium berghei ANKA
PCR	Polymerase chain reaction

PD-1	Programmed cell death 1
PDZ	PSD-95/Dig/ZO-1
PFA	Paraformaldehyde
PfeMP1	Plasmodium falciparum-encoded erythrocyte membrane protein 1
PGF	Placental growth factor
PMA	Phorobol 12-myristate 13-acetate
PRR	Pattern recognition receptor
PY	Plasmodium yoelii
qPCR	Quantitative PCR
RMCBS	rapid murine coma and behaviour scale
ROIs	Regions of interest
SDF-1β	Stromal cell-derived factor 1
Sema	Semaphorin
T_A	Annealing temperature
T_{CM}	Central memory T cells
TCR	T cell receptor
T_{EM}	Effector memory T cells
T_{FH}	Follicular T helper cell
TGF-β	Transforming growth factor β
T_H	T helper cell
Tim-3	T-cell immunoglobulin and mucin-domain 3
TLRs	Toll-like receptors
TM	Transmembrane
T_N	Naïve T cells
TNFR	Tumour necrosis factor receptor
TNF-α	Tumour necrosis factor α
TPPs	Tumour-penetrating peptides
Tregs	Regulatory T cells
VCAM-1	Vascular cell adhesion molecule 1
VEGFR	Vascular endothelial growth factors receptor
VEGFs	Vascular endothelial growth factors
VLA-4	Very late antigen 4
WHO	World health organisation
WT	Wildtype

10 List of figures

11 List of tables

12 Acknowledgments

Die Danksagung ist in der Online-Version nicht enthalten.

13 Curriculum Vitae

Der Lebenslauf ist in der Online-Version aus Gründen des Datenschutzes nicht enthalten.

14 Declarations

Hiermit erkläre ich, gem. § 7 Abs. 2 d) und f) der Promotionsordnung der Fakultät für Biologie zur Erlangung des Dr. rer. nat., dass ich die vorliegende Dissertation selbstständig verfasst und mich keiner anderen als der angegebenen Hilfsmittel bedient, bei der Abfassung der Dissertation nur die angegebenen Hilfsmittel benutzt und alle wörtlich oder inhaltlich übernommenen Stellen als solche gekennzeichnet habe.

Essen, den _____ _____

Hanna Abberger

Hiermit erkläre ich, gem. § 7 Abs. 2 e) und g) der Promotionsordnung der Fakultät für Biologie zur Erlangung des Dr. rer. nat., dass ich keine anderen Promotionen bzw. Promotionsversuche in der Vergangenheit durchgeführt habe und dass diese Arbeit von keiner anderen Fakultät/Fachbereich abgelehnt worden ist.

Essen, den _____ _____

Hanna Abberger

Hiermit erkläre ich, gem. § 6 Abs. 2 g) der Promotionsordnung der Fakultät für Biologie zur Erlangung der Dr. rer. nat., dass ich das Arbeitsgebiet, dem das Thema „Neuropilin-1-dependent modulation of T cell responses during blood-stage and experimental cerebral malaria“ zuzuordnen ist, in Forschung und Lehre vertrete und den Antrag von Hanna Abberger befürworte.

Essen, den _____ _____

Prof. Dr. Wiebke Hansen